Insulation Coordination of Solid State Devices Connected Directly to the Electric Power Distribution System

by

Xuening Rong

A Thesis Presented in Partial Fulfillment
of the Requirements for the Degree
Master of Science

Approved July 2017 by the
Graduate Supervisory Committee:

George Karady, Chair
Gerald Heydt
Raja Ayyanar

ARIZONA STATE UNIVERSITY

August 2017

ABSTRACT

With the penetration of distributed renewable energy and the development of semiconductor technology, power electronic devices could be utilized to interface renewable energy generation and the distribution power grid. However, when directly connected to the power grid, the semiconductors inside the power electronic devices could be vulnerable to the power system transient, especially to lightning strikes.

The work of this research focuses on the insulation coordination of power electronic devices connected directly to the power distribution system. The Solid State Transformer (SST) in Future Renewable Electric Energy Delivery and Management (FREEDM) system could be a good example for grid connected power electronic devices. Simulations were conducted in Power Systems Computer Aided Design (PSCAD) software. A simulation done to the FREEDM SST showed primary results which were then compare to simulation done to the grid-connected operating Voltage Source Converter (VSC) to get more objective results.

Based on the simulation results, voltage surges caused by lightning strikes could result in damage on the grid-connected electronic devices. Placing Metal Oxide Surge Arresers (MOSA, also known as Metal Oxide Surge Varistor, MOV) at the front filter could provide effective protection for those devices from power transient. Part of this research work was published as a conference paper and was presented at CIGRE US National Conference: Grid of the Future Symposium [1] and North American Power Symposium [2].

ACKNOWLEDGMENTS

I would like to express the deepest appreciation to my advisor and mentor, Dr George Karady, for providing me with this opportunity to work on the FREEDM project, and for his guidance, patience and persistent help during the research.

I would like to thank my committee members, Dr Heydt and Dr Ayyanar, for their valuable time and comments.

I am grateful to my parents for providing generous love and enormous support to me. In addition, a thank you to all my friends for their help, company and encouragement.

TABLE OF CONTENTS

CHAPTER Page

CHAPTER Page

CHAPTER Page

LIST OF TABLES

LIST OF FIGURES

Figure Page

Figure Page

LIST OF SYMBOLS

AWG	American Wire Gauge
BIL	Basic Lightning Impulse Insulation Level
DC	Direct Current
DESD	Distributed Energy Storage Devices
DGI	Distributed Grid Intelligence
DHB	Dual-Half-Bridge
DRER	Distributed Renewable Energy Resources
ERC	Engineering Research Center
FACTS	Flexible Alternating Current Transmission Systems
FREEDM	Future Renewable Electric Energy Delivery and Management
IEM	Industrial Ethernet Module
IGBT	Insulated Gate Bipolar Transistor
IPC	Interphase Power Controller
MOSA	Metal-Oxide Surge Arrester
MSC	Mechanically Switched Capacitor bank
MSR	Mechanically Switched Reactor bank
NSF	National Science Foundation
PSCAD	Power Systems Computer Aided Design
PWM	Pulse Width Modulation
SPD	Surge Protection Device
SSSC	Static Series Synchronous Compensator
SST	Solid State Transformer
STATCOM	Static Compensator
SVC	Static VAR Compensator
TCR	Thyristor Controlled Reactor
THD	Total Harmonic Distortion
TSC	Thyristor Switched Capacitor
VSC	Voltage Source Converter

Chapter 1

INTRODUCTION

1.1 Statement of Problem and Motivation

In the smart grid, the application of Distributed Renewable Energy Resources (DRERs) and Distributed Energy Storage Devices (DESDs) is getting more and more attention. Grid-connected power electronic devices, for instance, the Static VAR Compensator (SVC), Voltage Source Converter (VSC), Static Compensator (STATCOM) and Solid State Transformer (SST), are utilized to integrate DRERs and DESDs into power distribution systems. However, when directly connected to transmission and distribution lines, those solid-state devices might be exposed to voltage surges caused by lightning strikes. For this reason, the insulation coordination of the grid-connected power electronic devices should be studied.

The purpose of insulation coordination is to organize the insulation strength, making it high enough for Metal Oxide Surge Arreser (MOSA) to operate but low enough to be economical. Compared with power circuit components, power electronic devices have very poor over-voltage withstanding capability. Even transient voltages with comparatively small magnitudes could damage these devices. For this reason, it is of great importance to have surge protection and insulation coordination for these power electronic devices. Taking the Insulated Gate Bipolar Transistor (IGBT) as an example [8]. For a 6.5 kV IGBT, its rated current is 250 A. The impulse characteristics of this IGBT are:

$$max\frac{dV}{dt} = 16.25kV/\mu s \tag{1.1}$$

$$max\frac{dI}{dt} = 0.63kA/\mu s \tag{1.2}$$

Based on IEC 61000 [9], for the 60 kV 1.2/50 μs voltage impulse, the voltage increasing rate is:

$$max\frac{dV}{dt} = \frac{60kV}{1.2\mu s} = 50kV/\mu s \tag{1.3}$$

In conclusion, when directly connected to the power distribution system, the power electronic devices need to be protected.

1.2 The Scope of This Research and Objectives

The main focus of this thesis deals with the lightning protection of power electronic devices when they operate in power distribution network. The SST in Future Renewable Electric Energy Delivery and Management (FREEDM) system is taken as an example for analysis. The dynamic performance and protection of typical elements in the FREEDM SST will be studied. Similar simulations will also be done to other directly connected power electronic devices, namely the Voltage Source Converter (VSC).

The FREEDM system is a highly distributed, scalable, automated and flexible power system. The SST is the fundamental component of the FREEDM system. It could manage distributed renewable energy resources (DRERs), distributed energy storage devices (DESDs) and loads, acting as an energy router. Since the SST is directly connected to the power distribution primaries, the SST front filter or the semiconductor components inside the SST might be damaged by the voltage surge caused by lightning strikes. The protection of the SST under lightning strike could be a good example of the insulation coordination of solid state devices when connected directly to the distribution primaries.

According to the IEC 61000 and IEC 60071 [9][10], the SST or other electronic components must be tested by short duration impulse. They must withstand the 1.2/50 μs impulse with a peak value defined by the IEC standards [10]. The peak

value of this impulse is called the Basic Lightning Impulse Insulation Level (BIL). Depending on the rated AC voltage, the BIL could vary. For example, the BIL at 15 kV line-to-line distribution level would be 60 kV instantaneous phase-to-ground.

The standard allows that the tested equipment is protected by MOSAs. The surge arrester is a nonlinear resistance, which has high resistance at the rated AC voltage, but the resistance is reduced by the increasing voltage. This diverts the lightning current to the ground and protects the equipment.

Simulations are conducted to the FREEDM SST under non-operating and operating conditions respectively. To do so, simulations are done in Power Systems Computer Aided Design (PSCAD) software. According to the simulation results, the lightning strike could be harmful to the grid-connected power electronic devices. Installing MOSAs could protect them from the voltage surge caused by power transient and lightning strikes.

1.3 Thesis Outline

Chapter 1 provides a brief introduction including statement of problem, motivation for the research, and the objective of the thesis.

Chapter 2 comprises background literature review related to the application and protection of power electronic devices connected directly to transmission lines, the concept of insulation coordination, and the role the SST plays in the FREEDM system. The set-up, standards and testing method for lightning test is also introduced in Chapter 2.

In Chapter 3, the over-voltage response and protection of typical components in the SST are analyzed when a single-phase SST, in FREEDM system, is stricken by lightning under non-operating conditions.

Chapter 4 deliberates the dynamic performance and insulation coordination of the SST when a single-phase SST, in the FREEDM system, is struck by lightning under operating conditions.

In Chapter 5 similar simulations are done to grid-connected operating VSCs to get more objective results. The robustness of the VSCs are tested under 60 kV 1.2/50 μs over-voltage, and the protection methodology is analyzed for VSC protection.

Chapter 6 includes significant conclusions for the research and discusses future work that can be taken into consideration.

Chapter 2

BACKGROUND LITERATURE REVIEW

2.1 Application of Solid State Devices in Power System

With the development of semiconductor technology, the application of power electronic devices in the power system has gained increasing popularity. Grid-tied power electronic facilities are widely applied in Flexible Alternating Current Transmission Systems (FACTS) because of their excellent dynamic performance. An LCL filter is usually adopted for those facilities to decrease harmonic distortion and to have better dynamic performance [11] [12]. This increases the probability that those grid-connected power electronic devices, like, grid-connected Voltage Source Converters (VSCs), Static VAR Compensators (SVCs), Static Compensators (STATCOMs), and Solid State Transformers (SSTs), might be subjected to voltage surges caused by lightning or circuit switching. The protection provided by the filter capacitor is reasonable but limited [13]. Thus, transient overvoltage is lethal to the LCL front filter or semiconductor components inside the devices.

For these grid-tied power facilities, there are insulation standards which are determined by power system nominal voltages and voltage surges induced by lightning. In order to fulfill the requirements, the MOSAs are used to decrease the voltage strength to protect the power devices. In this chapter, several grid-tied power electronics facilities and the insulation standards are introduced. Furthermore, the mechanism of lightning and MOSA protection methods are also investigated.

2.1.1 Static VAR Compensator (SVC)

SVC is a set of power electronic device connected in shunt with transmission lines to provide reactive power quickly and reliably. It can be a combination of Thyristor Controlled Reactor (TCR), Thyristor Switched Capacitor (TSC), Harmonic filter, Mechanically Switched Capacitor bank (MSC) or Mechanically Switched Reactor bank (MSR). At least one of the elements in the SVC should include thyristors. As indicated in Fig 2.1, it can be operated at inductive or capacitive compensation when it is in the form of TCR or TSC, respectively [14]. The high-power harmonic filters are adopted to eliminate the undesirable harmonics caused by the switches and thyristors.

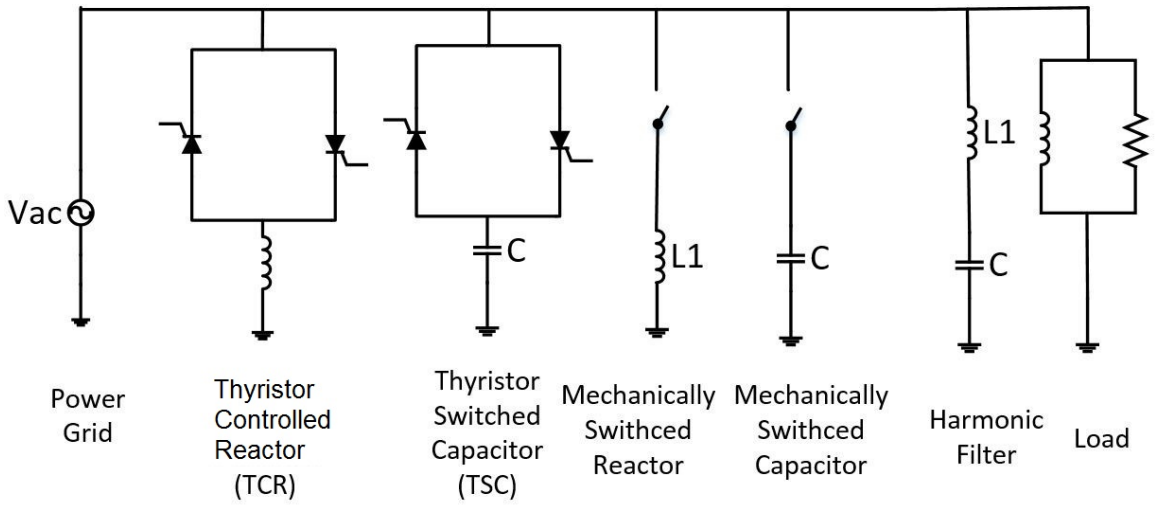

Figure 2.1: Single Phase Diagram of SVC Compensated Power System [3]

SVC is one of the most popular type of FACTS devices to improve power system performance. It could regulate the grid voltage, which is usually influenced by load variation and system operating condition changes [15], and adjust the power factor to unity by dynamically compensating the reactive power in the power grid to avoid voltage collapse in a weak distribution network [16] [17]. It could also improve power system stability, and alleviate power system oscillation by producing supplementary

control signals to the point where voltage is set as certain value [15] [18]. In addition, it helps to transfer power economically, minimize active power loss in the power system, and achieve optimal power flow [3] [19].

2.1.2 Grid-Connected Voltage Source Converter (VSC)

VSC is adopted to convert electric power from direct current (DC) to alternating current (AC) using insulated-gate bipolar transistors (IGBTs). IGBTs give the VSC more controllability. Unlike other converters based on thyristors, IGBTs do not depend on the external AC system to turn it off. For this reason, VSC can have a higher switching frequency and better harmonic performance. It could be more compact in size because it needs less harmonic filtering. Fig 2.2 shows a VSC connected to the grid through an LCL filter.

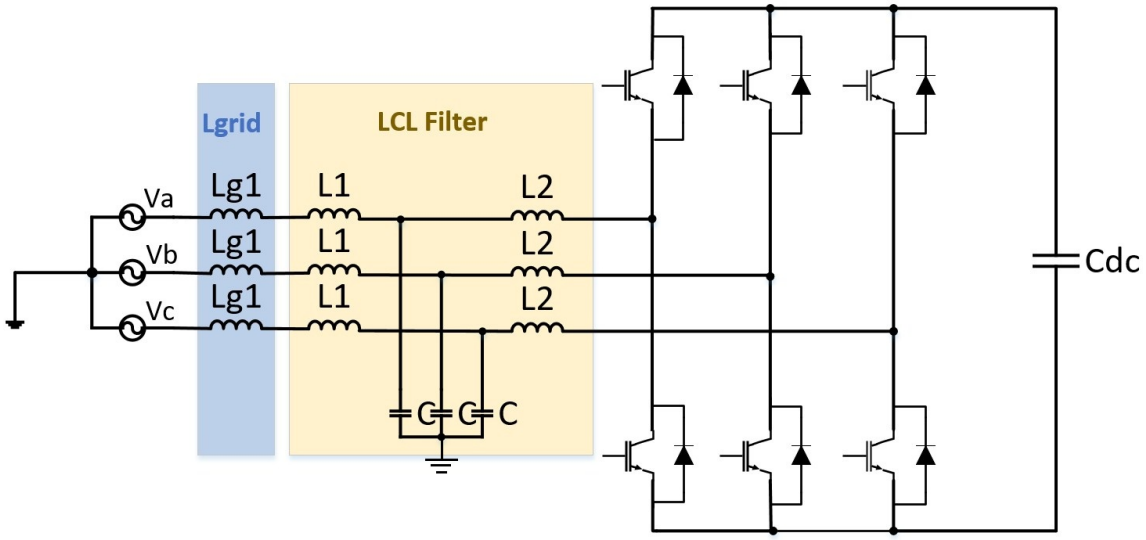

Figure 2.2: A VSC Connected to the Grid Through an LCL Filter [4]

VSC is vital for power system control [20]. Firstly, it could be adopted to interface renewables, such as solar panels, thermoelectric generators and wind turbines, with the distribution network. Also because the fuel cells have low output voltages, a static

converter is needed to increase the source voltage magnitude to match the regulated DC bus [21].

Secondly, VSCs could be used to improve power system stability, regulating active and reactive power delivered to the power grid [22]. For instance, VSC-based Interphase Power Controllers (IPC) are able to control power flow and limit short circuit current [23]. In addition, VSCs could be applied to incorporate Static Series Synchronous Compensators (SSSCs) and Static Synchronous Compensators (STATCOMs) in FACTS to correct power factor and improve power quality [4].

2.1.3 Static Synchronous Compensator (STATCOM)

The STATCOM (also known as a static synchronous condenser, STATCON) is a VSC-based device. Between the VSC and the AC power grid are inductors. On the DC side of a VSC, a capacitor and energy storage device are connected. The electrical structure of STATCOM is shown in Fig 2.3. DC voltage provided by a storage device is converted by VSC into balanced three-phase AC voltage. Reactive power will be injected into the system from STATCOM if voltage at a STATCOM terminal is higher than system voltage; under this condition, STATCOM would behave like a capacitor. Similarly, if the voltage at a STATCOM terminal is lower than the voltage of the power system, the STATCOM would act like an inductor, and reactive power can be absorbed from the power system [24]. Compared with SVC, STATCOM has a shorter response time because the IGBTs in the VSC could switch on and off quickly.

The STATCOM is also one of the core components of FACTS controller used as the shunt compensator to control reactive power in the transmission and distribution system. It is used to provide power system with power factor correction and voltage regulation. STATCOM without a storage system could provide voltage support for the grid, control power flow [25], mitigate power loss [26], suppress harmonic currents

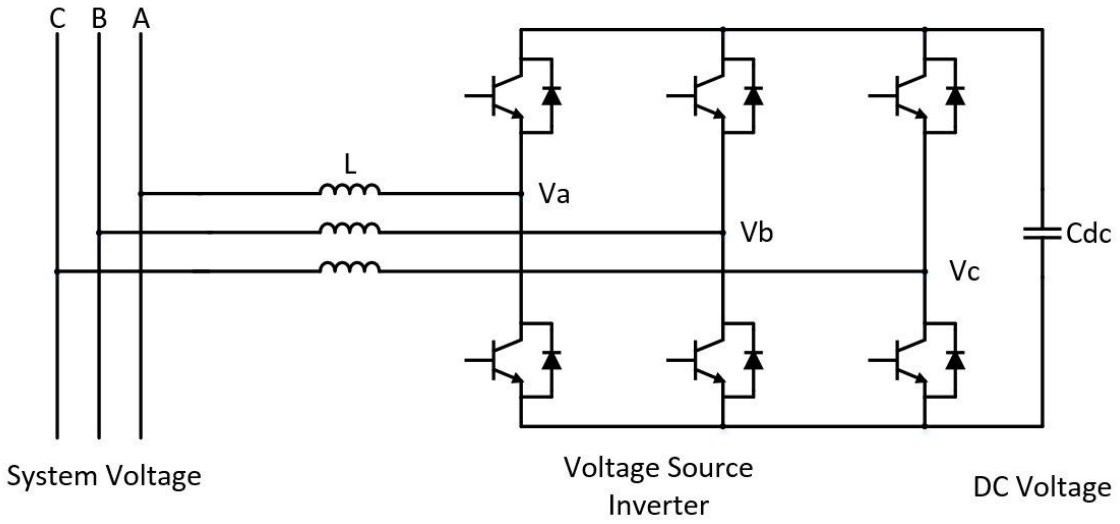

Figure 2.3: Basic Structure of STATCOM [5]

[5], and balance loading. Equipping the STATCOM with a storage system across the DC capacitor could increase its active power capability. In this way, STATCOM could also regulate the power system frequency, improve power quality, correct power factor, and provide uninterruptable power supply (UPS) service [27].

STATCOM is widely used to advance power system stability and improve power system dynamic performance because of its fast speed, small size and wide operation range [5].

2.1.4 Solid State Transformer(SST)

The SST combines power electronics and high frequency technology to reach adjustable power conversion, the FREEDM Gen II SST will be used as an example. The SST consists of three parts, rectifier, Dual-Half-Bridge (DHB) and inverter, as shown in Fig 2.4. The parameters of FREEDM GEN II SST are stated in Table 2.1. L_g, L_f, R_g, R_f, and C_f in Table 2.1 are the inductances, resistances and capacitance in the SST front filter.

The section following the front filter is the high voltage rectifier that converts 3.6

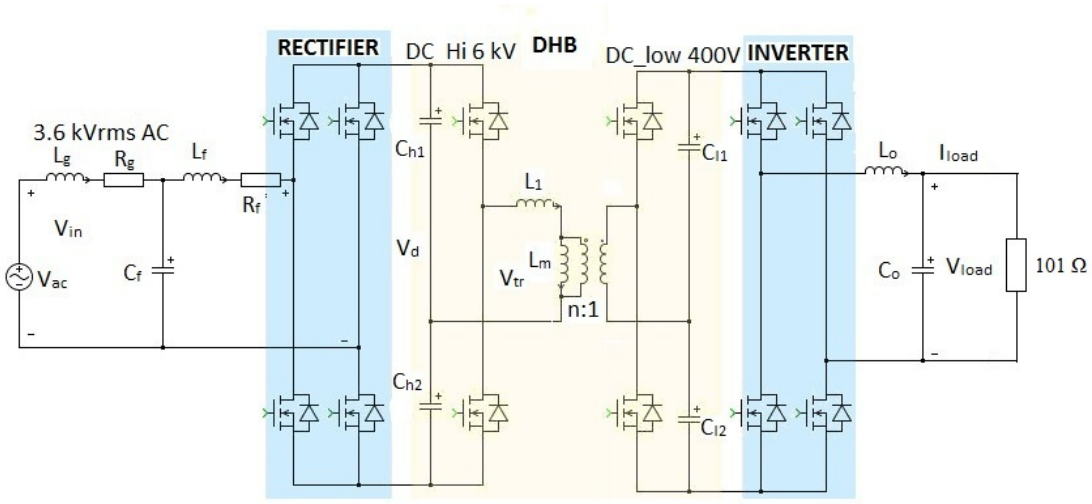

Figure 2.4: Basic Structure of SST [1]

kV_{rms} AC to 6 kV DC voltage. The control of this section regulates grid currents and high voltage DC-link voltage using Pulse Width Modulation (PWM) [1]. The second part is the DHB that transfers 6 kV high DC voltage to 400 V low DC voltage. The high frequency transformer with a turns ratio of 15:1 in the DHB makes it possible for DHB to provide isolation between high and low voltage circuits. On the primary side of transformer in Fig 2.4, L_1 and L_m are leakage inductance and magnetic inductance respectively. Then, the low voltage inverter converts 400 V DC to 120 V_{rms} AC voltage, supplying power on the load side [28] [29].

For the SST front filter, at least one inductance should be working as the filter on the AC side of the rectifier part. If a single inductance is chosen as the filter, the value of the inductance can influence the Total Harmonic Distortion (THD) of the current on the grid side according to the equation below. Systems with lower THD has better power quality, and larger inductance can reduce THD in the system. In the equation, I_1 is the rated RMS value of the line current fundamental component, T_s is the switching time period, V_{dc} is the DC voltage, V_{acpk} is the peak voltage on

Table 2.1: GEN II SST Parameters [1]

Rectifier Parameters			
Grid Voltage RMS	3.6 kV	HV DC Voltage	6 kV
L_g	121.3 mH	R_g	36.87 Ω
L_f	170 mH	R_f	11 Ω
C_f	0.04 μF	Switching Frequency	6 kHz
C_{h1}, C_{h2}	42 μF	Sampling Frequency	12 kHz
DHB Parameters			
L_m	44 mH	C_{f1}, C_{f2}	500 μF
L_f	6.77 mH	Switching Frequency	15 kHz
Turns ratio n:1	15:1	Sampling Frequency	12 kHz
Inverter Parameters			
L_o	1.686 mH	Switching Frequency	10 kHz
C_o	30 μF	Sampling Frequency	20 kHz

AC side,

$$THD = \frac{I_{RMS}}{I_1}\ 100\% \tag{2.1}$$

$$I_{RMS} = \frac{1}{\sqrt{12\pi}}\ T_s\ \frac{V_{dc}}{L}\ \frac{V_{acpk}}{V_{dc}}\ \sqrt{\frac{3\pi}{8}\ (\frac{V_{acpk}}{V_{dc}})^{2} - \frac{8}{3}\ \frac{V_{acpk}}{V_{dc}} + \frac{\pi}{2}} \tag{2.2}$$

For FREEDM GEN II SST, the calculation for inductor L is as follows:

The DC voltage is $V_{dc} = 6$ kV, the RMS AC voltage is $V_{acRMS} = 3.6$ kV. So the peak AC voltage is

$$V_{acpk} = \sqrt{2}\ V_{acRMS} = 5.09\ kV \tag{2.3}$$

The switching frequency of the rectifier part of FREEDM SST is $f_s = 6$ kHz, so the switching time is

$$T_s = \frac{1}{f_s} \tag{2.4}$$

The SST capacity is S = 10 KVA, the rated RMS AC voltage is 3.6 kV, so the

rated RMS value of the line current I_1 is

$$I_1 = \frac{S}{V} = 2.778\ A \tag{2.5}$$

Set THD=6%, then

$$I_{RMS} = I_1\ THD = 0.167\ A \tag{2.6}$$

According to Equation 2.2, the total inductance value is

$$L_T = 328\ mH \tag{2.7}$$

For the FREEDM SST, the front filter is updated from an inductor to an LCL filter. If a single inductance is adopted to decrease current harmonics, the inductance has to be of comparatively high value, which would be very expensive since the capacity of the system is very large. However, the LCL filter has the advantage of smaller inductances and capacitance, faster dynamic response and better performance [30] [31].

For FREEDM GEN II SST, the calculation for LCL filter is as follows:

The base impedance is

$$Z_b = \frac{(V_{acRMS})^2}{S} = 1296\ \Omega \tag{2.8}$$

The power system frequency is f = 60 Hz, so the value of the base capacitance is

$$C_b = \frac{1}{2\pi\ f\ Z_b} = 2.047\ \mu F \tag{2.9}$$

Assume that the capacitor absorbs 2% of the reactive power under the rated condition, set x equals to 2%, so the base capacitance value is adjusted as

$$C_f = x\ C_b = 0.041\ \mu F \tag{2.10}$$

Assume the current ripple is decreased from 36% to 6%, set the desired attenuation as

$$k = \frac{6\%}{36\%} = 0.165 \tag{2.11}$$

The first filter inductor can be calculated as

$$L_g = \frac{\sqrt{\frac{1}{k^2} + 1}}{C_f \ (2 \ \pi \ f_{sw})^2} = 121 \ mH \tag{2.12}$$

The second inductor can be calculated as

$$L_f = L_T - L_g = 197 \ mH \tag{2.13}$$

From the data sheet ASU received as listed in Table 2.1, the values for the inductances and capacitance in SST front filter is $C_f = 0.04$ μF, $L_g = 121.3$ mH, and $L_f = 170$ mH. The calculations above are very closed to the value provided by the data sheet.

The bode plot of the frequency response of the filter with a single inductance and the LCL filter can be plotted in Matlab software is shown in Fig 2.5,

For the 60 kV 1.2/50 μs lightning impulse, according to the bode plot, when at high frequency f = 10 kHz, the magnitude attenuation for L filter is approximately -100 dB, but for LCL filter is around -120 dB. So the LCL filter has better attenuation for high frequency transient.

The SST, enabled by power semiconductor devices, is one promising technology to interconnect Medium Voltage (MV) and Low Voltage (LV) networks, to interface between the generation sources and the main grid, and to manage the end-user and local renewable resources [28]. It could be adopted as an empowering technology for the modernized power distribution system where renewable energy is taking a more and more important role [32]. This power electronic device can act as a potential replacement for the conventional bulk size distribution transformer, particularly in renewable energy applications and smart grids [33].

Compared with traditional low frequency transformer, the SST has significant advantages. It is smaller in size, lighter in weight, and is more environmentally friendly

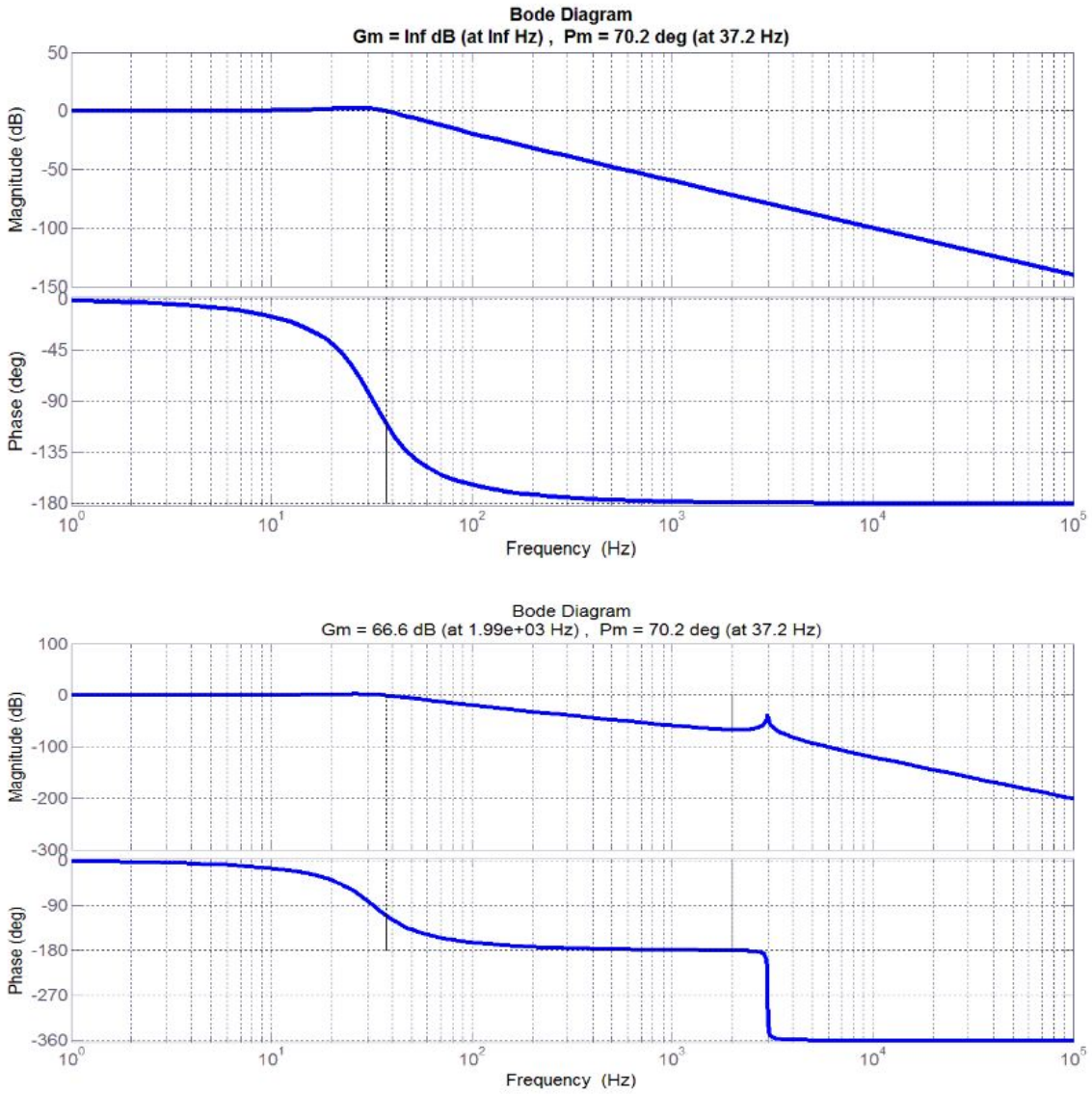

Figure 2.5: L Filter and LCL Filter Frequency Response (a) L Filter Frequency Response (b) LCL Filter Frequency Response

[34]. Most importantly it has the capability to facilitate the operating conditions of the distribution system, regulating voltage on the load side dynamically, controlling reactive power and correcting power factor simultaneously. Besides, it can also achieve isolation, operational efficiency improvement, overload capability increase, and fault current limitation. Therefore, it is beneficial to enhancing power system performance, improving power quality, ensuring domestic power system network flex-

ibility and strengthening power system stability [29].

2.2 Basic Insulation Level (BIL) and Insulation Coordination

In power transmission and distribution networks, insulation is provided to all equipment in the system. In IEEE standard [35], it is stated that insulation coordination is the arrangement of electrical insulation strength to acquire an accepted failure risk when the system is under expected over-voltages. The main purpose of insulation coordination is to protect the system from insulation failure both practically and economically, that is, to provide the system with reliable protection at minimum cost. In order to conduct insulation coordination analysis, the system voltage stresses need to be analyzed first. The over-voltage stress could be evaluated by the maximum crest value, a statistic crest value distribution or a statistic over-voltage value. In addition, the insulation strength should be determined to achieve the required failure rate.

Insulation level of a power system is determined based on its ability to withstand surge voltage caused by lightning. The minimum level of all the components in the system is called basic insulation level. According to IEEE standard [35], Basic Lightning Impulse Insulation Level is usually expressed by the crest value of a standard lightning impulse, representing the electrical strength of the insulation.

IEEE standard [36] addresses Metal-Oxide Surge Arresters (MOSAs) that can suppress voltage surges by allowing surge discharge current to pass through MOSA, so as to protect the power system itself or equipment directly connected to it from harmful over-voltages caused by lightning. The arrester should function below the minimum insulation level in order to protect the system or equipment from surges. The selection of MOSA is also suggested in standard [36] (Appendix A).

This research focuses on the protection of power electronic devices connected di-

rectly to the power system. Different from power circuit components, power electronic devices function at lower power and voltage levels. For this reason, the power electronic devices, when connected directly to the power grid, is very vulnerable when exposed to power transient, for instance, the voltage surge caused by lightning strike. The study of insulation coordination of power electronic devices that connect directly to the power system is of great importance.

2.3 Voltage Surge Caused by Lightning

2.3.1 Lightning Induced Power System Transient

A transient is a sudden voltage or current surge that is generated in or injected to the power system. It could damage the system or any component connected to the system. In [13] it is stated that over-voltage or over-current events contributed to more than 75% of the field failures of the power electronic systems. Over-voltage happens when the system voltage is ten times higher than the nominal rated voltage. It can result in damage to the electrical component or insulation failure of the equipment [37]. Transient over-voltage in power system is mainly caused by power system re-energizing, arcing, short circuiting, capacitor switching and lightning [32] [31]. Since those complicated power electronic devices are extremely vulnerable to voltage surges [13], transient over-voltage caused by lightning is one of the primary concerns of the electrical or electronic components damage in power system.

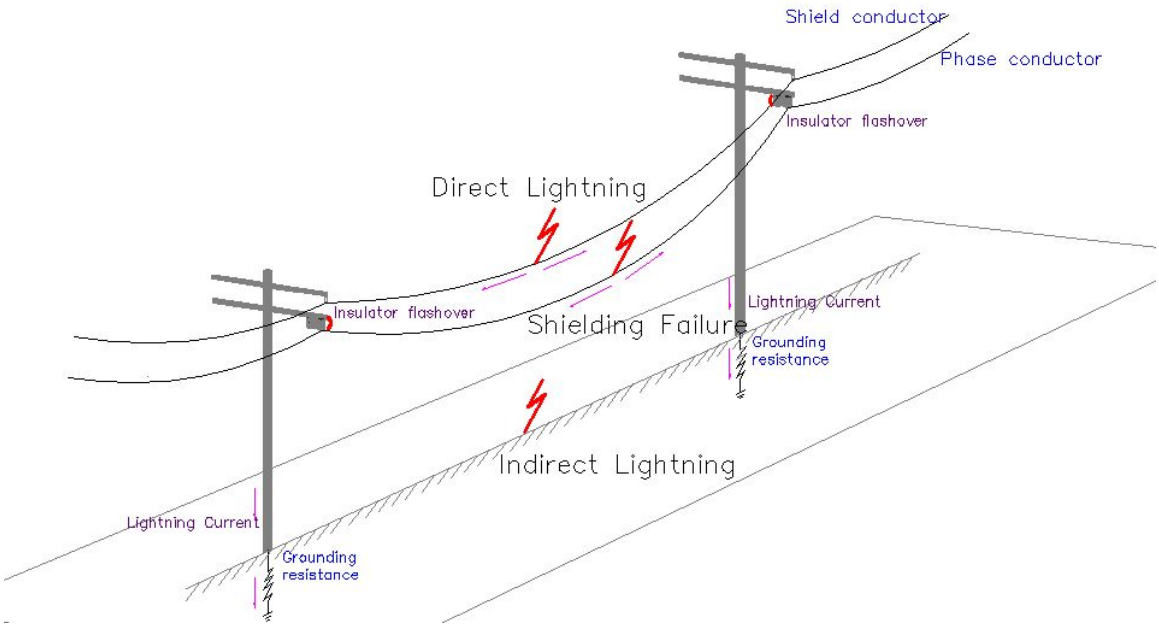

Figure 2.6: Lightning Strike: Insulator Flash-Over, Shielding Failure and Indirect Lightning

Lightning is the electrical discharge between cloud and earth or between clouds. It can cause severe and unpredictable damage to power electronic devices [13]. The frequency of lightning impulse is very high, ranging from tens of kilohertz to several megahertz [38]. Lightning strikes can affect the power system in two ways. One is direct injection, during which the lightning discharge directly from the cloud to the subject component. It is related to the lightning current, energy and heating [39]. As indicated in Fig 2.6, for high voltage power system, grounded shield conductors are placed at the top of the tower to protect transmission lines, the lightning current flows directly to the ground when the lightning hits the shield wire. In this case, when the impulse resistance of the ground is high, the lightning is not able to be discharged, this can cause flash-over on insulators. During shielding failure, the lightning directly hits the phase conductor. The other way that lightning strikes affect the power system is indirect strike, during this event, traveling waves are induced when charged clouds suddenly discharge to earth or other clouds, which is indicated in Fig 2.6. It is related

to induced transient over-voltage in directly connected power electrical and electronic systems. Direct strike is usually the most severe, while indirect strike happens more frequently in the power distribution system [13]. Hence, the voltage surge caused by indirect lightning strike is studied in this research.

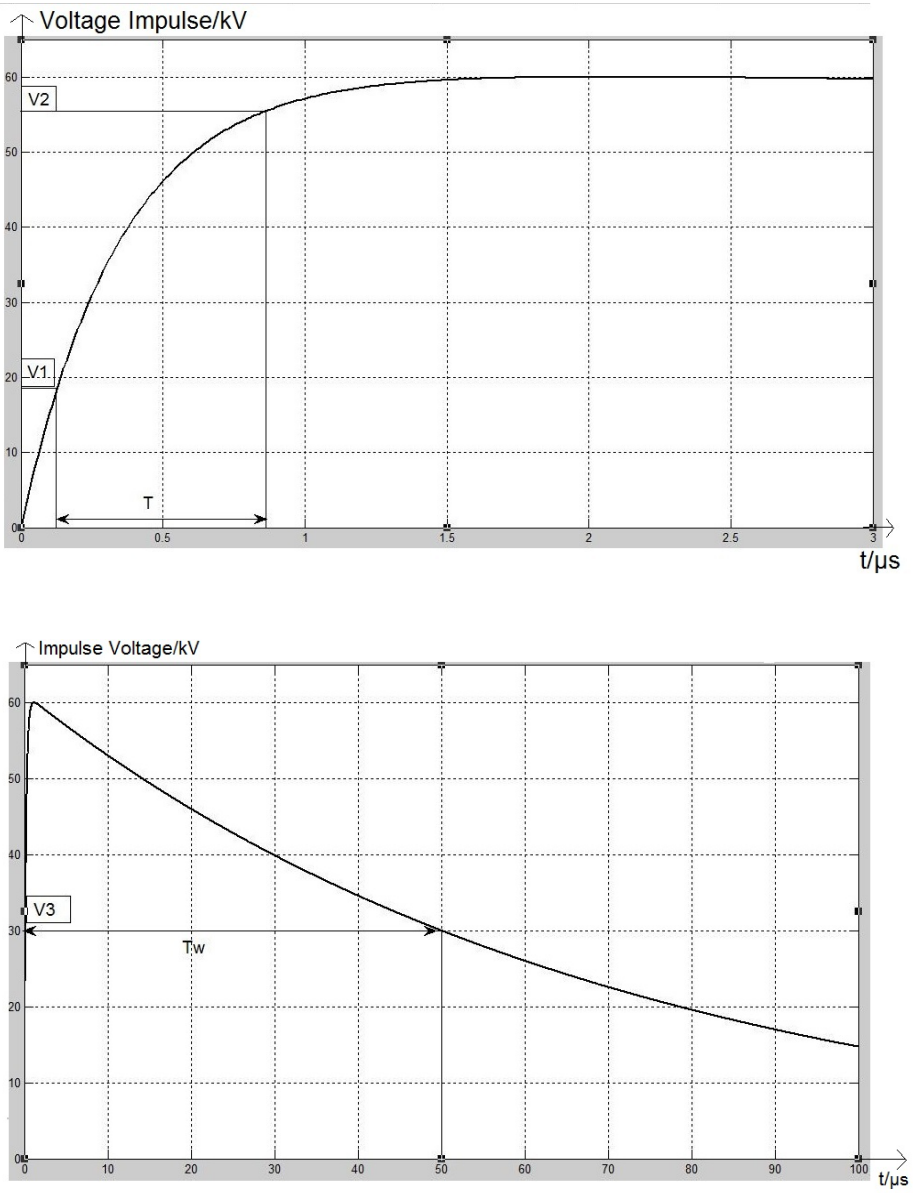

Figure 2.7: 1.2/50 μs Lightning Impulse

The rated voltage for FREEDM system is designed to be 15 kV phase-to-phase, according to IEC 60076 [40], the rated lightning impulse withstand voltage for the

transformer winding is set to be 60 kV. Based on IEC 61000 [9], the standard lightning waveform 60 kV 1.2/50 μs is adopted for this research. This waveform (Fig 2.7) denotes the surge wave that increase to 60 kV (its peak value) in 1.2 μs and drops to 30 kV (half of its peak value) in 50 μs.

In Fig. 2.7, $V_1 = 30\%\ \ V_{peak} = 18$ kV, $V_2 = 90\%\ \ V_{peak} = 54$ kV, $V_3 = 50\%\ \ V_{peak} = 30$ kV. The front time $T_f = 1.67\ \ T = 1.2$ μs, the duration is $T_D = T_W = 50$ μs.

2.3.2 Lightning Protection Using MOSA

Power electronic devices connected directly to the power grid contain semiconductor components which could be jeopardized by voltage surge caused by lightning [41]. Thus, it is necessary to properly select and install Surge Protection Devices (SPDs) to protect those power electronic devices from electrical transient resulted from lightning stroke, to reduce number of failures caused by lightning strike, so as to ensure both the safety of the electronic devices and an uninterrupted power supply [13] [42].

Surge Protection Device (SPD) are the devices that can protect power electronic equipment from electrical transients [43]. Over-voltage suppressors, break-over diodes, and MOSAs could act as protective devices for power electronic equipment and also improve power system reliability [41]. Despite the fact that installing MOSA will cause undesirable energy consumption, the MOSA wins its reputation for small size, high surge current capability and tight voltage regulating ability [13] [44]. It is an economic option for over-voltage protection in this research.

MOSA is a ZnO based voltage dependent semiconductor ceramic device [36]. It works like an insulator at normal voltages, but works as a conductor under high voltages. In this way, it diverts current into the ground and constrain both positive and negative over-voltage [13]. When 10 kA current flows through the MOSA, the voltage

across the MOSA is defined as V10 [45]. Fig 2.8 indicates the V-I characteristics of a 12 kV MOSA, with a V10 of 23.93 kV. Little current flows through the MOSA until the voltage reaches approximately 20 kV. Until then the voltage across the MOSA can be considered the same as the surge voltage. When the voltage across the MOSA is larger than 20 kV, the MOSA diverts current into the ground to restrain voltage surge.

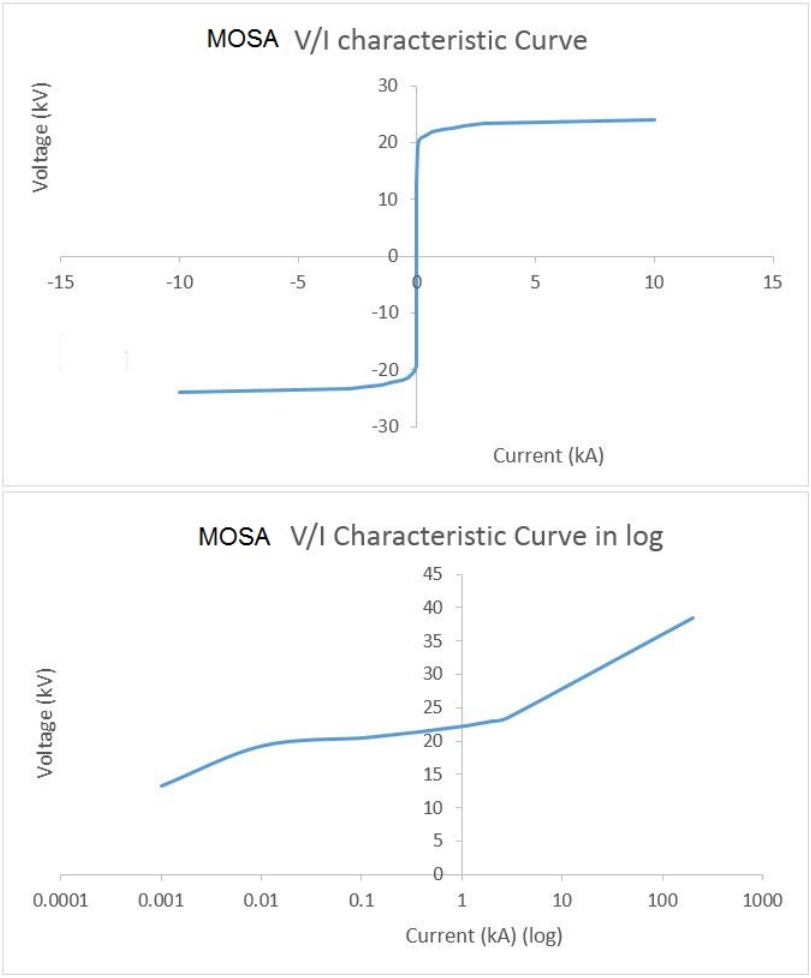

Figure 2.8: MOSA V/I Characteristic Curve

Fig 2.9 describes the MOSA model defined by the IEEE Working Group 3.4.11. The RL filter separates non-linear resistance A0 and A1 into two parts. When slow-front surge occurs, the RL filter has low impedance. In this way, the non-linear

resistance A0 and A1 are connected in parallel. As for fast-front surge, the impedance of RL filter is high, the current flows mostly through non-linear resistance A0 [46] [47].

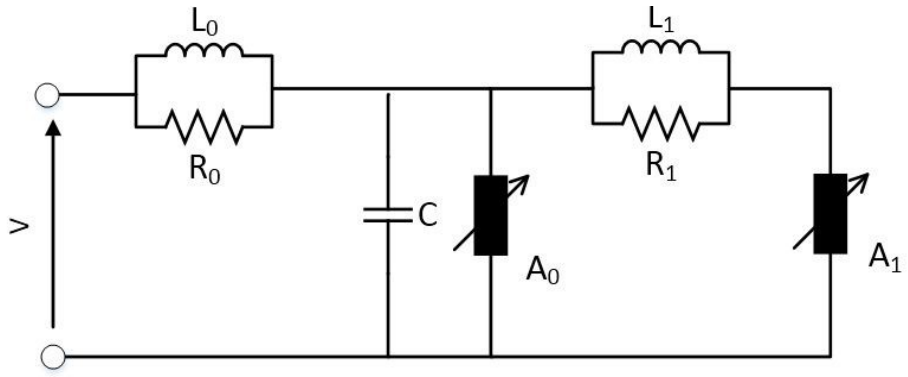

Figure 2.9: MOSA Model Defined by IEEE

2.4 Future Renewable Electric Energy Delivery and Management (FREEDM) System

2.4.1 Future Grid and the FREEDM System

The energy generation depend heavily on fossil fuel that is non-sustainable and not environmentally-friendly. This may lead to many side effects, for instance, the uncertainty of resource supply, the non-renewable essence of the resource and the environmental pollution. Burning the fossil can release carbon dioxide, which is one of the major reason for global warming. In addition, during the combustion, nitrogen dioxide, sulfur dioxide and carbon monoxide could also be released and cause serious air pollution. In order to alleviate these issues, renewable energy resources should be utilized widely and efficiently.

The FREEDM Engineering Research Center (ERC) is sponsored by National Science Foundation (NSF) in 2008 [6], it is consisted of five universities, namely, North Caroline State University, Arizona State University, Florida State University, Missouri

University of Science and Technology, and Florida Agriculture and Technological University. The FREEDM system is an innovative and efficient smart power grid that can integrate highly distributed renewable power generation and storage facilities. This proposed infrastructure enables a sustainable electric power system, which could help to avoid the energy crisis [7]. The FREEDM system structure is shown in Fig 2.10.

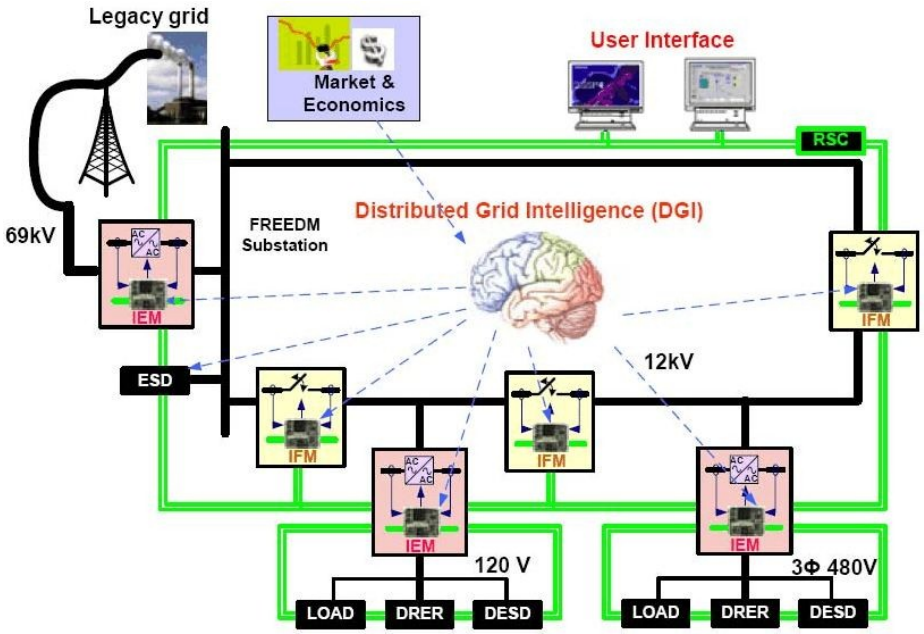

Figure 2.10: FREEDM System Diagram [6]

2.4.2 FREEDM System Structure

The architecture of this FREEDM system could be described as Energy Internet, a network of DRERs that can manage power intelligently using advanced power electronics, communication technology and control system. It is a plug-and-play interface for highly distributed resource generation. It makes possible flexible energy sharing among DRERs (such as solar power and wind power) on the residential side, Distributed Energy Storage Devices (DESDs) and the power distribution grid. The basic objective of the FREEDM system is to automatically manage load, storage

and generation in the power system using power electronics, control and information technology [6].

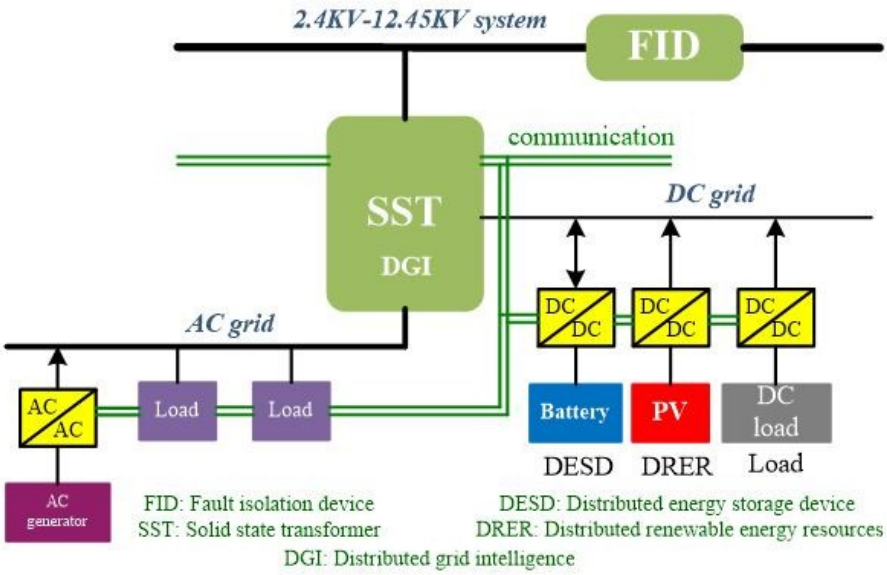

Figure 2.11: FREEDM System Structure [7]

2.4.3 The Role SST Play in the FREEDM System

The 12.47 kV FREEDM loop is a major element of the FREEDM system, it is divided into different parts. SST, together with the communication interface and Distributed Grid Intelligence (DGI) software, form the Industrial Ethernet Module (IEM) node to enable the plug-and-play of large amounts of DRER, DESD and loads, making the FREEDM system compatible and flexible [7].

Previously it was stated that FREEDM system could be described as Internet of Energy, then the SST could be compared to the router in the energy Internet, which is a fundamental part in the FREEDM system. It is a power electronic device that not only performs voltage step-down function like traditional distribution transformer, but could also control both power and energy in the system and respond in very short time, because of the fast switching of the semiconductors inside SST. SST is

also able to isolate the power grid from the harmonics and disturbances from DRER and DESD, making the power system more stable [7]. It could also help to transport high quality electric energy efficiently, supplying reactive power and correct power factor if necessary [48].

2.5 The Lightning Test Set-up

Simulation is done in PSCAD platform in order to evaluate the robustness of the grid-tied power electronic devices when they are under lightning strike, and analyze the proper protection methodology. A 60 kV 1.2/50 μs voltage surge will be applied at the filter front end, the FREEDM GEN II single-phase SST switching model is adopted for simulation. The SST is under non-operating and operating conditions respectively.

Similar simulation is done to grid-tied operating VSC to get more objective results.

Chapter 3

SST ROBUSTNESS TEST AND PROTECTION UNDER NON-OPERATING CONDITION

3.1 Non-Operating SST Robustness Test

In this robustness test, the FREEDM GEN II single-phase SST switching model (Fig 3.1) is adopted for simulation. The SST is under non-operating condition, the control of rectifier, DHB and inverter is not functioning, the grid voltage is set as zero. This simulation is done in PSCAD platform.

Simulation of SST over-voltage response is conducted when the SST front end witnesses a voltage surge of 60 kV 1.2/50 μs, according to IEC standard [10]. The voltage across the front filter components and semiconductors in SST is measured and analyzed when this impulse is applied. MOSA is selected and implemented to protect the semiconductors and the SST front filter from lightning strike.

The voltage impulse is applied at the filter front end at 0.12 s. According to IEC standard [10], the voltage surge due to transmission line direct lightning is simulated, the parameters used for impulse wave shape are: $T_1 = 1.2$ μs, $T_2 = 50$ μs, $V_{peak} = 60$ kV. This wave shape is automatically defined in PSCAD software.

The voltage impulse caused by lightning strike on the grid side mainly affects the front filter, the rectifier and the DHB front part in the SST, the behavior of the semiconductors in DHB front part is the same as the ones in rectifier under lightning strike. Therefore, the voltage and current across inductances and the capacitance in the front filter and semiconductors in the rectifier are simulated and analysed.

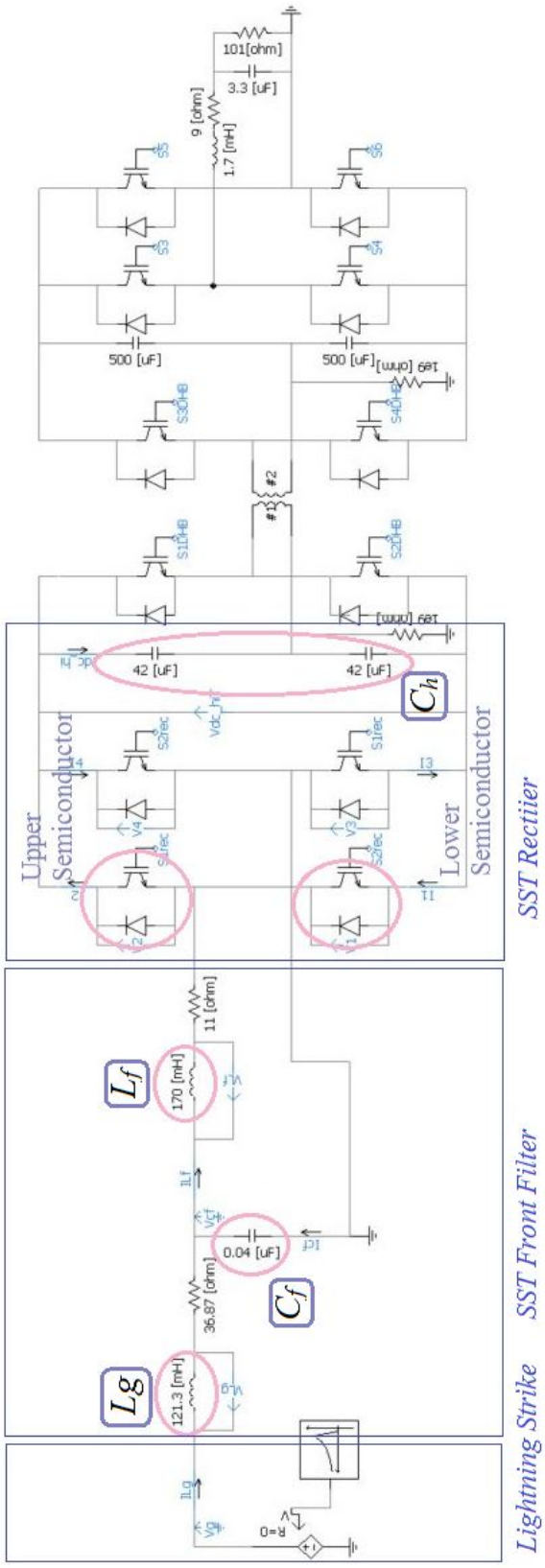

Figure 3.1: Schematic of Non-Operating SST in PSCAD [1]

The increasing rate of the voltage and current across each component is determined by the derivative calculation modules in PSCAD software (Fig 3.2). Take the voltage across the front filter inductance L_g (V_{Lg}) as an example. The voltage across L_g (V_{Lg}) is measured by the voltmeter in Fig 3.1, and the voltage value is put at the input terminal of the derivative module. The value of the increasing rate of the voltage (dV_{Lg}/dt) can be obtained at the output terminal of the derivative module.

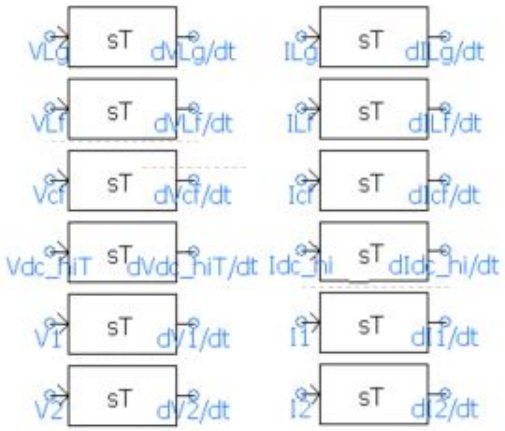

Figure 3.2: The Derivative Modules in PSCAD Software [1]

3.1.1 The Voltage and Current Across Front Filter Inductance L_g

As shown in Fig 3.3, the maximum values and increasing rates of voltage across front filter inductance L_g ($V_{Lg.pk}$) and current through front filter inductance L_g ($I_{Lg.pk}$) are:

maximum voltage across L_g: $V_{Lg.pk} = 57.41$ kV,

maximum increasing rate: max $\frac{dV_{Lg}}{dt} = 0.91$ kV/μs,

maximum current through L_g: $I_{Lg.pk} = 25.71$ A,

maximum increasing rate: max $\frac{dI_{Lg}}{dt} = 0.48$ A/μs.

The magnitudes of the voltage and current surges on L_g are excessive as seen in this case, the insulation of the inductance winding is under risk. The American Wire

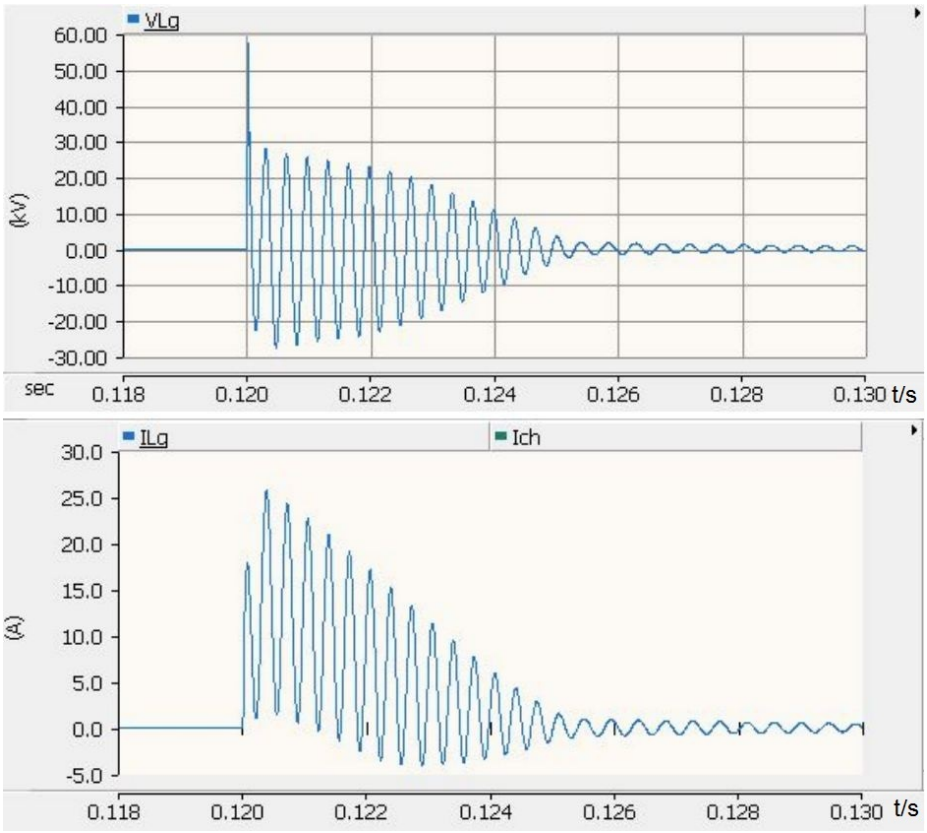

Figure 3.3: V_{Lg} I_{Lg} When Impulse Is Applied

Gauge (AWG) for the inductance winding is chosen as 10 based on the maximum impulse current [49], the maximum voltage it can withstand is 20 kV [50]. However, the peak voltage across the inductance is 57.41 kV, higher than rated. Measures should be taken to protect L_g in the front filter.

3.1.2 The Voltage and Current Across Front Filter Inductance L_f

As shown in Fig 3.4, the maximum values and increasing rates of voltage across front filter inductance L_f (V_{Lf}) and current through front filter inductance L_f (I_{Lf}) are:

maximum voltage across L_f: $V_{Lf.pk} = 31.26$ kV,

maximum increasing rate: max $\frac{dV_{Lf}}{dt} = 2.85$ kV/μs,

maximum current through L_f: $I_{Lf.pk} = 22.56$ A,

maximum increasing rate: max $\frac{dI_{Lf}}{dt} = 0.18$ A/μs.

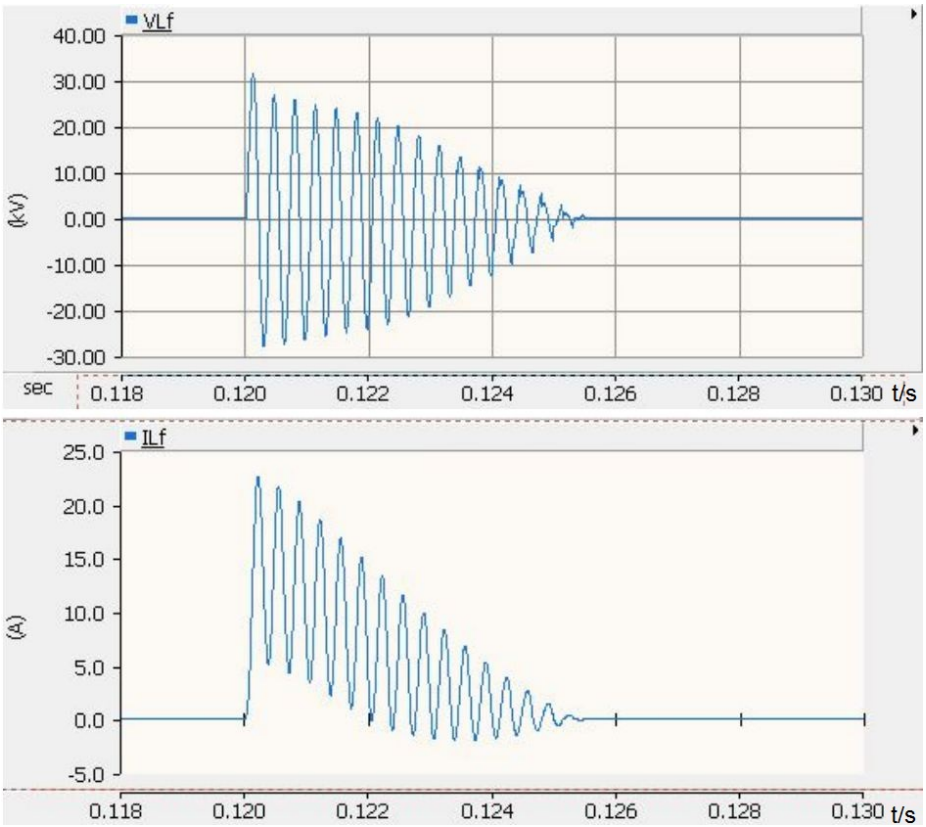

Figure 3.4: V_{Lf} I_{Lf} When Impulse Is Applied

The magnitudes of the voltage and current surges on L_f are excessive as seen in this case, the insulation of the inductance winding is under risk. The AWG for the inductance winding is chosen as 10 based on the maximum impulse current [49], the maximum voltage it can withstand is 20 kV [50]. However, the peak voltage across the inductance is 31.28 kV, higher than rated. Measures should be taken to protect L_f in the front filter.

3.1.3 The Voltage and Current Across Front Filter Capacitance C_f

As shown in Fig 3.5, the maximum values and increasing rates of voltage across front filter capacitance C_f (V_{Cf}) and current through front filter capacitance C_f (I_{Cf}) are:

maximum voltage across C_f: $V_{Cf.pk} = 31.47$ kV,

maximum increasing rate: max $\frac{dV_{Cf}}{dt} = 0.54$ kV/μs,

maximum current through C_f: $I_{Cf.pk} = 21.46$ A,

maximum increasing rate: max $\frac{dI_{Cf}}{dt} = 0.48$ A/μs.

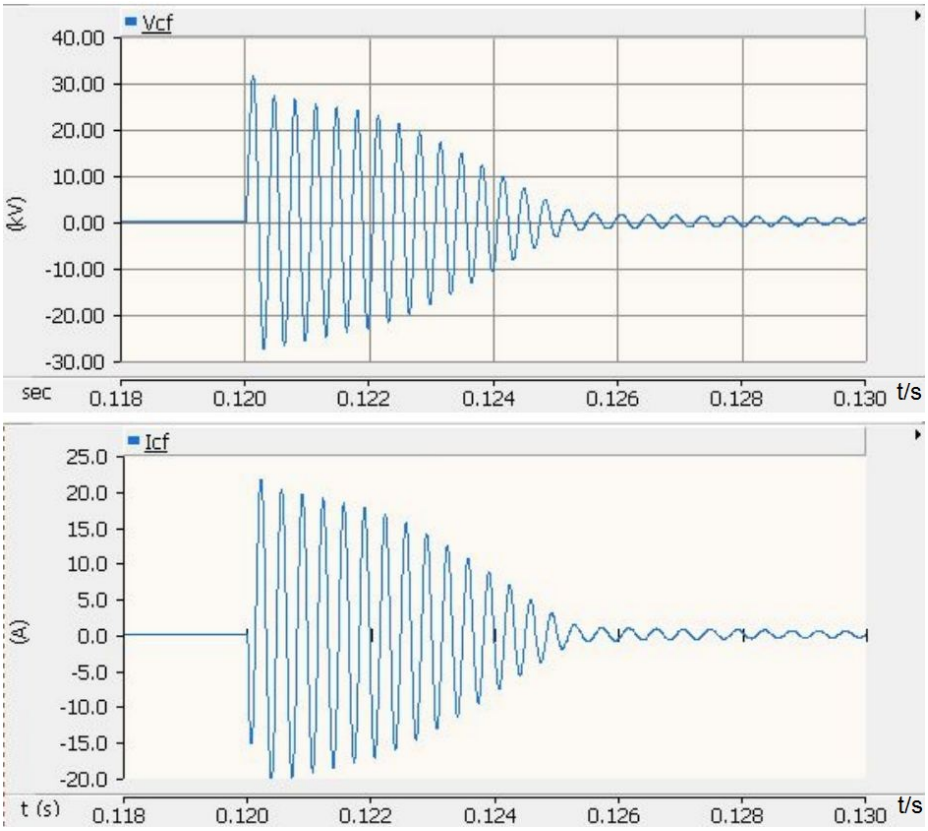

Figure 3.5: V_{Cf} I_{Cf} When Impulse Is Applied

The magnitudes of the voltage and current surges on C_f are excessive as seen in this case. The highest withstanding voltage of a commercial 0.04 F capacitance is 10 kV [51], but the impulse voltage can reach up to 31.37 kV, higher than rated, so the

insulation of the capacitance is under risk. Measures should be taken to protect C_f in the front filter.

3.1.4 The Voltage and Current Across Semiconductors

a. Lower Semiconductor

Fig 3.6 is an example of voltage and current surges on semiconductors in the rectifier. The maximum values and increasing rates of voltage across the lower semiconductor in the rectifier (V_{r1}) and current through lower semiconductor in rectifier (I_{r1}) are:

maximum voltage across lower IGBT: $V_{r1.pk} = 1.54$ kV,

maximum increasing rate: max $\frac{dV_{r1}}{dt} = 1.48$ kV/μs,

maximum current through lower IGBT: $I_{r1.pk} = 1.92$ A,

maximum increasing rate: max $\frac{dI_{r1}}{dt} = 0.07$ A/μs.

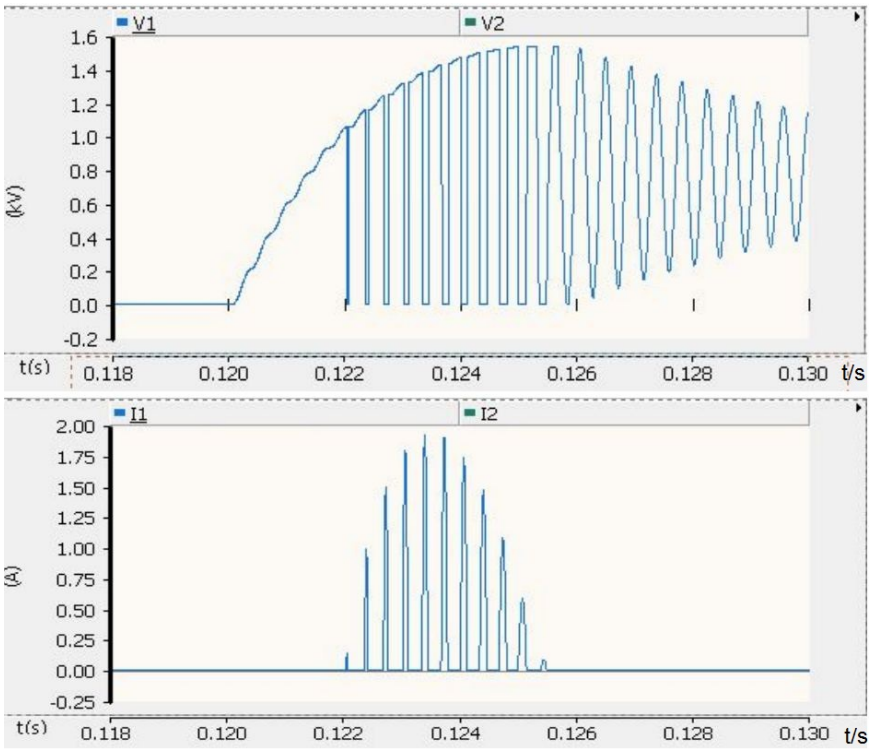

Figure 3.6: V_{r1} I_{r1} When Impulse Is Applied

The shape of V_{r1} waveform can be explained as follows. In PSCAD simulation, when the system is under non-operating condition, the IGBTs are considered open circuit, and the equivalent circuit for the rectifier part could be derived as in Fig 3.7. When the current is going through the diode on upper side, the voltage across D1 is almost zero, and all the impulse voltage is on D3.

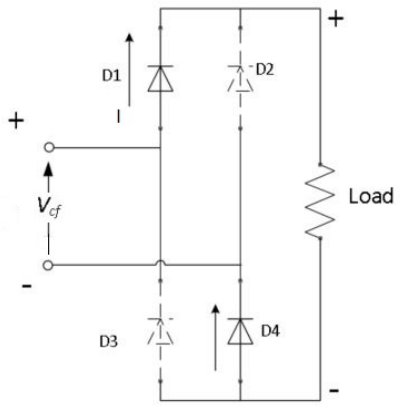

Figure 3.7: Simplified Model to Analyze the Lower Semiconductor

The cut off in V_{r1} is due to the fluctuates of voltage (V_{cf}) on C_f. When V_{cf} crosses zero, the current changes its direction to D2 and D3, causing the voltage drop to zero.

Since the rating of the semiconductors is 6.5 kV, which is much higher than the 1.54 kV maximum over-voltage, and SST will witness larger rising rate when it is under operating condition, the over-voltage and over-current on semiconductors are tolerable. Compared with the impulse characteristics of IGBT in Chapter 1, the maximum increasing rates of voltage and current for 6.5 kV IGBT are 16.25 kV/μs and 0.625 kA/μs, which is much higher than the increasing rates of voltage and current on lower semiconductor. Thus, the increasing rates of voltage and current on lower semiconductor are tolerable.

b. Upper Semiconductor

The maximum values and increasing rates of voltage across upper semiconductor

in rectifier (V_{r2}) and current through upper semiconductor in rectifier (I_{r2}) are:

maximum voltage across lower IGBT: $V_{r2.pk} = 1.54$ kV,

maximum increasing rate: max $\frac{dV_{r2}}{dt} = 1.48$ kV/μs,

maximum current through lower IGBT: $I_{r2.pk} = 22.56$ A,

maximum increasing rate: max $\frac{dI_{r2}}{dt} = 0.18$ A/μs.

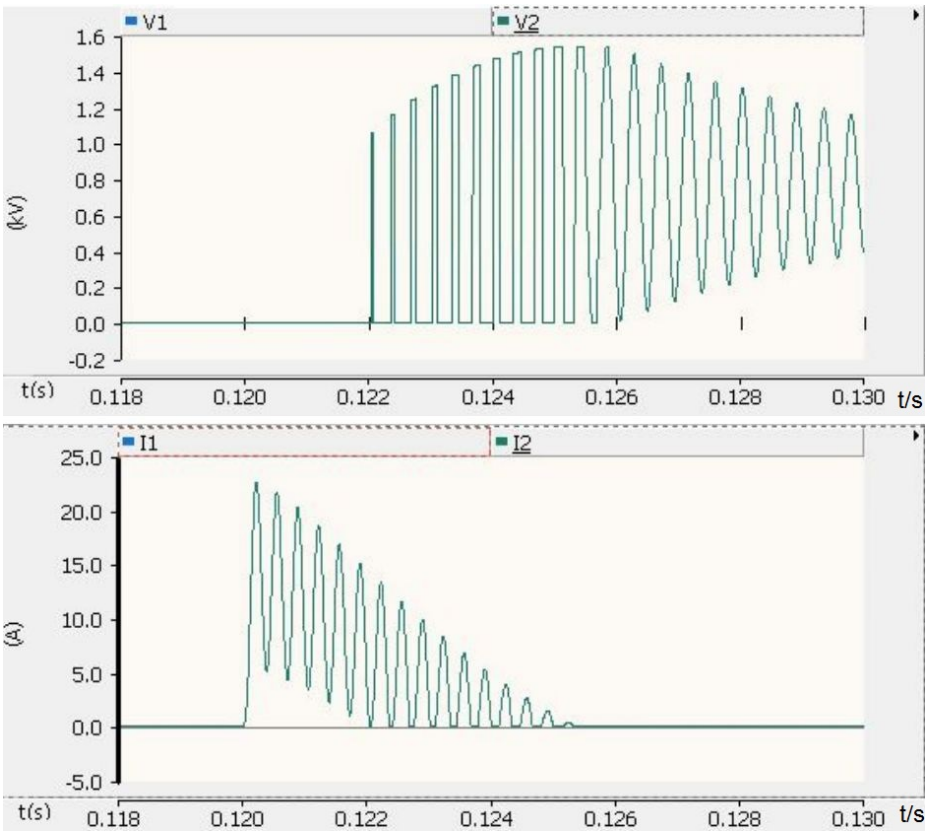

Figure 3.8: V_{r2} I_{r2} When Impulse Is Applied

The shape of V_{r2} waveform can be explained as follows. In PSCAD simulation, when the system is under non-operating condition, the IGBTs are considered open circuit, and equivalent circuit for the rectifier part could be derived as in Fig 3.9. When current is going through the diode on lower side, the voltage across D3 is almost zero, and all the impulse voltage is on D1.

The cut off in V_{r2} is due to the fluctuates of voltage (V_{cf}) on C_f. When V_{cf} crosses

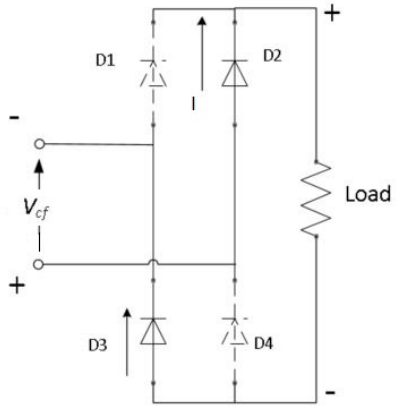

Figure 3.9: Simplified Model to Analyze the Upper Semiconductor

zero, the current changes its direction to D1 and D4, causing the voltage drop to zero.

Since the rating of the semiconductors is 6.5 kV, which is much higher than the 1.54 kV maximum over-voltage, and SST will witness larger rising rate when it is under operating condition, the over-voltage and current on semiconductors are tolerable. Compared with the impulse characteristics of IGBT in Chapter 1, the maximum increasing rates of voltage and current for 6.5 kV IGBT are 16.25 kV/μs and 0.625 kA/μs, which is much higher than the increasing rates of voltage and current on higher semiconductor. Thus, the increasing rates of voltage and current on higher semiconductor are tolerable.

3.1.5 The Voltage and Current Across Capacitance C_h

As shown in Fig 3.10, the maximum values and increasing rates of voltage across capacitance C_h ($V_{dc.hi}$) and current through capacitance C_h ($I_{dc.hi}$) are,

maximum voltage across C_h: $V_{dc.hi.pk} = 1.54$ kV,

maximum increasing rate: max $\frac{dV_{dc.hi}}{dt} = 1.07$ V/μs,

maximum current through C_h: $I_{dc.hi.pk} = 22.56$ A,

maximum increasing rate: max $\frac{dI_{dc.hi}}{dt} = 0.18$ A/μs.

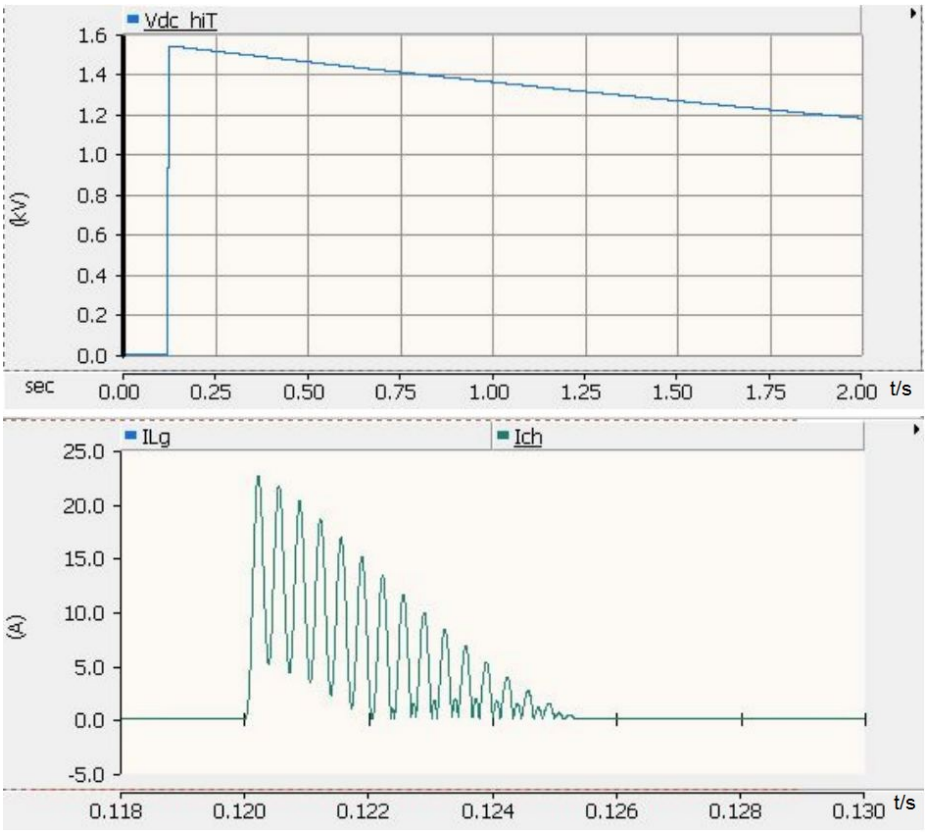

Figure 3.10: $V_{dc.hi}$ $I_{dc.hi}$ When Impulse Is Applied

Under operating condition, the voltage across this DC capacitance is higher than 6 kV. Now the over-voltage on capacitance C_h is 1.54 kV, so the over-voltage on capacitance C_h is tolerable in this design.

3.1.6 The Voltage and Current Across Capacitance C_l

As shown in Fig 3.11, the maximum values of voltage across capacitance C_l ($V_{dc.lo}$) and current through capacitance C_l ($I_{dc.lo}$) are,

maximum voltage across C_l: $V_{dc.lo.pk} = 5.42 * 10^{-9}$ V,

maximum current through C_l: $I_{dc.lo.pk} = 7.35 * 10^{-10}$ A,

Therefore, the lightning has little effect on the components after the high frequency transformer.

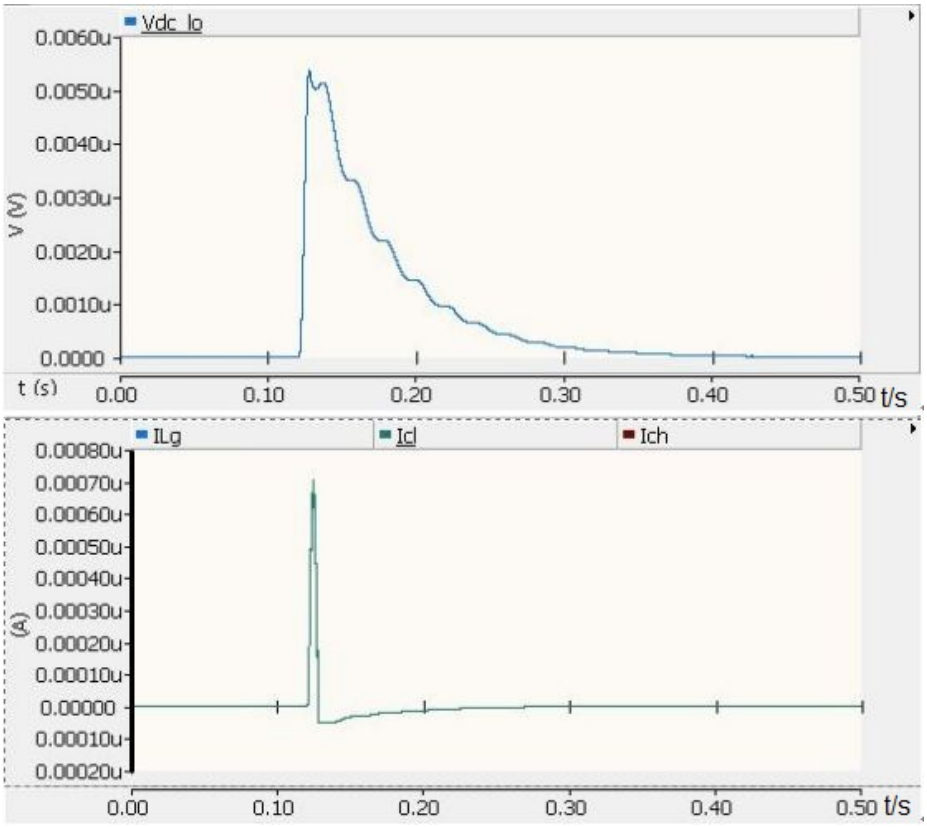

Figure 3.11: $V_{dc.lo}$ $I_{dc.lo}$ When Impulse Is Applied

3.1.7 Conclusions

Lightning impulse could cause unacceptable high voltage surges across filter inductances and capacitance in the SST. Under 60 kV 1.2/50 μs lightning voltage surge, the maximum voltage on L_g reaches 57.41 kV, and the maximum voltage on L_f reaches 31.28 kV, much higher than the rated 20 kV. The maximum over-voltage across C_f can reach up to 31.37 kV, much larger than the rated 10 kV. The over-voltage and over-current on semiconductors in SST rectifier are tolerable. The components after the high frequency transformer are barely affected. Accordingly, the components in the SST front filter need to be protected.

3.2 Improvement of the Non-Operating SST Front Filter

According to the simulation results, the lightning impulse could damage the FREEDM SST. Thus, MOSAs are implemented to protect the SST and the SST front filter is improved.

For the lightning protection of non-operating SST, as shown in Fig 3.13, a surge arrester is placed in parallel with the capacitance C_f in the front filter to protect C_f, L_f and semiconductors from the voltage surge. The filter inductances are designed as three inductances connected in series, since the maximum voltage the inductance winding can withstand is 20 kV [50] [49], and the total voltage impulse is 57.41 kV. Same topology is applied for front filter inductance L_f.

According to Fig 3.12, the energy consumed by the MOSA is

$$Q = P \times t = 147.48\ kW \times 0.0004\ s = 0.059\ kJ \tag{3.1}$$

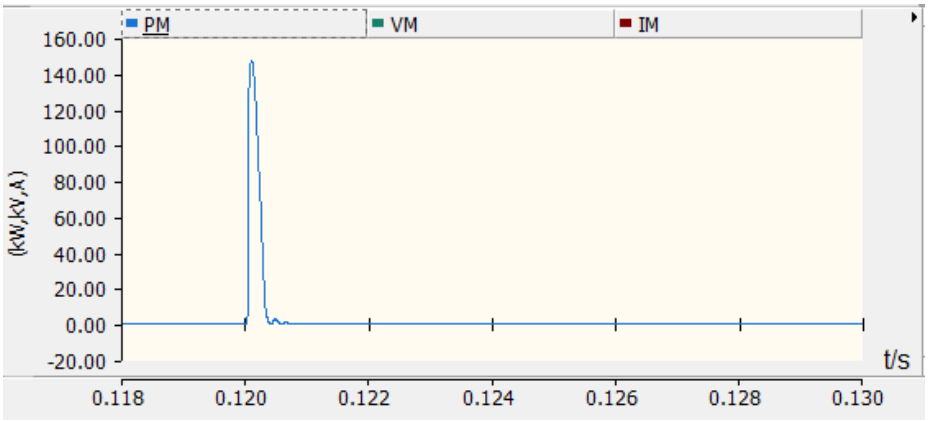

Figure 3.12: Energy Consumed by MOSA When Impulse Is Applied

Since AC voltage on the filter front terminal is set as 3.6 kVrms, the peak AC voltage is

$$V_{acpk} = \sqrt{2} \times 3.6 = 5.1\ kV \tag{3.2}$$

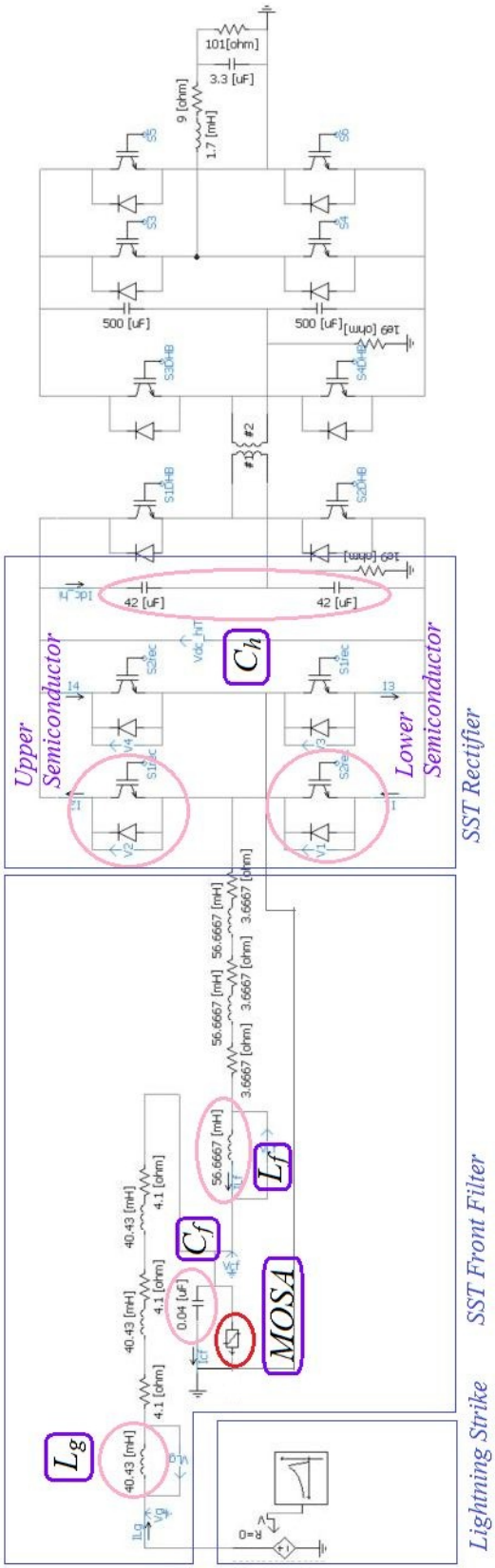

Figure 3.13: Protection of the Non-Operating SST Front Filter in PSCAD [1]

The rating for MOSA is selected as 5.1 kV. Similar result is indicated according to the ANSI standard (Appendix A). During the simulation, the voltage impulse is applied at the filter front end at 0.12s.

Table 3.1 compares the performance of non-operating SST before and after the front filter improvement. The reduction ratio is calculated using equation 3.3.

$$\text{Reduction Ratio} = \frac{\text{Value without MOSA} - \text{Value with MOSA}}{\text{Value without MOSA}} * 100\% \qquad (3.3)$$

Table 3.1: Performance of SST Before and After the Front Filter Improvement

Model Property	With MOSAs	MOSAs	
		Value	Reduction Ratio (%)
$V_{Lg.pk}$/kV	57.41	19.98	60.20
$I_{Lg.pk}$/A	25.71	22.15	13.85
$V_{Lf.pk}$/kV	31.26	2.73	91.27
$I_{Lf.pk}$/A	22.56	14.97	33.64
$V_{Cf.pk}$/kV	31.47	8.21	73.91
$I_{Cf.pk}$/A	21.46	11.46	46.60
$V_{r1.pk}$/kV	1.54	1.25	18.83
$I_{r1.pk}$/A	1.92	0.00	100.00
$V_{r2.pk}$/kV	1.54	0.78	49.35
$I_{r2.pk}$/A	22.56	14.97	33.64
$V_{dc.hi.pk}$/kV	1.54	1.25	18.83
$I_{dc.hi.pk}$/A	22.56	14.97	33.64

3.2.1 *The Voltage and Current Across Front Filter Inductance L_g*

The voltage surge on the front filter inductance L_g is reduced from 57.41 kV to 19.98 kV, current surge drops from 25.71 A to 22.15 A. Over-voltage on L_g caused by lightning strike is significantly reduced. Oscillations of voltage and current are both reduced. Since the maximum voltage the inductance winding can withstand is 20 kV [50][49], the front filter inductance L_g is well protected.

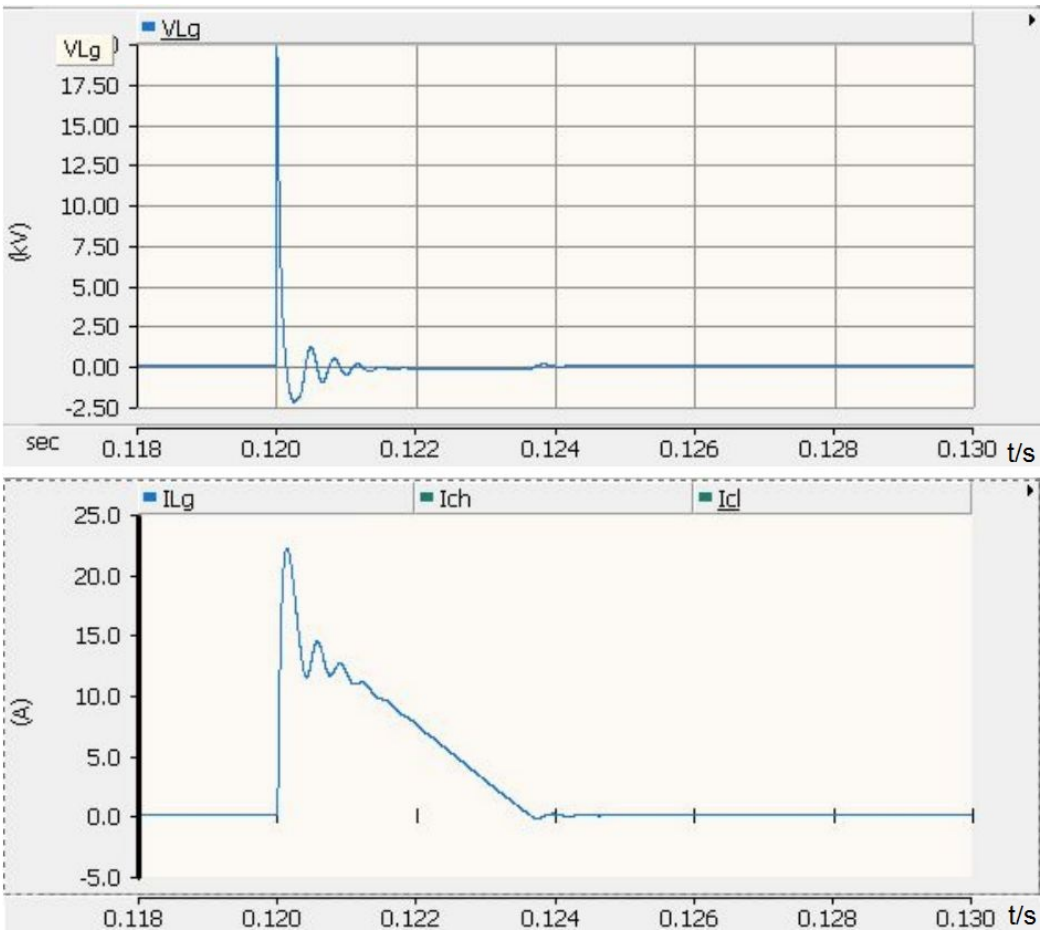

Figure 3.14: V_{Lg} I_{Lg} After the Filter Improvement

3.2.2 *The Voltage and Current Across Front Filter Inductance L_f*

The voltage surge on the front filter inductance L_f is reduced from 31.26 kV to 2.73 kV, current surge drops from 22.56 A to 14.97 A. Over-voltage on L_f caused by lightning strike is significantly reduced. Oscillations of voltage and current are both reduced. Since the maximum voltage the inductance winding can withstand is 20 kV [50][49], the front filter inductance L_f is well protected.

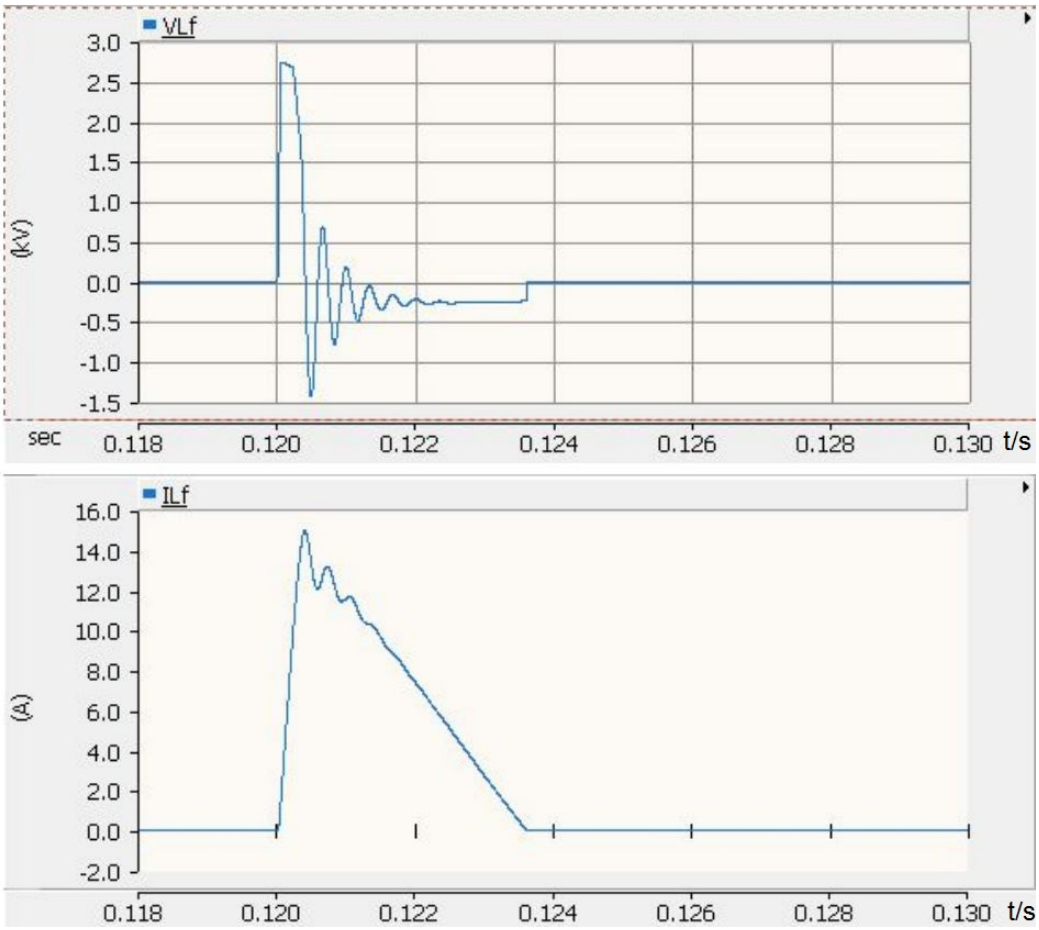

Figure 3.15: V_{Lf} I_{Lf} After the Filter Improvement

3.2.3 The Voltage Across Front Filter Capacitance C_f

The voltage surge on the front filter capacitance C_f is reduced from 31.47 kV to 8.21 kV, current surge drops from 21.46 A to 11.46 A. Over-voltage on C_f caused by lightning strike is significantly reduced. Oscillations of voltage and current are both reduced. The highest withstanding voltage of a commercial 0.04 μF capacitance is 10 kV [51]. Thus the front filter capacitance C_f is well protected.

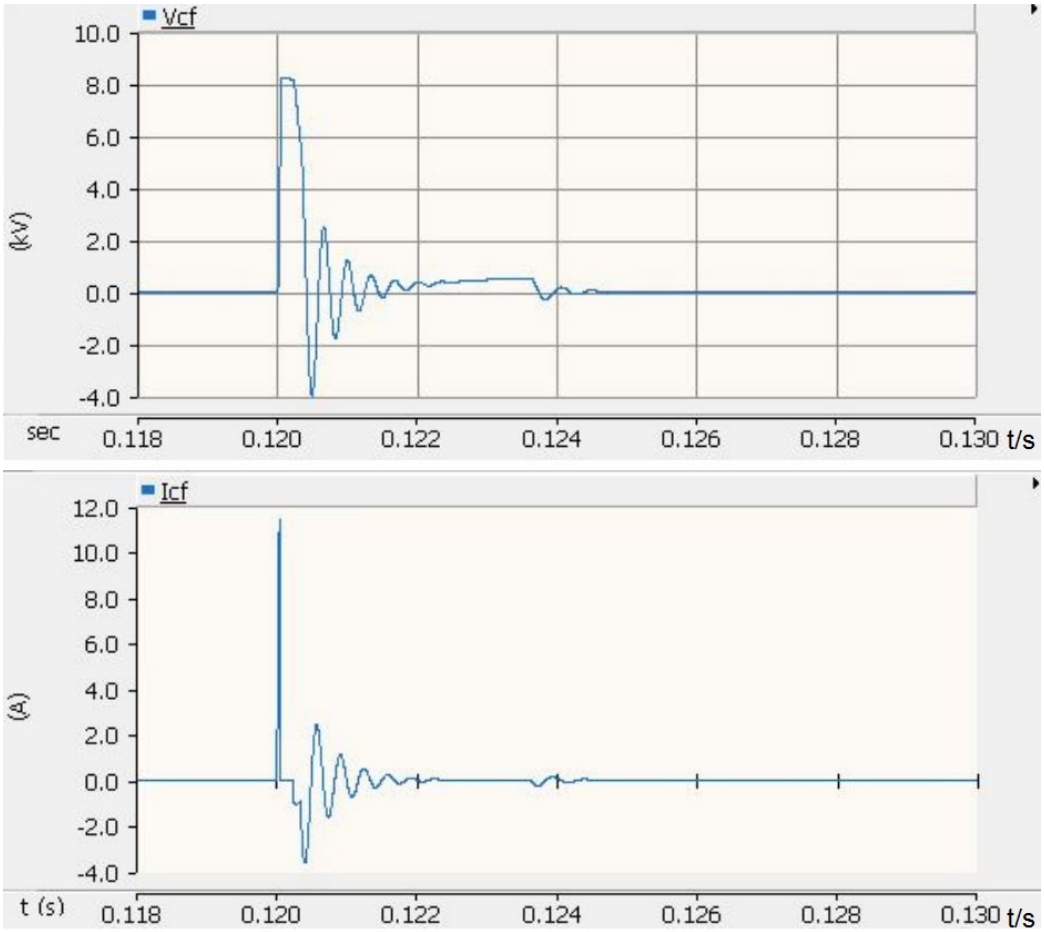

Figure 3.16: V_{Cf} I_{Cf} After the Filter Improvement

3.2.4 The Voltage and Current Across Semiconductors

a. Lower Semiconductor

The voltage surge on the lower semiconductor is reduced from 1.54 kV to 1.25 kV, current surge drops from 1.92 A to $2.50 * 10^{-3}$ A. Oscillation of voltage is reduced.

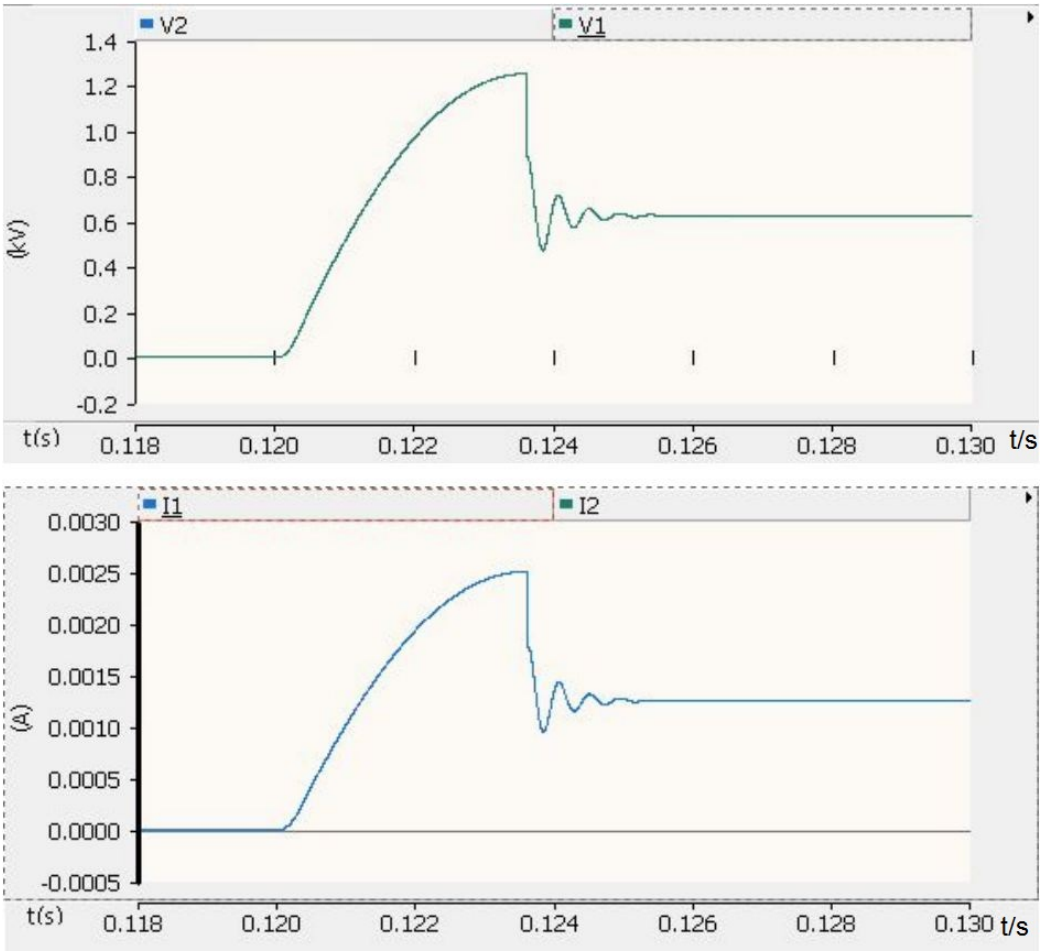

Figure 3.17: V_{r1} I_{r1} After the Filter Improvement

b. Upper Semiconductor

The voltage surge on the upper semiconductor is reduced from 1.54 kV to 0.78 kV, current surge drops from 22.56 A to 14.97 A.

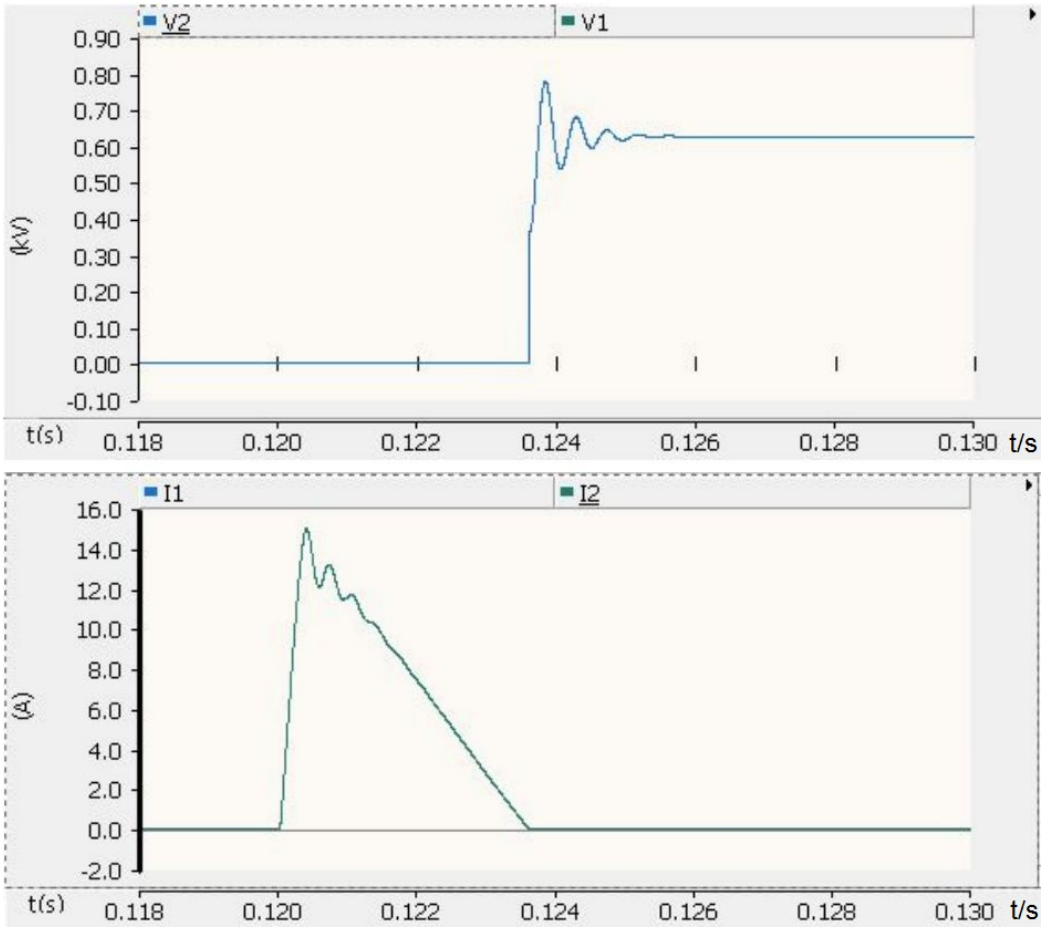

Figure 3.18: V_{r2} I_{r2} After the Filter Improvement

3.2.5 The Voltage and Current Across Capacitance C_h

The voltage surge on capacitance C_h is reduced from 1.54 kV to 1.25 kV, current surge drops from 22.56 A to 14.97 A.

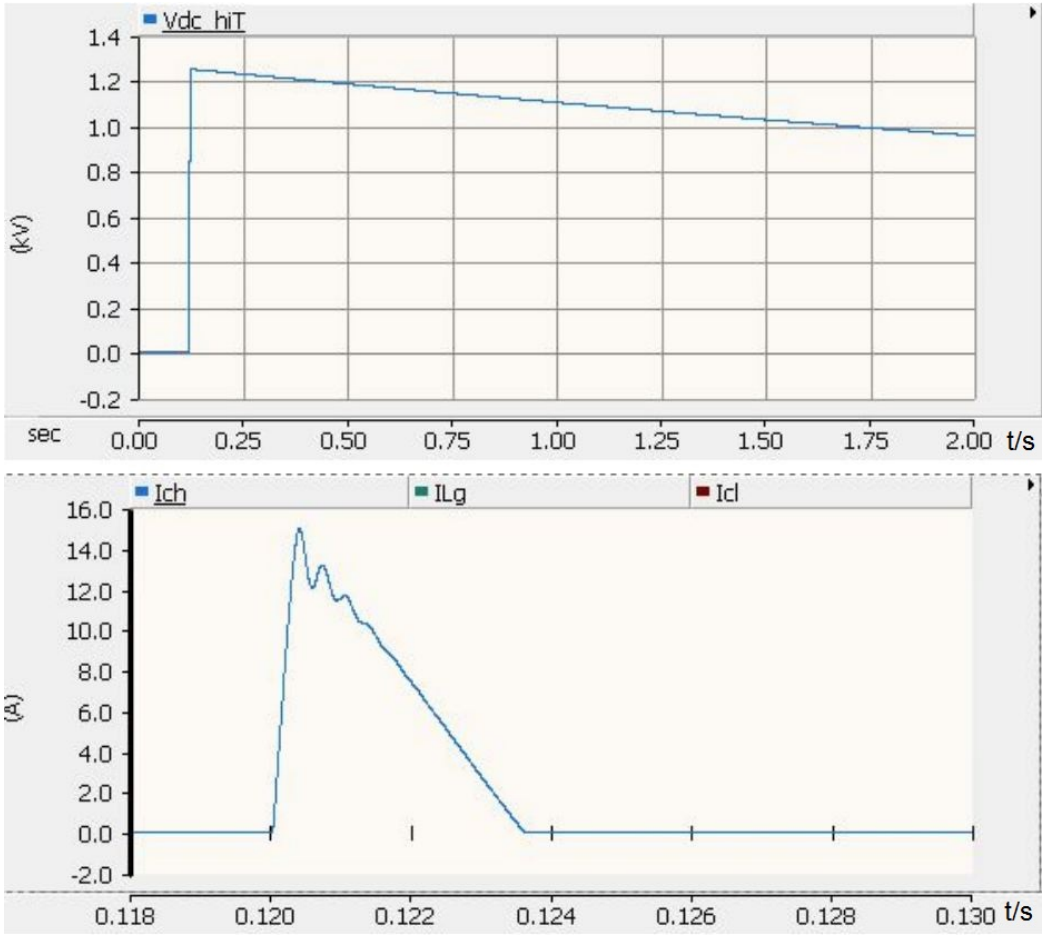

Figure 3.19: $V_{dc.hi}$ $I_{dc.hi}$ After the Filter Improvement

3.2.6 Conclusions

It can be seen in the table and figures that the surge arrester has effects on over-voltage and over-current protection if lightning happens, reducing the amplitudes of voltage and current surges on L_g, L_f and C_f by almost 90%.

Chapter 4

SST ROBUSTNESS TEST AND PROTECTION UNDER OPERATING CONDITION

4.1 Operating SST Robustness Test

In this test, the SST is under operating condition, the control of the rectifier, DHB and inverter is functioning. The grid voltage is set as 3.6 kVrms. Assuming the equation for the sine wave is:

$$V_{ac} = 3.6\ sin(2\ \pi\ 60 + \alpha)kV \tag{4.1}$$

When the 60 kV 1.2/50 μs voltage impulse is applied at $\alpha = 0^{\circ}$, 90°, 270°, the impulse and sinusoidal AC supply voltage is shown in Fig 4.1. According to equation 2.3, the peak AC voltage on the filter front terminal is $V_{acpk} = 5.1$ kV, so

$$\frac{V_{acpk}}{V_{Lightning}} = \frac{5.1kV}{60kV} = 8.5\% \tag{4.2}$$

Compared with lightning voltage surge, the effect of grid voltage can be neglected. Accordingly, the value of α (where the voltage surge is applied) has little effect on the simulation results. Therefore, the voltage impulse is applied at filter front end at 0.12 s during the analysis, when $\alpha = 90^{\circ}$, and the grid voltage has maximum positive value. Fig 4.2 is the schematic of operating SST in PSCAD.

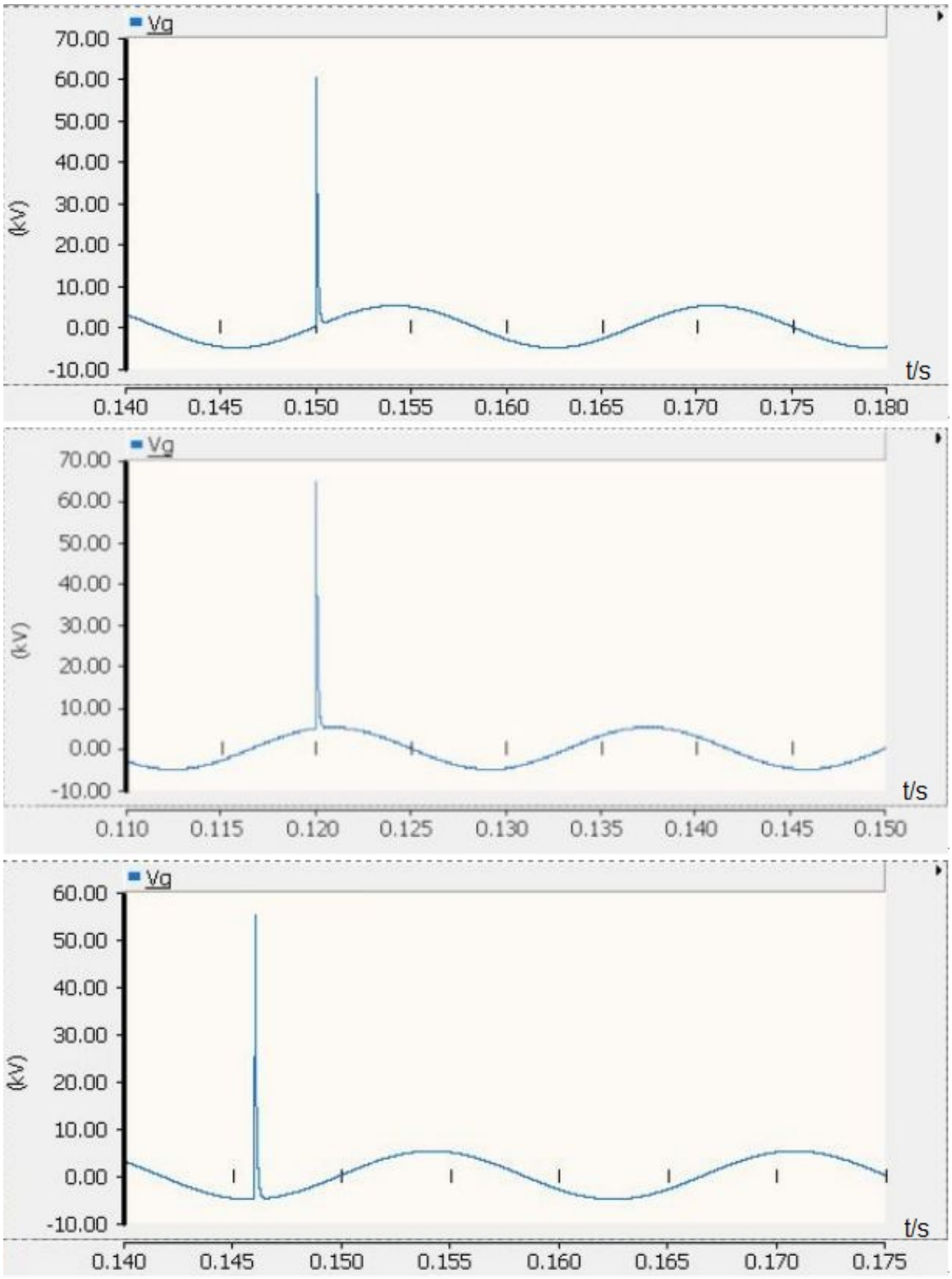

Figure 4.1: The Impulse and Sinusoidal AC Supply Voltage When the Voltage Impulse Is Applied at $\alpha = 0^{\circ}$, 90°, 270° Respectively

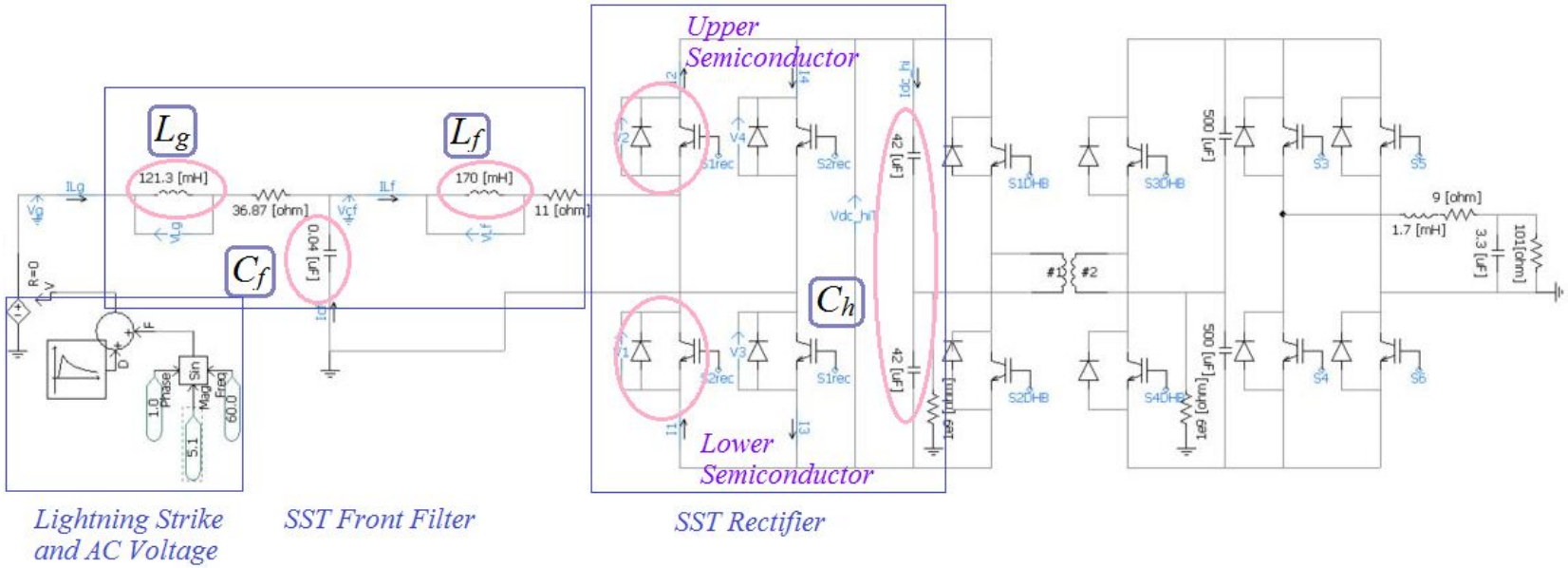

Figure 4.2: Schematic of Operating SST in PSCAD [1]

4.1.1 The Voltage and Current Across Front Filter Inductance L_g

As shown in Fig 4.3, the maximum values and increasing rates of voltage across front filter inductance L_g ($V_{Lg.pk}$) and current through front filter inductance L_g ($I_{Lg.pk}$) are:

maximum voltage across L_g: $V_{Lg.pk} = 60.23$ kV,

maximum increasing rate: max $\frac{dV_{Lg}}{dt} = 0.91$ kV/μs,

maximum current through L_g: $I_{Lg.pk} = 34.42$ A,

maximum increasing rate: max $\frac{dI_{Lg}}{dt} = 0.50$ A/μs.

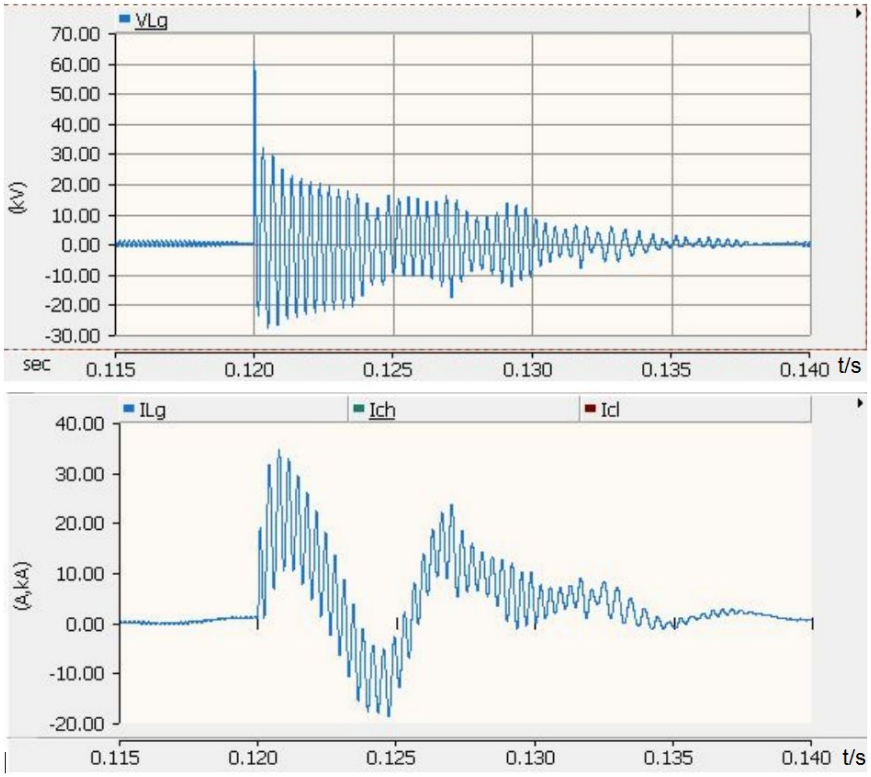

Figure 4.3: V_{Lg} I_{Lg} When Impulse Is Applied

The magnitudes of the voltage and current surges on L_g are excessive as seen in this case, the insulation of the inductance winding is under risk. The AWG for the inductance winding is chosen as 10 based on the maximum impulse current [49], the maximum voltage it can withstand is 20 kV [50]. However, the peak voltage across

the inductance is 60.23 kV, higher than rated. Measures should be taken to protect L_g in the front filter.

4.1.2 The Voltage and Current Across Front Filter Inductance L_f

As shown in Fig 4.4, the maximum values and increasing rates of voltage across front filter inductance L_f (V_{Lf}) and current through front filter inductance L_f (I_{Lf}) are:

maximum voltage across L_f: $V_{Lf.pk} = 31.24$ kV,

maximum increasing rate: max $\frac{dV_{Lf}}{dt} = 141.52$ kV/μs,

maximum current through L_f: $I_{Lf.pk} = 29.78$ A,

maximum increasing rate: max $\frac{dI_{Lf}}{dt} = 0.18$ A/μs.

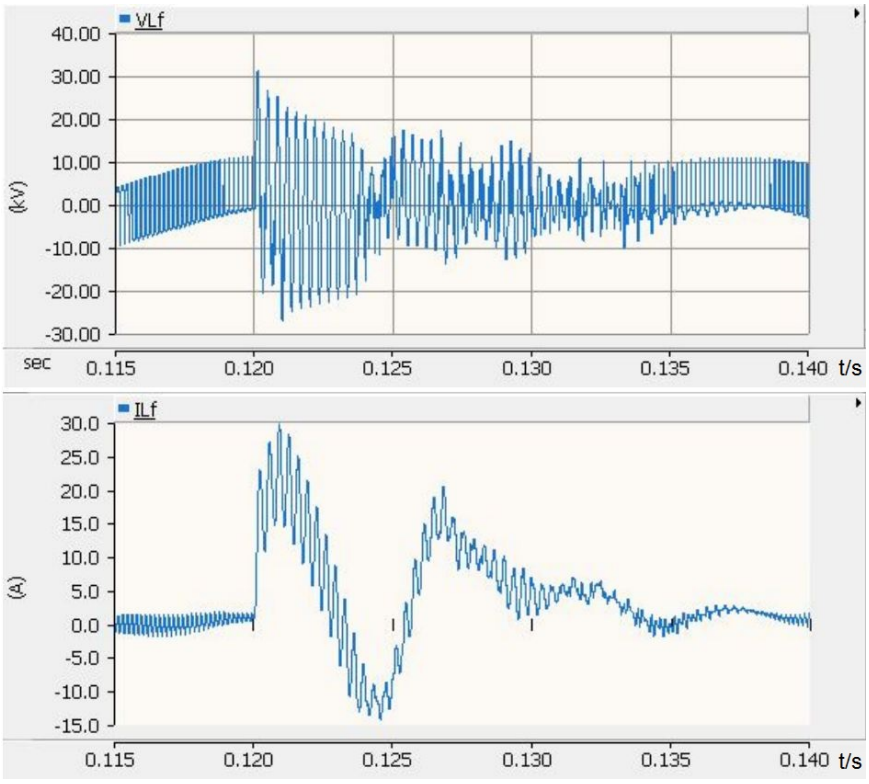

Figure 4.4: V_{Lf} I_{Lf} When Impulse Is Applied

The magnitudes of the voltage and current surges on L_f are excessive as seen in this case, the insulation of the inductance winding is under risk. The AWG for the inductance winding is chosen as 10 based on the maximum impulse current [49], the maximum voltage it can withstand is 20 kV [50]. However, the peak voltage across the inductance is 31.24 kV, higher than rated. Measures should be taken to protect L_f in the front filter.

4.1.3 The Voltage and Current Across Front Filter Capacitance C_f

As shown in Fig 4.5, the maximum values and increasing rates of voltage across front filter capacitance C_f (V_{Cf}) and current through front filter capacitance C_f (I_{Cf}) are:

maximum voltage across C_f: $V_{Cf.pk} = 37.34$ kV,

maximum increasing rate: max $\frac{dV_{Cf}}{dt} = 0.54$ kV/μs,

maximum current through C_f: $I_{Cf.pk} = 21.99$ A,

maximum increasing rate: max $\frac{dI_{Cf}}{dt} = 0.50$ A/μs.

The magnitudes of the voltage and current surges on C_f are excessive as seen in this case. The highest withstanding voltage of a commercial 0.04 μF capacitance is 10 kV [51], but the impulse voltage can reach up to 37.34 kV, higher than rated, so the insulation of the capacitance is under risk. Measures should be taken to protect C_f in the front filter.

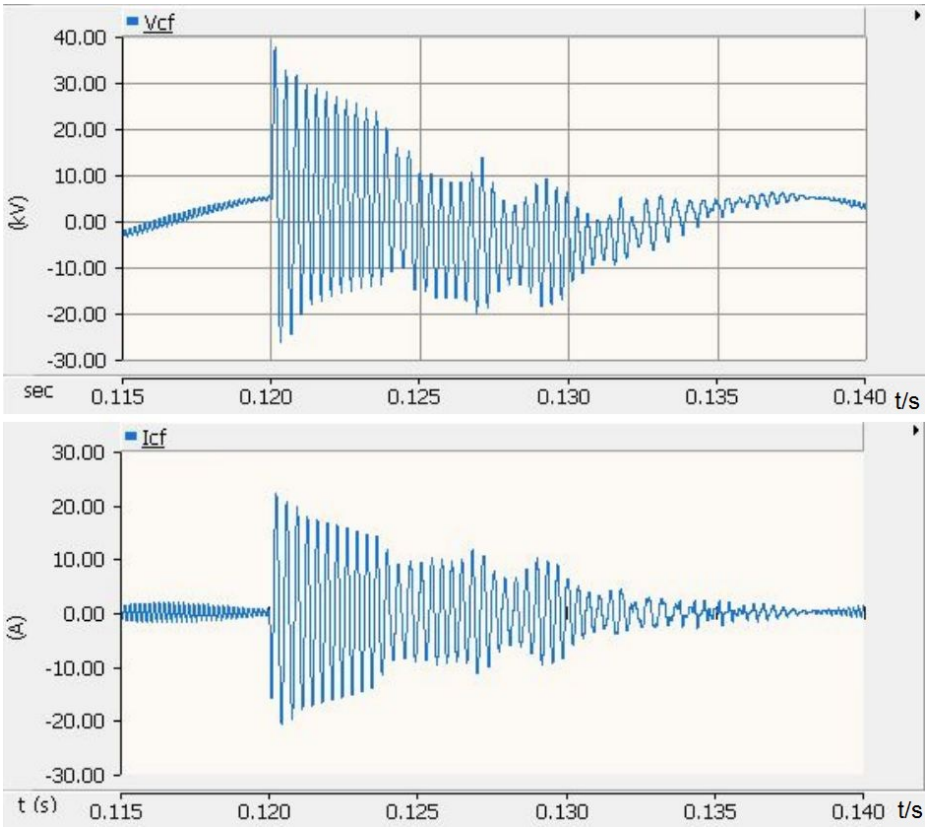

Figure 4.5: V_{Cf} I_{Cf} When Impulse Is Applied

4.1.4 The Voltage and Current Across Semiconductors

a. Lower Semiconductor

Fig 4.6 is an example of voltage and current surges on semiconductors in the rectifier. The maximum values and increasing rates of voltage across the lower semiconductor in the rectifier (V_{r1}) and current through the lower semiconductor in rectifier (I_{r1}) are:

maximum voltage across lower IGBT: $V_{r1.pk} = 7.38$ kV,

maximum increasing rate: max $\frac{dV_{r1}}{dt} = 70.81$ kV/μs,

maximum current through lower IGBT: $I_{r1.pk} = 25.72$ A,

maximum increasing rate: max $\frac{dI_{r1}}{dt} = 73.55$ A/μs.

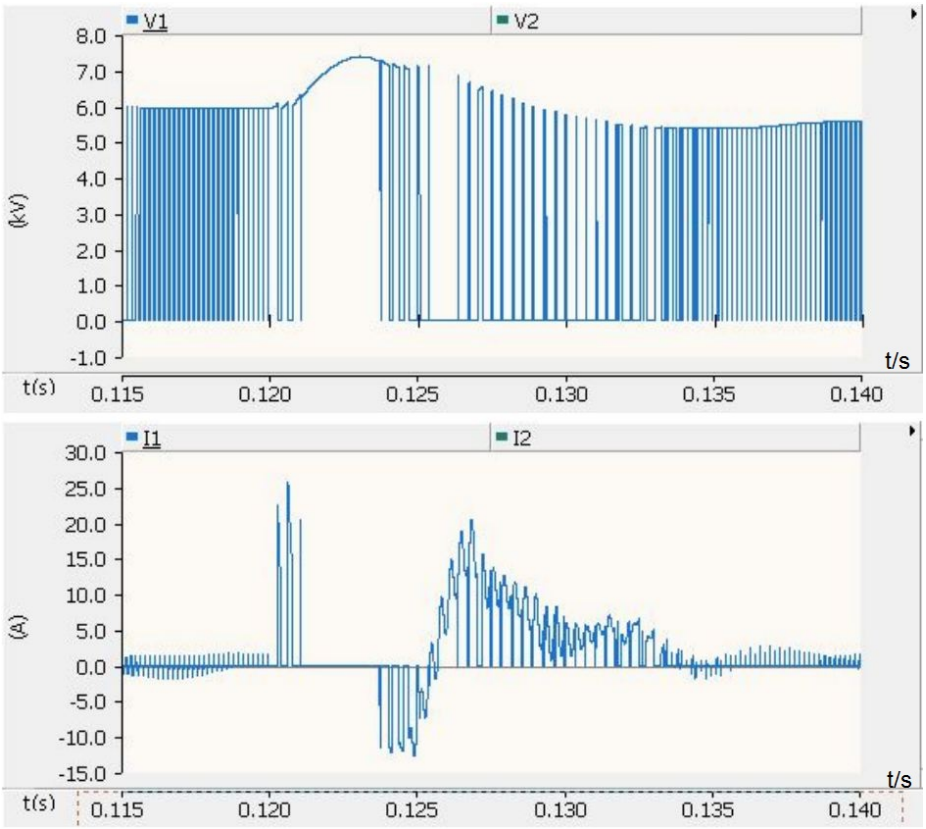

Figure 4.6: V_{r1} I_{r1} When Impulse Is Applied

Since the voltage rating of the semiconductors is 6.5 kV, which is lower than the 7.38 kV maximum over-voltage, the semiconductors in rectifier part need over-voltage protection. The current rating of the semiconductors is 250 A, so the 25.72 A current surge is tolerable in this design.

The increasing rates of voltage and current are not accurate in this simulation model. During the simulation, the IGBTs in the rectifier are operating under ideal condition, which does not coincide with physical models.

The voltage and current characteristics of a 6.5 kV IGBT can be found in the data sheet [8]. Accordingly, the maximum increasing rates of the voltage and current across the semiconductors in SST rectifier are:

$$max\frac{dV}{dt} = 18.45kV/\mu s \tag{4.3}$$

$$max\frac{dI}{dt} = 0.06kA/\mu s \tag{4.4}$$

Compare with the impulse characteristics of IGBT in Chapter 1,

$$max\frac{dV}{dt} = 16.25kV/\mu s \tag{4.5}$$

$$max\frac{dI}{dt} = 0.63kA/\mu s \tag{4.6}$$

The increasing rate of current is within limit, but the increasing rate of voltage is higher than rated. The lower semiconductors in SST rectifier part need protection.

b. Upper Semiconductor

The maximum values and increasing rates of voltage across upper semiconductor in rectifier (V_{r2}) and current through upper semiconductor in rectifier (I_{r2}) are:

maximum voltage across lower IGBT: $V_{r2.pk} = 7.25$ kV,

maximum increasing rate: max $\frac{dV_{r2}}{dt} = 70.81$ kV/μs,

maximum current through lower IGBT: $I_{r2.pk} = 29.78$ A,

maximum increasing rate: max $\frac{dI_{r2}}{dt} = 73.68$ A/μs.

Since the voltage rating of the semiconductors is 6.5 kV, which is lower than the 7.25 kV maximum over-voltage, the semiconductors in rectifier part need over-voltage protection. The current rating of the semiconductors is 250 A, so the 29.78 A current surge is tolerable in this design.

The increasing rates of voltage and current are not accurate in this simulation model. During the simulation, the IGBTs in the rectifier are operating under ideal condition, which does not coincide with physical models.

The voltage and current characteristics of a 6.5 kV IGBT can be found in the data sheet [8]. Accordingly, the maximum increasing rates of the voltage and current across the semiconductors in SST rectifier are:

$$max\frac{dV}{dt} = 18.13kV/\mu s \tag{4.7}$$

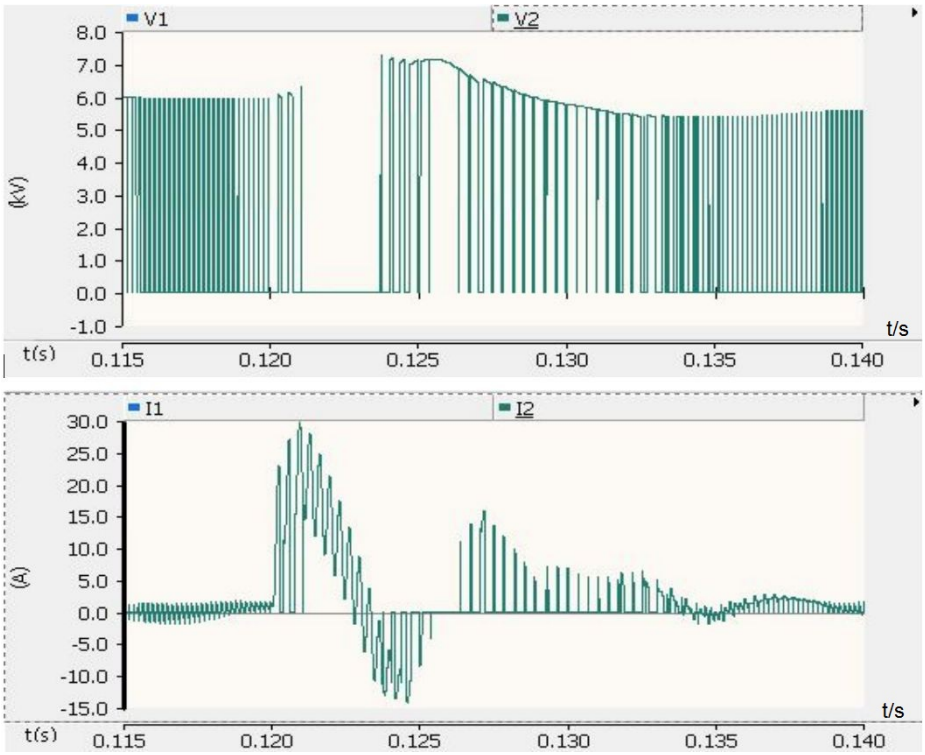

Figure 4.7: V_{r2} I_{r2} When Impulse Is Applied

$$max\frac{dI}{dt} = 0.07kA/\mu s \tag{4.8}$$

Compared with the impulse characteristics in equation 4.5 and 4.6, the increasing rate of current is within limit, but the increasing rate of voltage is higher than rated. The upper semiconductors in SST rectifier part need protection.

4.1.5 The Voltage and Current Across Capacitance C_h

As shown in Fig 4.8, the maximum values and increasing rates of voltage across capacitance C_h ($V_{dc.hi}$) and current through capacitance C_h ($I_{dc.hi}$) are,

maximum voltage across C_h: $V_{dc.hi.pk} = 7.38$ kV,

maximum increasing rate: max $\frac{dV_{dc.hi}}{dt} = 1.45$ V/μs,

maximum current through C_h: $I_{dc.hi.pk} = 30.32$ A,

maximum increasing rate: max $\frac{dI_{dc.hi}}{dt} = 205.38$ A/μs.

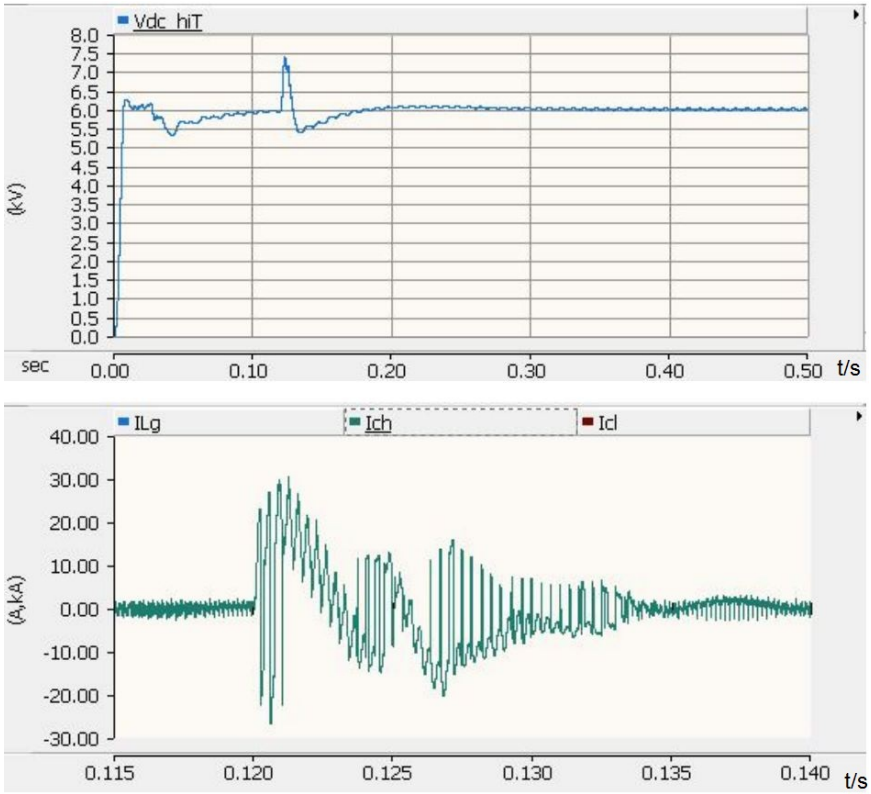

Figure 4.8: $V_{dc.hi}$ $I_{dc.hi}$ When Impulse Is Applied

The over-voltage and over-current on capacitance C_h in rectifier are tolerable in this design.

4.1.6 Conclusions

Lightning impulse could cause unacceptably high voltage surges across filter inductances and capacitance in the SST. Under 60 kV 1.2/50 μs lightning voltage surge, the maximum voltage on L_g reaches 60.23 kV, and the maximum voltage on L_f reaches 31.24 kV, much higher than the rated 20 kV. The maximum over-voltage across C_f can reach up to 37.34 kV, much larger than the rated 10 kV. The value and increasing rate of over-voltage on semiconductors in SST rectifier are also higher than rated. Accordingly, the components in the SST front filter and semiconductors in rectifier need to be protected.

4.2 Improvement of the Operating SST Front Filter

According to the simulation results, the lightning impulse could damage the FREEDM SST. Thus, MOSAs are implemented to protect the SST and the SST front filter is improved. According to Fig 4.9, the energy consumed by the MOSA is

$$Q = P \times t = 219.32\ kW \times 0.0008\ s = 0.175\ kJ \tag{4.9}$$

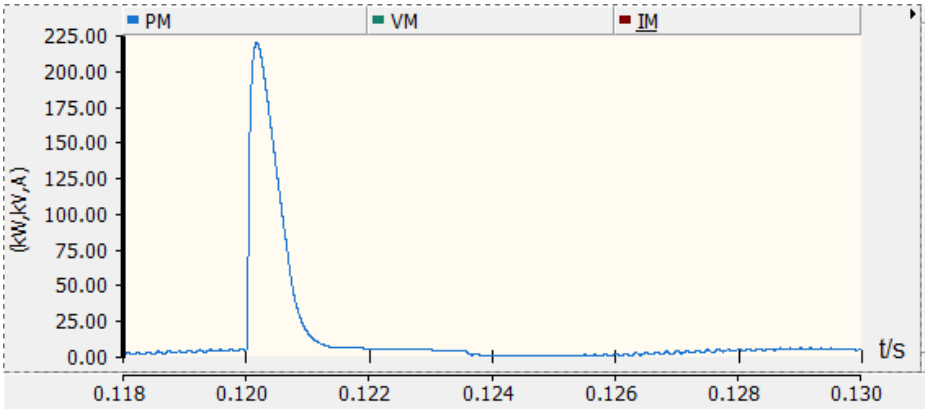

Figure 4.9: Energy Consumed by MOSA When Impulse Is Applied

The lightning protection of operating SST is shown in Fig 4.10, the same as the topology described in Chapter 3. Table 4.1 compares the performance of operating SST before and after the improvement of the front filter.

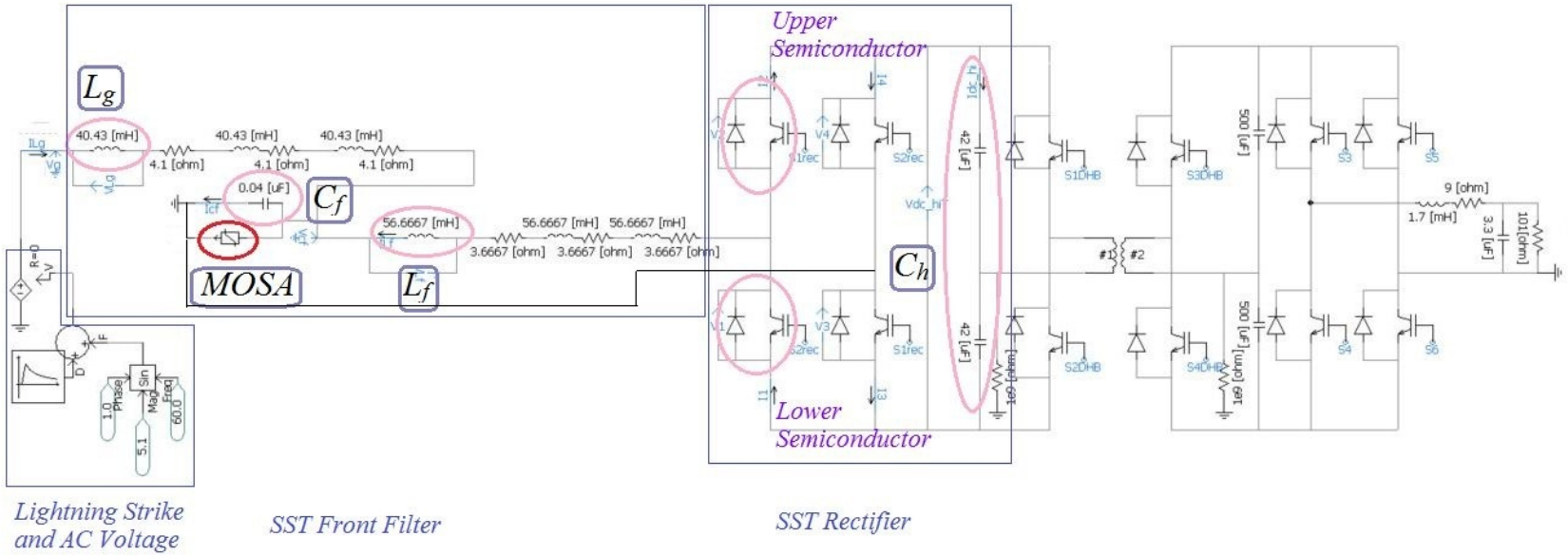

Figure 4.10: Protection of the Operating SST Front Filter in PSCAD [1]

Table 4.1: Performance of Operating SST Before and After the Front Filter Improvement

Model Property	With MOSAs	MOSAs	
		Value	Reduction Ratio (%)
V_{Lg}/kV	60.23	19.08	68.32
I_{Lg}/A	34.42	29.53	14.21
V_{Lf}/kV	31.24	4.14	86.75
I_{Lf}/A	29.78	11.03	62.96
V_{Cf}/kV	37.34	8.25	77.91
I_{Cf}/A	21.99	5.96	72.90
V_{r1}/kV	7.38	6.40	13.28
I_{r1}/A	25.72	11.00	57.23
V_{r2}/kV	7.25	6.28	13.38
I_{r2}/A	29.78	12.18	59.10
$V_{dc.hi}$/kV	7.38	6.28	14.91
$I_{dc.hi}$/A	30.32	13.29	56.17

4.2.1 *The Voltage and Current Across Front Filter Inductance L_g*

The voltage surge on the front filter inductance L_g is reduced from 60.23 kV to 19.08 kV, current surge drops from 34.42 A to 29.53 A. Over-voltage on L_g caused by lightning strike is significantly reduced. Oscillations of voltage and current are both reduced. Since the maximum voltage the inductance winding can withstand is 20 kV [50][49], the front filter inductance L_g is well protected.

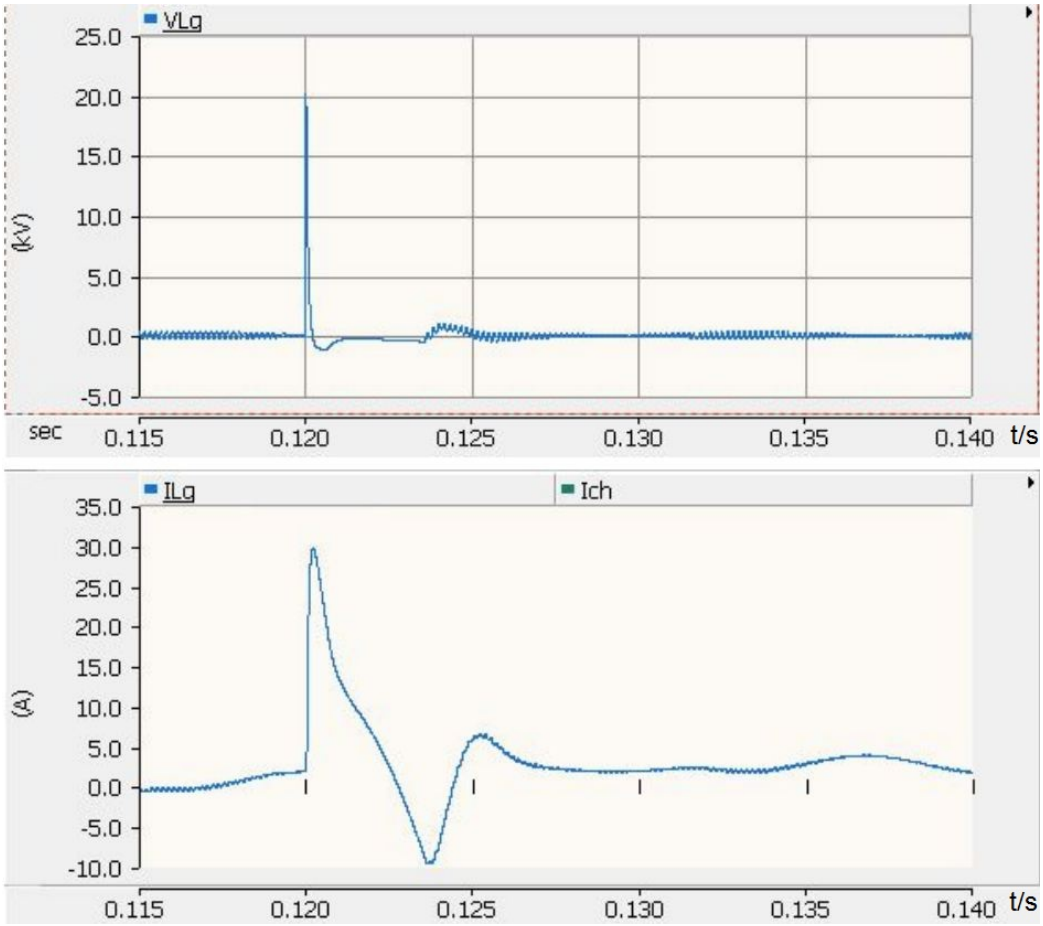

Figure 4.11: V_{Lg} I_{Lg} After the Filter Improvement

4.2.2 *The Voltage and Current Across Front Filter Inductance L_f*

The voltage surge on the front filter inductance L_f is reduced from 31.24 kV to 4.14 kV, current surge drops from 29.78 A to 11.03 A. Over-voltage on L_f caused by lightning strike is significantly reduced. Oscillations of voltage and current are both reduced. Since the maximum voltage the inductance winding can withstand is 20 kV [50][49], the front filter inductance L_f is well protected.

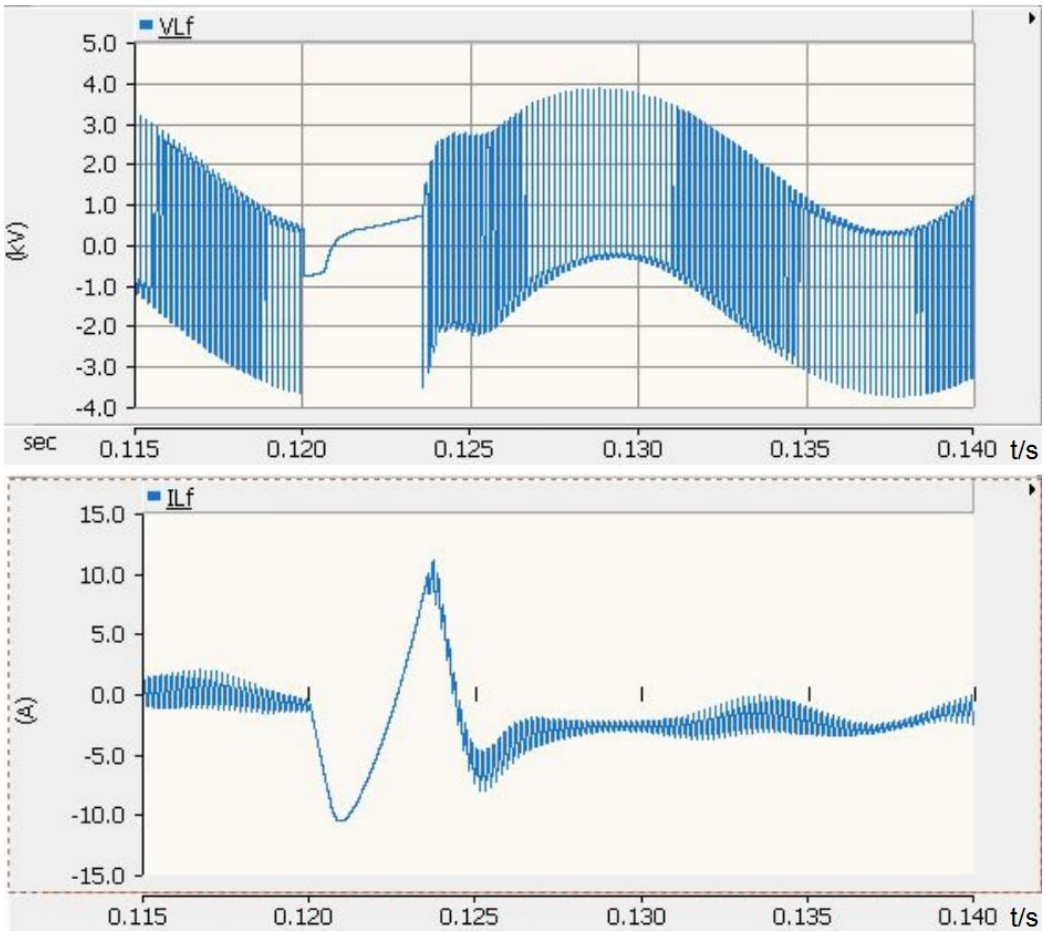

Figure 4.12: V_{Lf} I_{Lf} After the Filter Improvement

4.2.3 The Voltage Across Front Filter Capacitance C_f

The voltage surge on the front filter capacitance C_f is reduced from 37.34 kV to 8.25 kV, current surge drops from 21.99 A to 5.96 A. Over-voltage on C_f caused by lightning strike is significantly reduced. Oscillations of voltage and current are both reduced. The highest withstand voltage of a commercial 0.04 F capacitance is 10 kV [51]. Thus the front filter capacitance C_f is well protected.

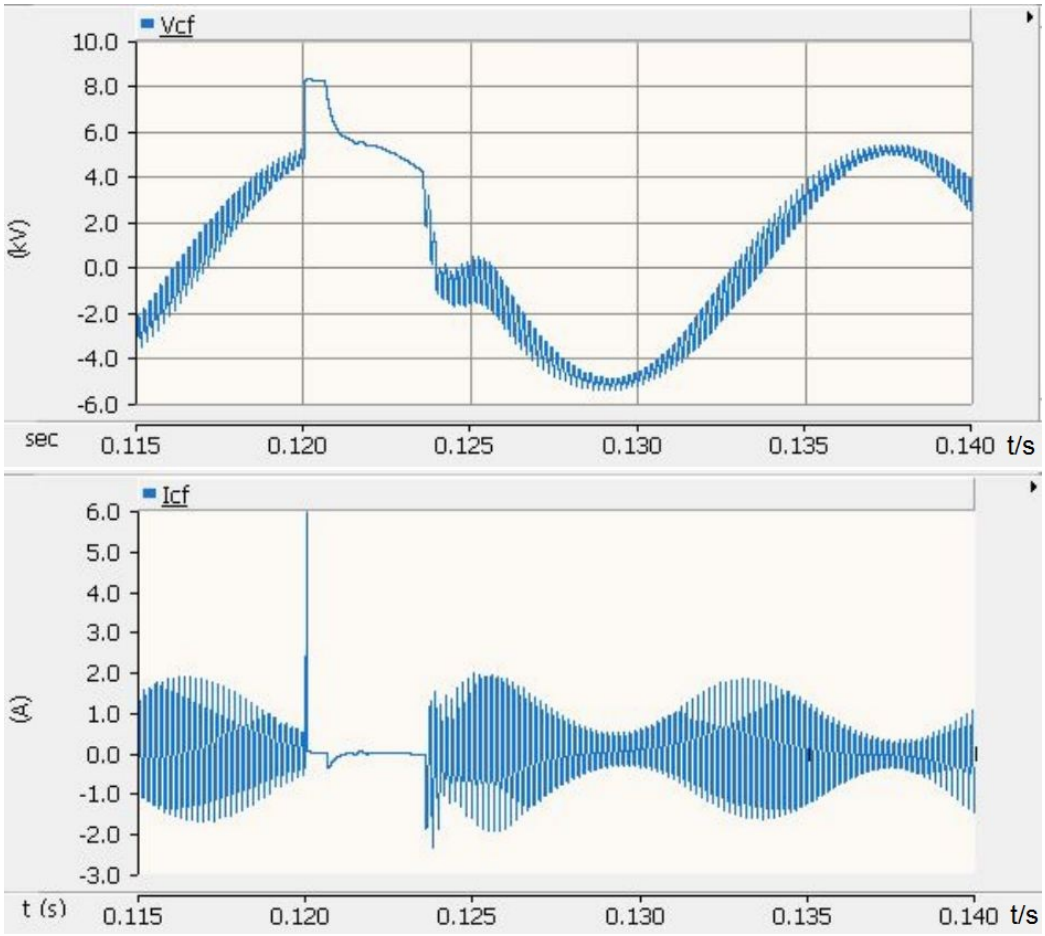

Figure 4.13: V_{Cf} I_{Cf} After the Filter Improvement

4.2.4 The Voltage and Current Across Semiconductors

a. Lower Semiconductor

The voltage surge on the lower semiconductor is reduced from 7.38 kV to 6.40 kV, lower than rated 6.50 kV. Voltage increasing rate $max\frac{dV}{dt} = 16.00kV/\mu s$, lower than rated $max\frac{dV}{dt} = 16.25kV/\mu s$. Current surge drops from 25.72 A to 11.00 A. The lower semiconductor is protected.

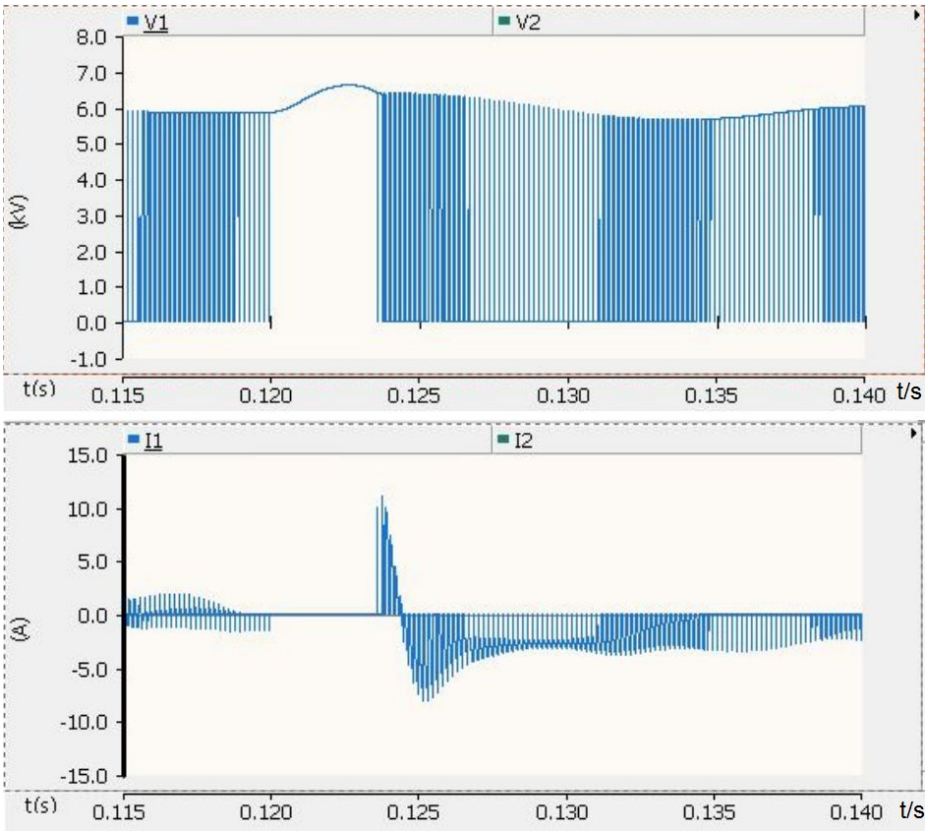

Figure 4.14: V_{r1} I_{r1} After the Filter Improvement

b. Upper Semiconductor

The voltage surge on the upper semiconductor is reduced from 7.25 kV to 6.28 kV, lower than rated 6.50 kV. Voltage increasing rate $max\frac{dV}{dt} = 15.30kV/\mu s$, lower than rated $max\frac{dV}{dt} = 16.25kV/\mu s$. Current surge drops from 29.78 A to 12.18 A. The upper semiconductor is protected.

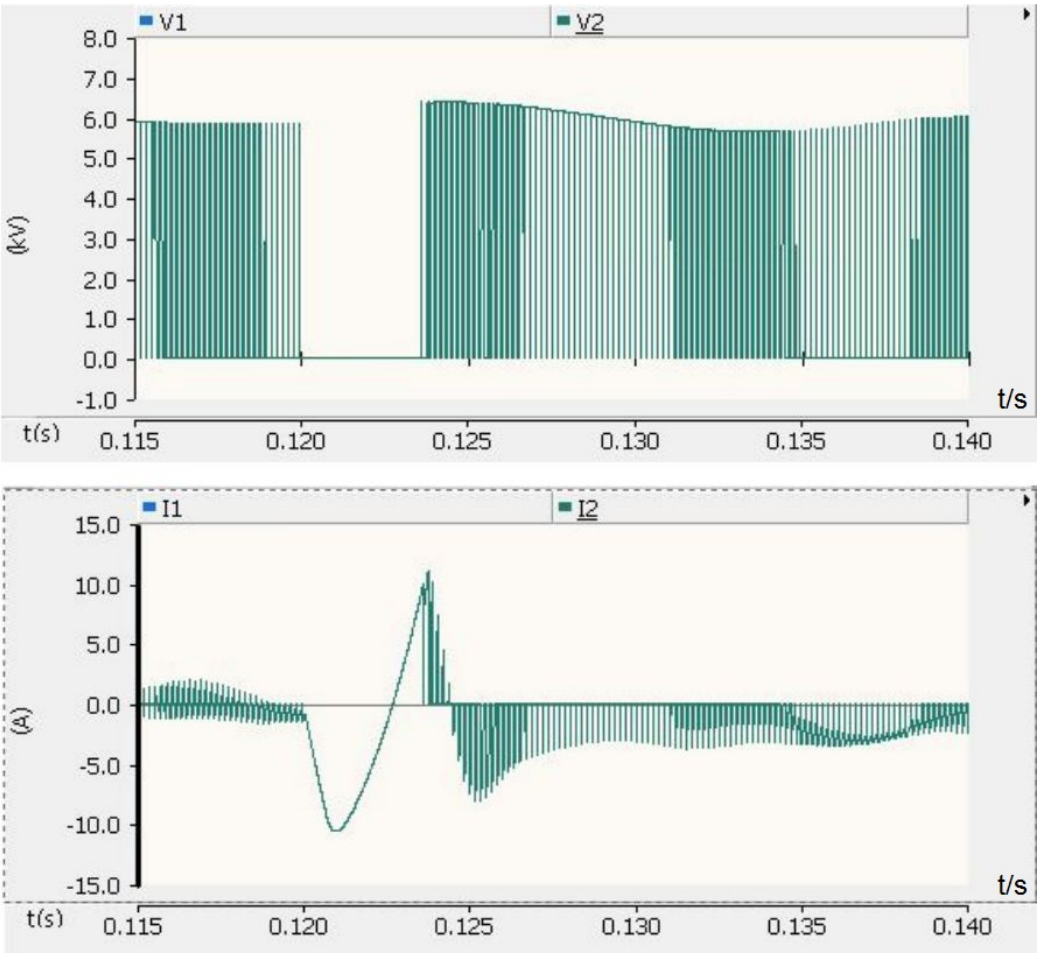

Figure 4.15: V_{r2} I_{r2} After the Filter Improvement

4.2.5 The Voltage and Current Across Capacitance C_h

The voltage surge on capacitance C_h is reduced from 7.38 kV to 6.28 kV, current surge drops from 30.32 A to 13.29 A. Thus the capacitance C_h is well protected, and

voltage surge on high DC output caused by lightning strike is significantly reduced.

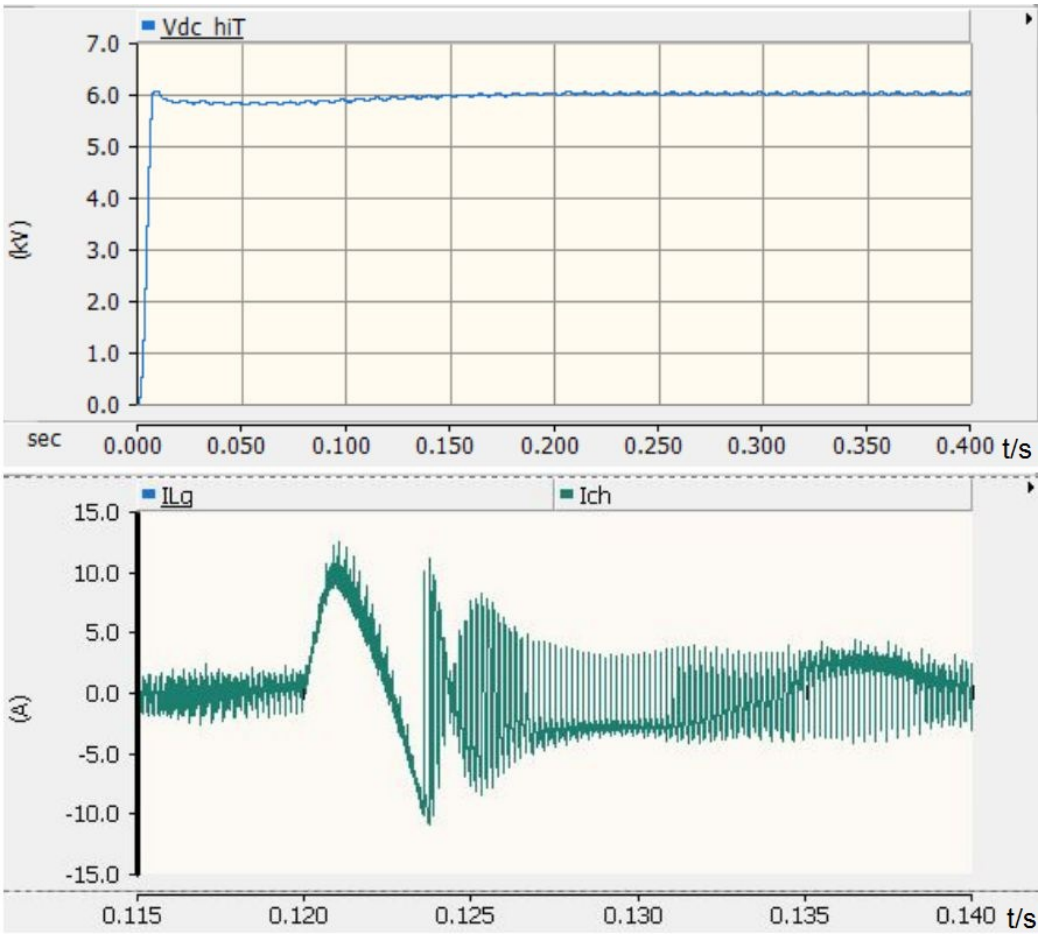

Figure 4.16: $V_{dc.hi}$ $I_{dc.hi}$ After the Filter Improvement

4.2.6 Conclusions

It can be seen in the table and figures that the surge arrester has effects on over-voltage and over-current protection if lightning happens, reducing amplitudes of voltage and current surges on L_g, L_f and C_f by almost 86%.

Chapter 5

VSC ROBUSTNESS TEST AND PROTECTION UNDER OPERATING CONDITION

5.1 Operating VSC Robustness Test

The Voltage Source Converter (VSC) is a grid-tied power electronic device that can be adopted to convert DC power to AC power using IGBTs. Simulation of robustness test and protection is done to VSC similar to that of SST in Chapter 4. In this test, the VSC is under operating condition, the control of rectifier is functioning. Since the three phase distribution line voltage in the FREEDM system is 12 kV, the AC voltage for this single phase VSC is set as 7.2 kVrms. The voltage surge is applied at filter front end at 0.12 s (Fig 5.1). The schematic of the operating VSC in PSCAD is described in Fig 5.2.

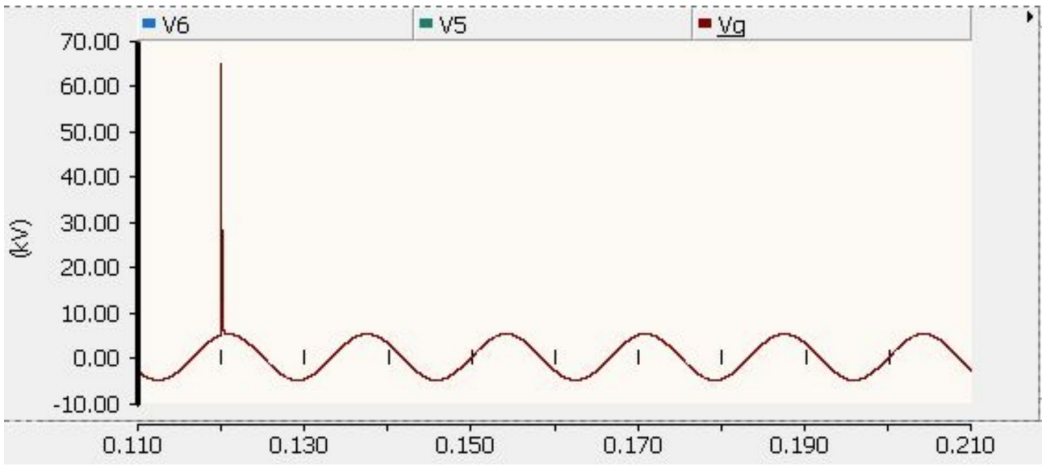

Figure 5.1: Impulse and Sinusoidal Grid Voltage

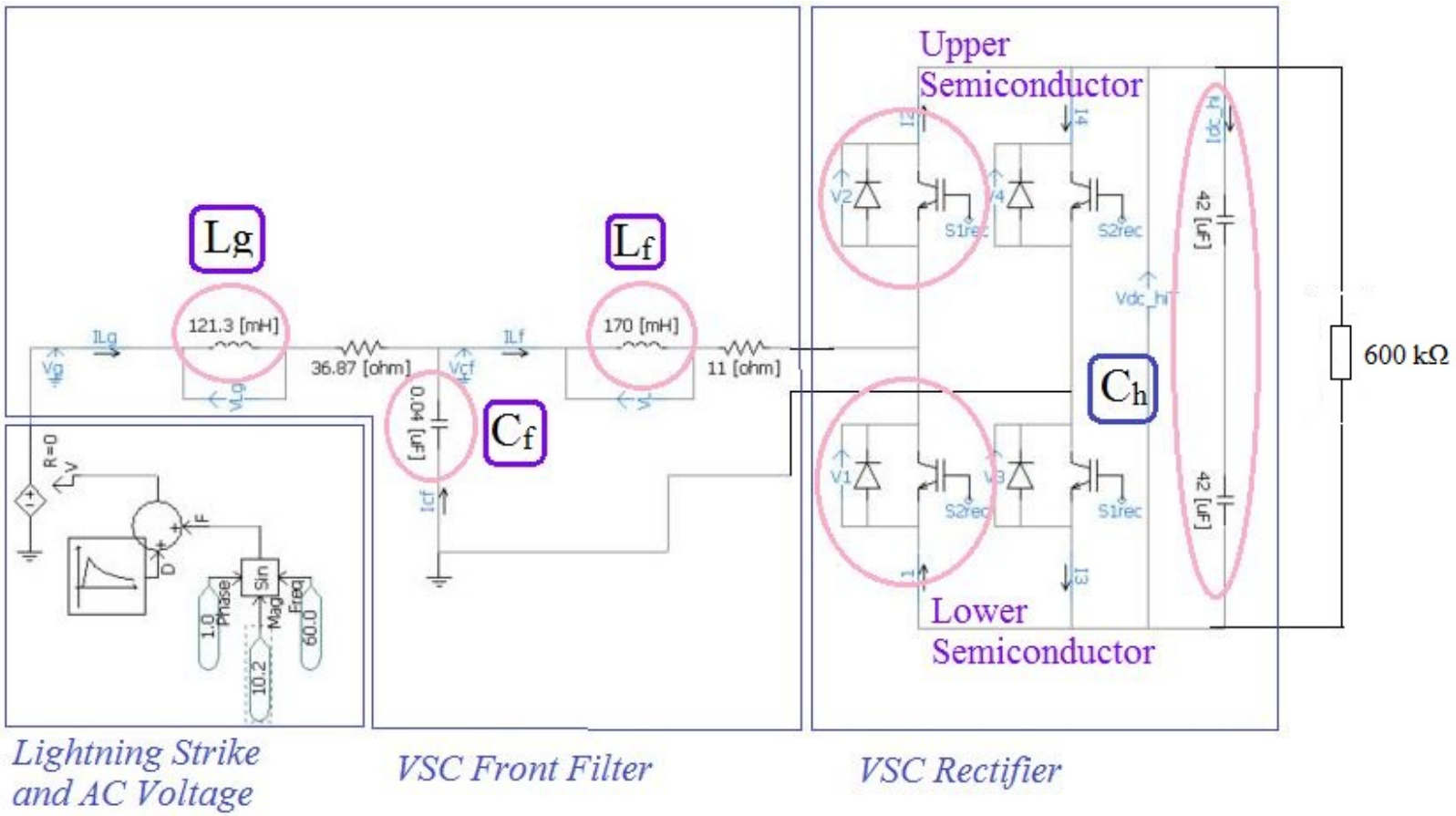

Figure 5.2: Schematic of Operating VSC in PSCAD [1]

5.1.1 *The Voltage and Current Across Front Filter Inductance L_g*

As shown in Fig 5.3, the maximum values and increasing rates of voltage across front filter inductance L_g ($V_{Lg.pk}$) and current through front filter inductance L_g ($I_{Lg.pk}$) are:

maximum voltage across L_g: $V_{Lg.pk} = 60.45$ kV,

maximum increasing rate: max $\frac{dV_{Lg}}{dt} = 0.91$ kV/μs,

maximum current through L_g: $I_{Lg.pk} = 34.30$ A,

maximum increasing rate: max $\frac{dI_{Lg}}{dt} = 0.51$ A/μs.

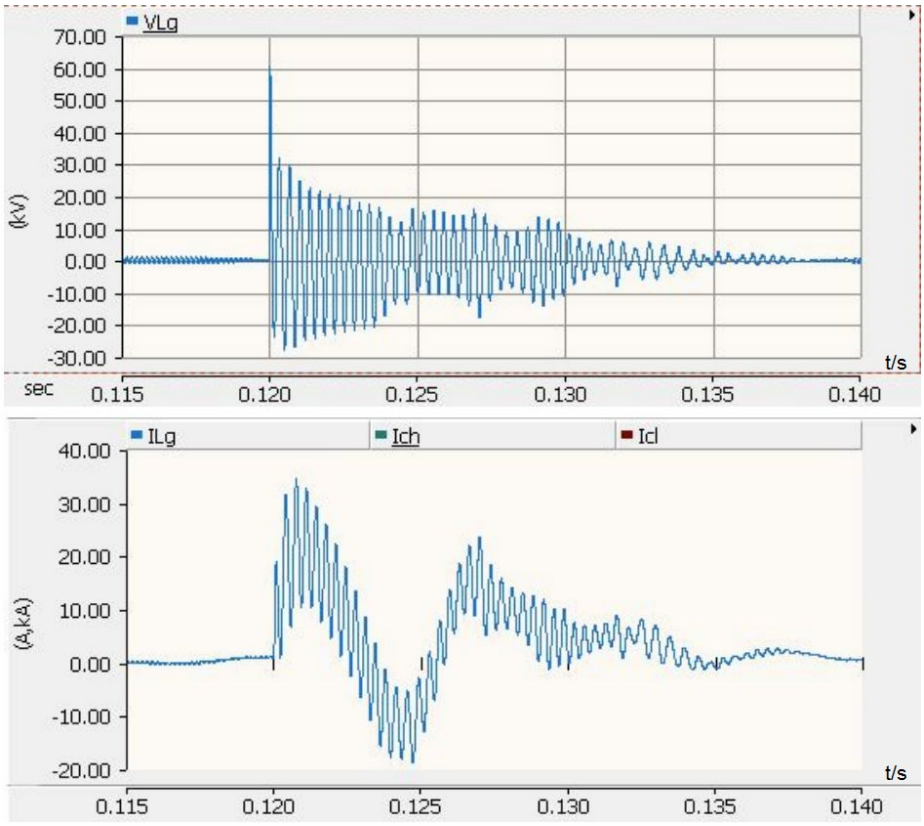

Figure 5.3: V_{Lg} I_{Lg} When Impulse Is Applied

The magnitudes of the voltage and current surges on L_g are excessive as seen in this case, the insulation of the inductance winding is under risk. The AWG for the inductance winding is chosen as 10 based on the maximum impulse current [49], the

maximum voltage it can withstand is 20 kV [50]. However, the peak voltage across the inductance is 60.45 kV, higher than rated. Measures should be taken to protect L_g in the front filter.

5.1.2 The Voltage and Current Across Front Filter Inductance L_f

As shown in Fig 5.4, the maximum values and increasing rates of voltage across front filter inductance L_f (V_{Lf}) and current through front filter inductance L_f (I_{Lf}) are:

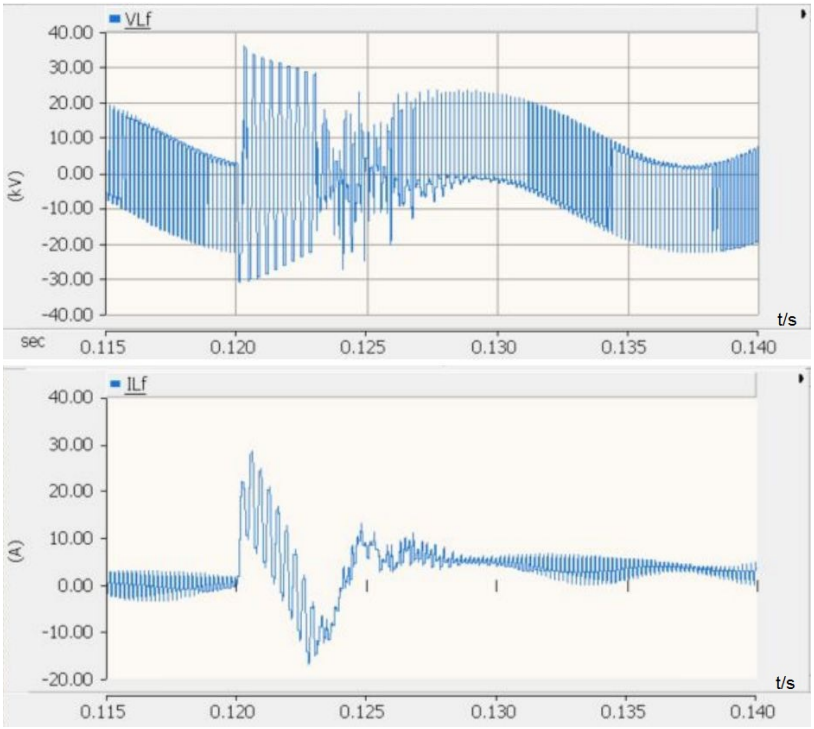

Figure 5.4: V_{Lf} I_{Lf} When Impulse Is Applied

maximum voltage across L_f: $V_{Lf.pk} = 36.10$ kV,

maximum increasing rate: max $\frac{dV_{Lf}}{dt} = 251.20$ kV/μs,

maximum current through L_f: $I_{Lf.pk} = 28.10$ A,

maximum increasing rate: max $\frac{dI_{Lf}}{dt} = 0.50$ A/μs.

The magnitudes of the voltage and current surges on L_f are excessive as seen in this case, the insulation of the inductance winding is under risk. The AWG for the inductance winding is chosen as 10 based on the maximum impulse current [49], the maximum voltage it can withstand is 20 kV [50]. However, the peak voltage across the inductance is 36.10 kV, higher than rated. Measures should be taken to protect L_f in the front filter.

5.1.3 The Voltage and Current Across Front Filter Capacitance C_f

As shown in Fig 5.5, the maximum values and increasing rates of voltage across front filter capacitance C_f (V_{Cf}) and current through front filter capacitance C_f (I_{Cf}) are:

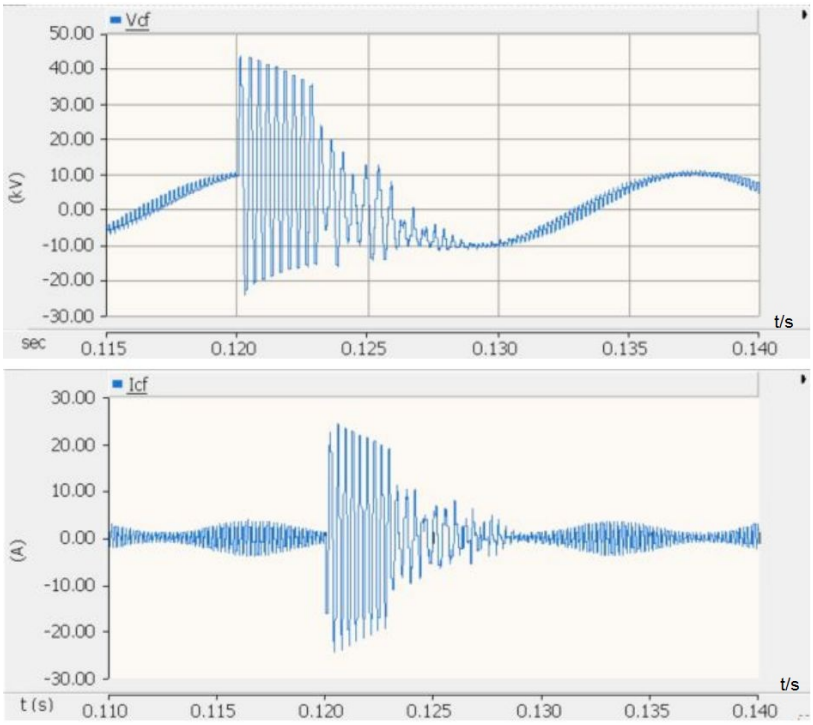

Figure 5.5: V_{Cf} I_{Cf} When Impulse Is Applied

maximum voltage across C_f: $V_{Cf.pk} = 43.30$ kV,

maximum increasing rate: max $\frac{dV_{Cf}}{dt} = 0.65$ kV/μs,

maximum current through C_f: $I_{Cf.pk} = 24.58$ A,

maximum increasing rate: max $\frac{dI_{Cf}}{dt} = 0.59$ A/μs.

The magnitudes of the voltage and current surges on C_f are excessive as seen in this case. The highest withstanding voltage of a commercial 0.04 F capacitance is 10 kV [51], but the impulse voltage can reach up to 43.30 kV, higher than rated, so the insulation of the capacitance is under risk. Measures should be taken to protect C_f in the front filter.

5.1.4 The Voltage and Current Across Semiconductors

a. Lower Semiconductor

Fig 5.6 is an example of voltage and current surges on semiconductors in the rectifier. The maximum values and increasing rates of voltage across the lower semiconductor in the rectifier (V_{r1}) and current through lower semiconductor in rectifier (I_{r1}) are:

maximum voltage across lower IGBT: $V_{r1.pk} = 12.72$ kV,

maximum increasing rate: max $\frac{dV_{r1}}{dt} = 120.38$ kV/μs,

maximum current through lower IGBT: $I_{r1.pk} = 20.96$ A,

maximum increasing rate: max $\frac{dI_{r1}}{dt} = 54.59$ A/μs.

Since the voltage rating of the semiconductors is 15 kV, which is higher than the 12.72 kV maximum over-voltage, the over-voltage is tolerable in this design. The current rating of the semiconductors is 20 A, which is lower than the 20.96 A maximum over-current. The semiconductors in rectifier part need protection.

The increasing rates of voltage and current are not accurate in this simulation model. During the simulation, the IGBTs in the rectifier are operating under ideal condition, which does not coincide with physical models.

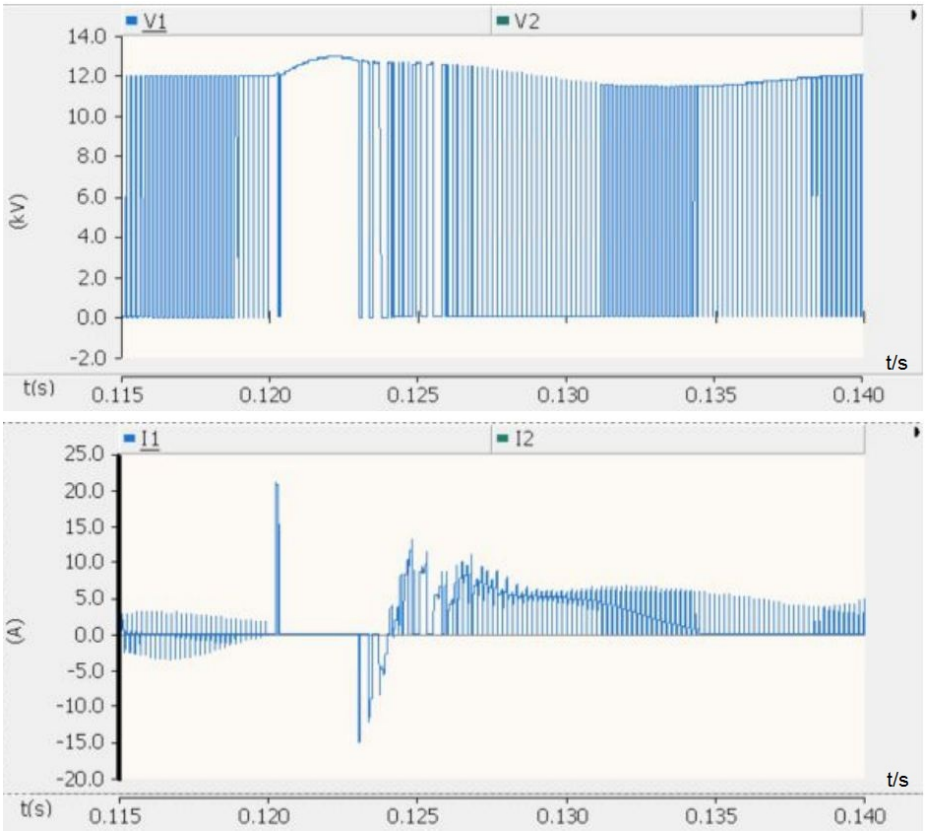

Figure 5.6: V_{r1} I_{r1} When Impulse Is Applied

According to the impulse characteristics of the IGBT in Chapter 1, the maximum increasing rates of the voltage and current across the semiconductors in VSC rectifier are:

$$max\frac{dV}{dt} = 31.80kV/\mu s \tag{5.1}$$

$$max\frac{dI}{dt} = 0.40kA/\mu s \tag{5.2}$$

Compare with the voltage and current characteristics of 15 kV 20 A IGBT [52], the voltage and current increasing rates can reach up to:

$$\frac{dV}{dt} = 45kV/\mu s \tag{5.3}$$

$$\frac{dI}{dt} = 0.63kA/\mu s \tag{5.4}$$

The increasing rates of voltage and current is within limit.

b. Upper Semiconductor

The maximum values and increasing rates of voltage across upper semiconductor in rectifier (V_{r2}) and current through upper semiconductor in rectifier (I_{r2}) are:

maximum voltage across lower IGBT: $V_{r2.pk} = 12.72$ kV,

maximum increasing rate: max $\frac{dV_{r2}}{dt} = 126.47$ kV/μs,

maximum current through lower IGBT: $I_{r2.pk} = 28.34$ A,

maximum increasing rate: max $\frac{dI_{r2}}{dt} = 54.52$ A/μs.

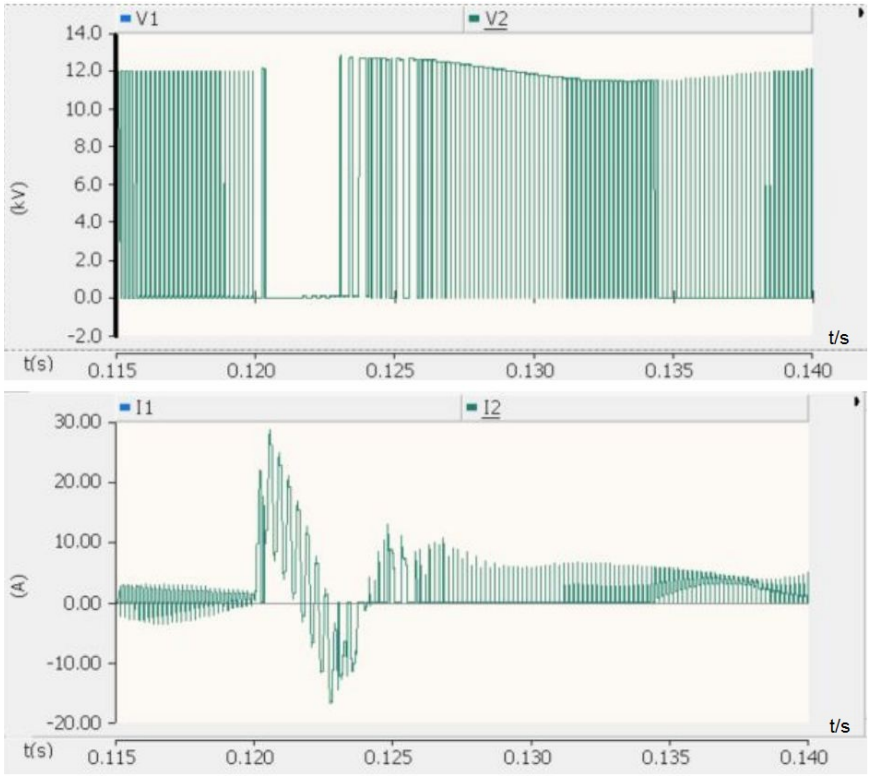

Figure 5.7: V_{r2} I_{r2} When Impulse Is Applied

Since the rating of the semiconductors is 15 kV, which is higher than the 12.72 kV maximum over-voltage. The over-voltage is tolerable in this design. The current rating of the semiconductors is 20 A, which is lower than the 28.34 A maximum over-current. The semiconductors in rectifier part need protection. Same as above, the increasing rate of voltage and current is within limit.

5.1.5 The Voltage and Current Across Capacitance C_h

As shown in Fig 5.8, the maximum values and increasing rates of voltage across capacitance C_h ($V_{dc.hi}$) and current through capacitance C_h ($I_{dc.hi}$) are,

maximum voltage across C_h: $V_{dc.hi.pk} = 12.72$ kV,

maximum increasing rate: max $\frac{dV_{dc.hi}}{dt} = 2.84$ V/μs,

maximum current through C_h: $I_{dc.hi.pk} = 28.26$ A,

maximum increasing rate: max $\frac{dI_{dc.hi}}{dt} = 109.10$ A/μs.

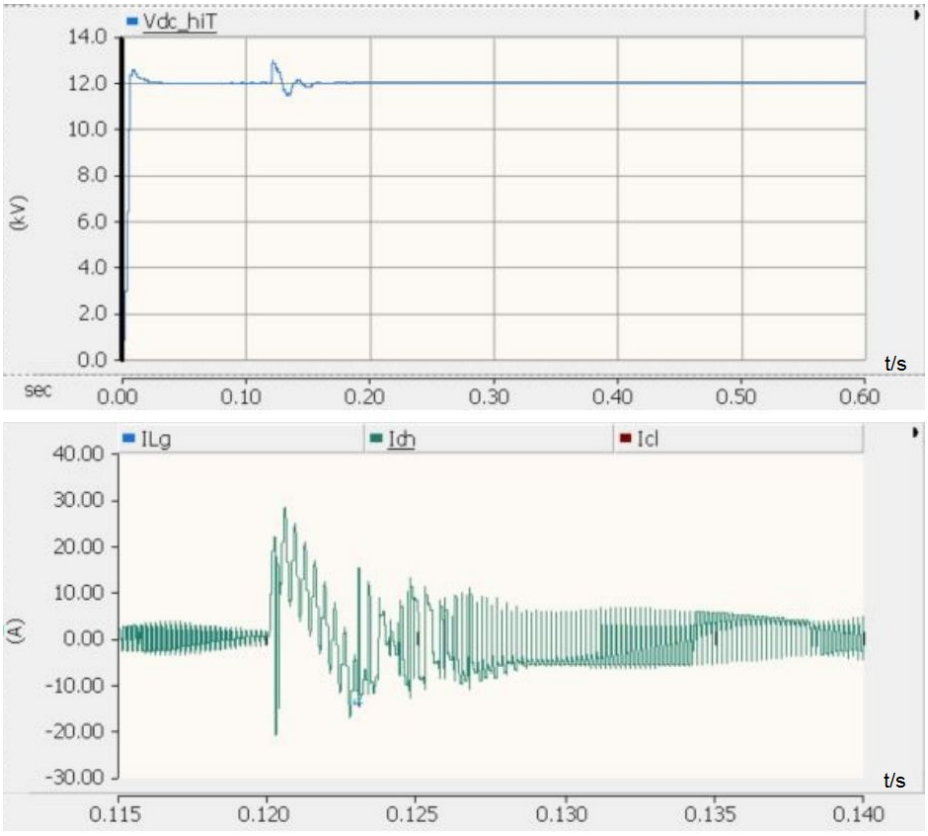

Figure 5.8: $V_{dc.hi}$ $I_{dc.hi}$ When Impulse Is Applied

The over-voltage and over-current on capacitance C_h in rectifier are tolerable in this design.

5.1.6 *Conclusions*

Lightning impulse could cause unacceptable high voltage surges across filter inductances and capacitance in the VSC. Under 60 kV 1.2/50 μs lightning voltage surge, the maximum voltage on L_g reaches 60.45 kV, and the maximum voltage on L_f reaches 36.10 kV, much higher than the rated 20 kV. The maximum over-voltage across C_f can reach up to 43.30 kV, much larger than the rated 10 kV. The over-voltage and over-current on semiconductors in VSC rectifier are tolerable. Accordingly, the components in the VSC front filter need to be protected.

5.2 Improvement of the Operating VSC Front Filter

According to the simulation results, the lightning impulse could damage the VSC. Thus, MOSAs are implemented to protect the VSC and the VSC front filter is improved. As shown in Fig 5.10, the protection topology is the same as non-operating SST in Chapter 2.

According to Fig 5.9, the energy consumed by the MOSA is

$$Q = P \times t = 376.52\ kW \times 0.001\ s = 0.38\ kJ \tag{5.5}$$

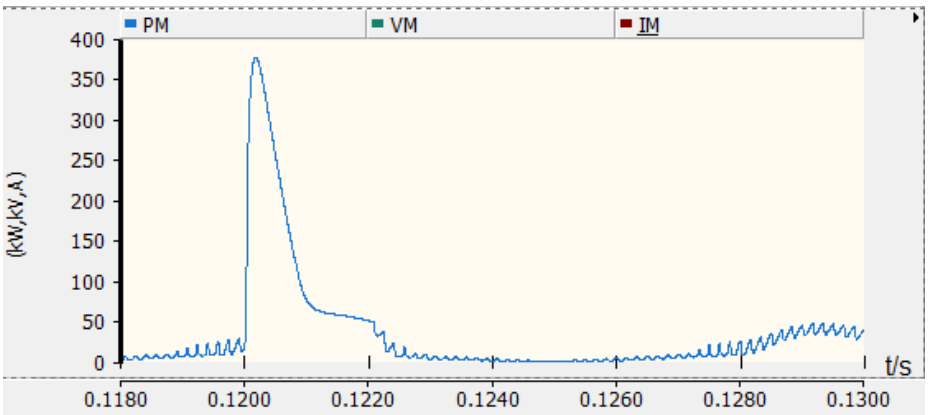

Figure 5.9: Energy Consumed by MOSA When Impulse Is Applied

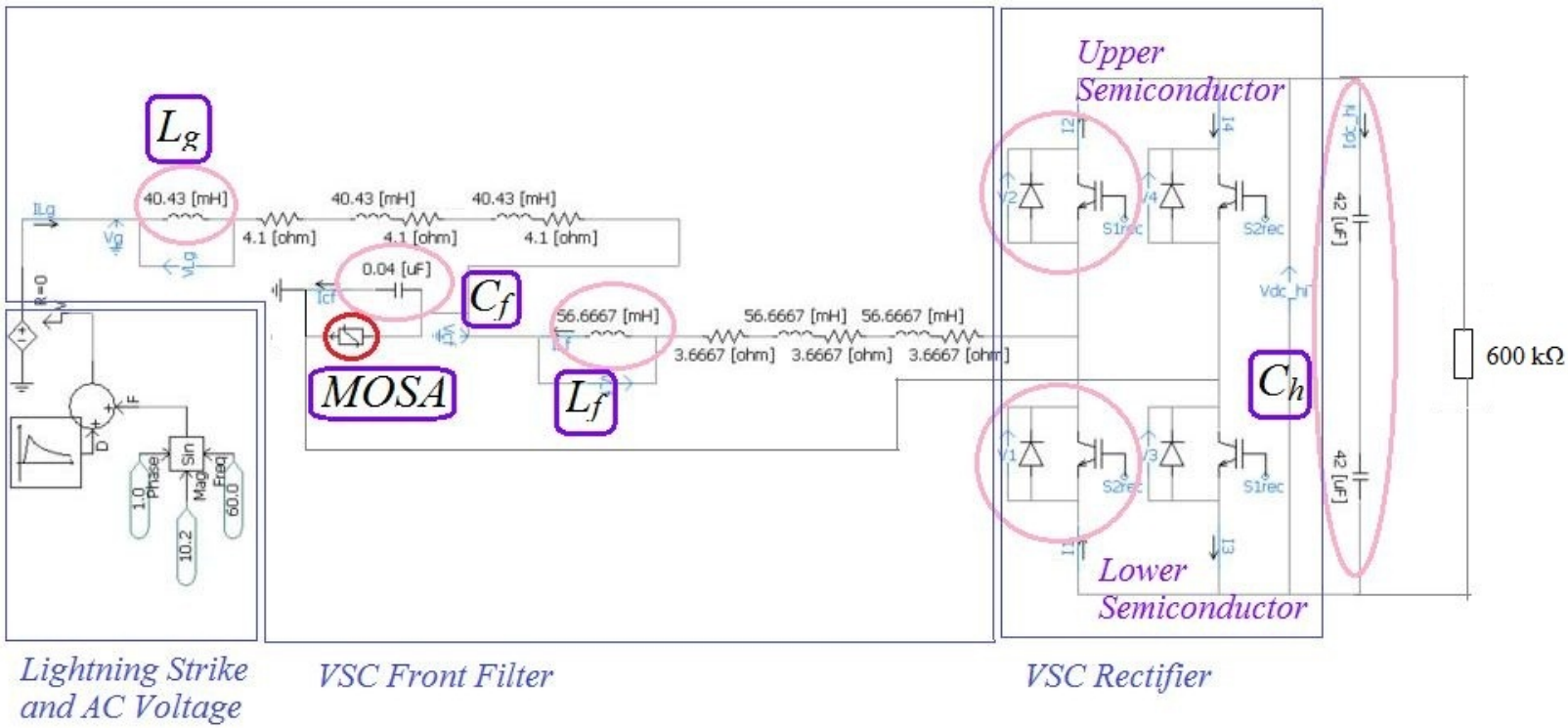

Figure 5.10: Protection of the Operating VSC Front Filter in PSCAD [1]

Table 5.1 compares the performance of VSC before and after the improvement of the front filter.

Table 5.1: Performance of VCS Before and After the Front Filter Improvement

Model Property	With MOSAs	MOSAs	
		Value	Reduction Ratio (%)
V_{Lg}/kV	60.45	19.09	68.42
I_{Lg}/A	34.30	32.69	4.69
V_{Lf}/kV	36.10	7.54	79.11
I_{Lf}/A	28.10	4.68	83.35
V_{Cf}/kV	43.30	12.97	70.05
I_{Cf}/A	24.58	5.59	77.26
V_{r1}/kV	12.72	12.43	2.28
I_{r1}/A	20.96	5.07	75.81
V_{r2}/kV	12.72	12.43	2.28
I_{r2}/A	28.34	5.57	80.35
$V_{dc.hi}$/kV	12.72	12.43	2.28
$I_{dc.hi}$/A	28.26	5.57	80.29

5.2.1 *The Voltage and Current Across Front Filter Inductance L_g*

The voltage surge on the front filter inductance L_g is reduced from 60.45 kV to 19.09 kV, current surge drops from 34.30 A to 32.69 A. Over-voltage on L_g caused by lightning strike is significantly reduced. Oscillations of voltage and current are both reduced. Since the maximum voltage the inductance winding can withstand is 20 kV [50][49], the front filter inductance L_g is well protected.

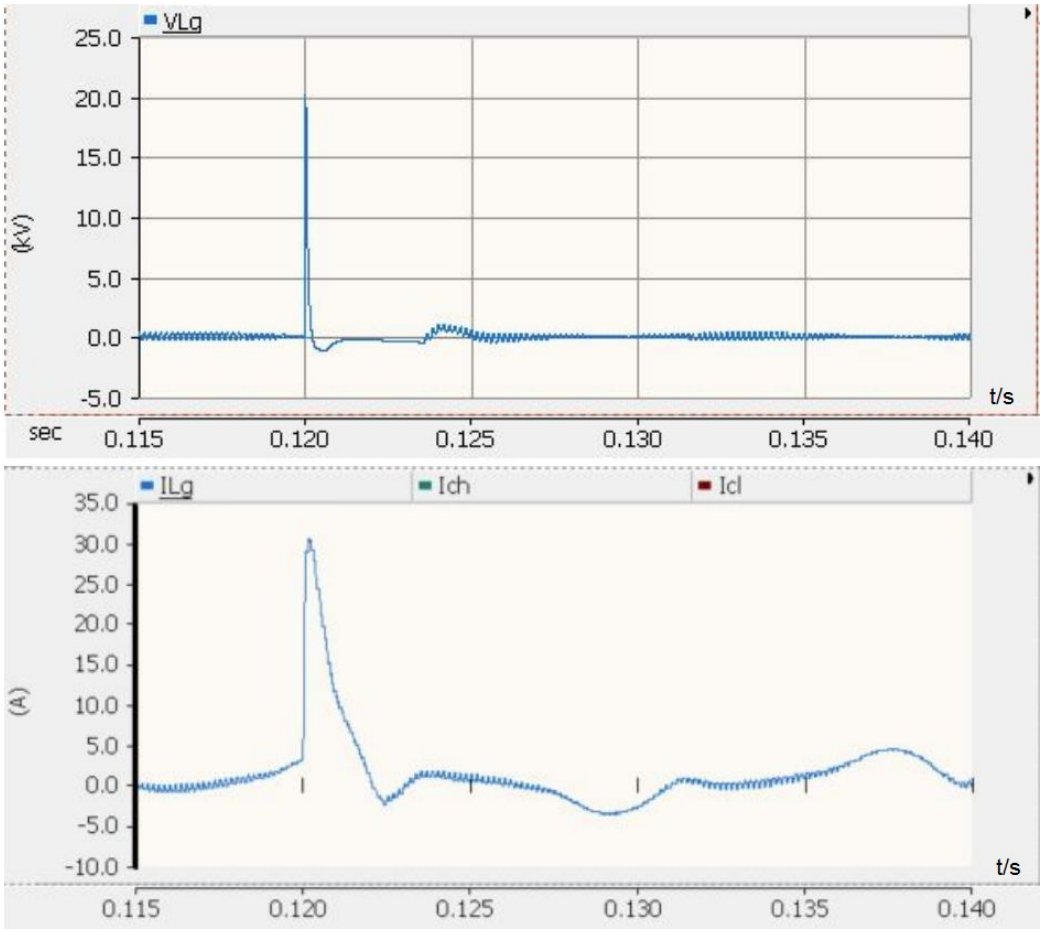

Figure 5.11: V_{Lg} I_{Lg} After the Filter Improvement

5.2.2 *The Voltage and Current Across Front Filter Inductance L_f*

The voltage surge on the front filter inductance L_f is reduced from 36.10 kV to 7.54 kV, current surge drops from 28.10 A to 4.68 A. Over-voltage on L_f caused by lightning strike is significantly reduced. Oscillations of voltage and current are both reduced. Since the maximum voltage the inductance winding can withstand is 20 kV [50][49], the front filter inductance L_f is well protected.

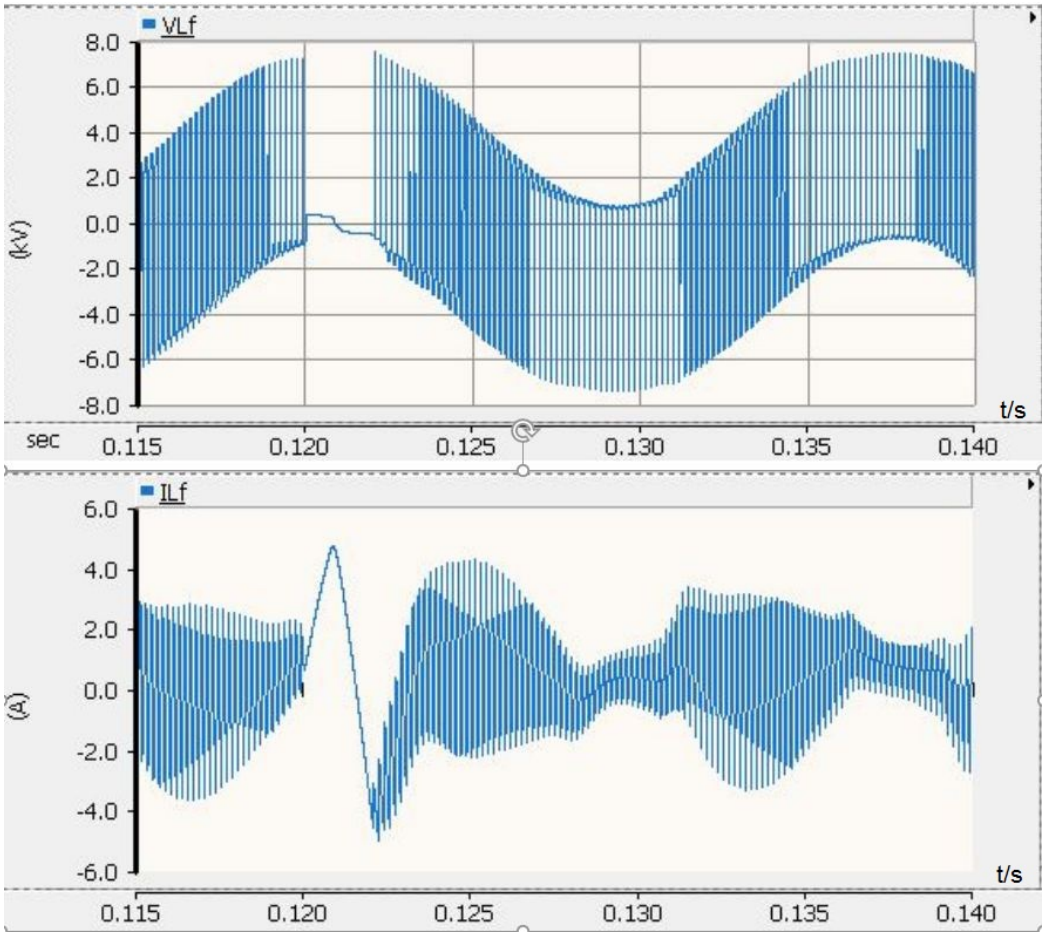

Figure 5.12: V_{Lf} I_{Lf} After the Filter Improvement

5.2.3 The Voltage Across Front Filter Capacitance C_f

The voltage surge on the front filter capacitance C_f is reduced from 43.30 kV to 12.97 kV, current surge drops from 24.58 A to 5.59 A. Over-voltage on C_f caused by lightning strike is significantly reduced. Oscillations of voltage and current are both reduced. The highest withstand voltage of a commercial 0.04 F capacitance is 10 kV [51]. Thus there should be two 0.08 F capacitances with the rating of 10 kV connected in series to protect the capacitances from over-voltage.

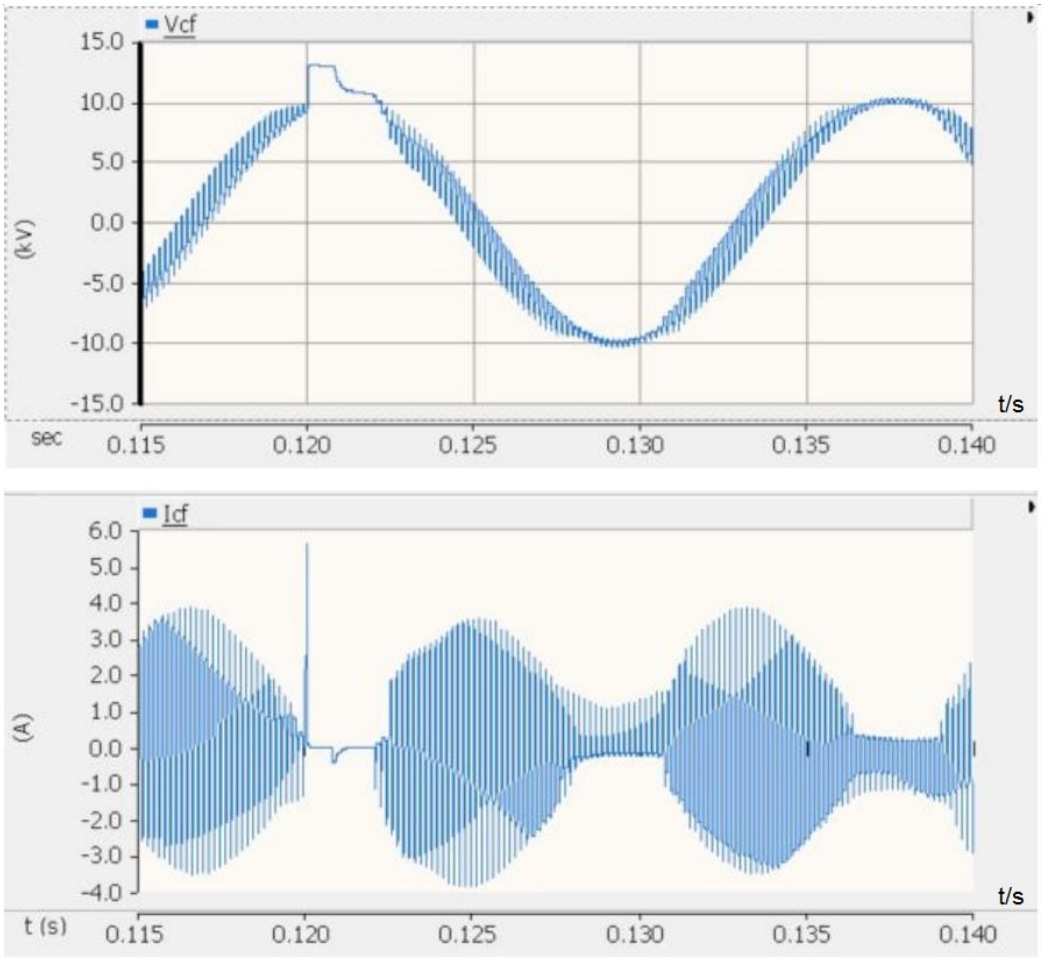

Figure 5.13: V_{Cf} I_{Cf} After the Filter Improvement

5.2.4 The Voltage and Current Across Semiconductors

a. Lower Semiconductor

The voltage surge on the lower semiconductor is reduced from 12.72 kV to 12.43 kV, current surge drops from 20.96 A to 5.07 A, lower than rated 20 A.

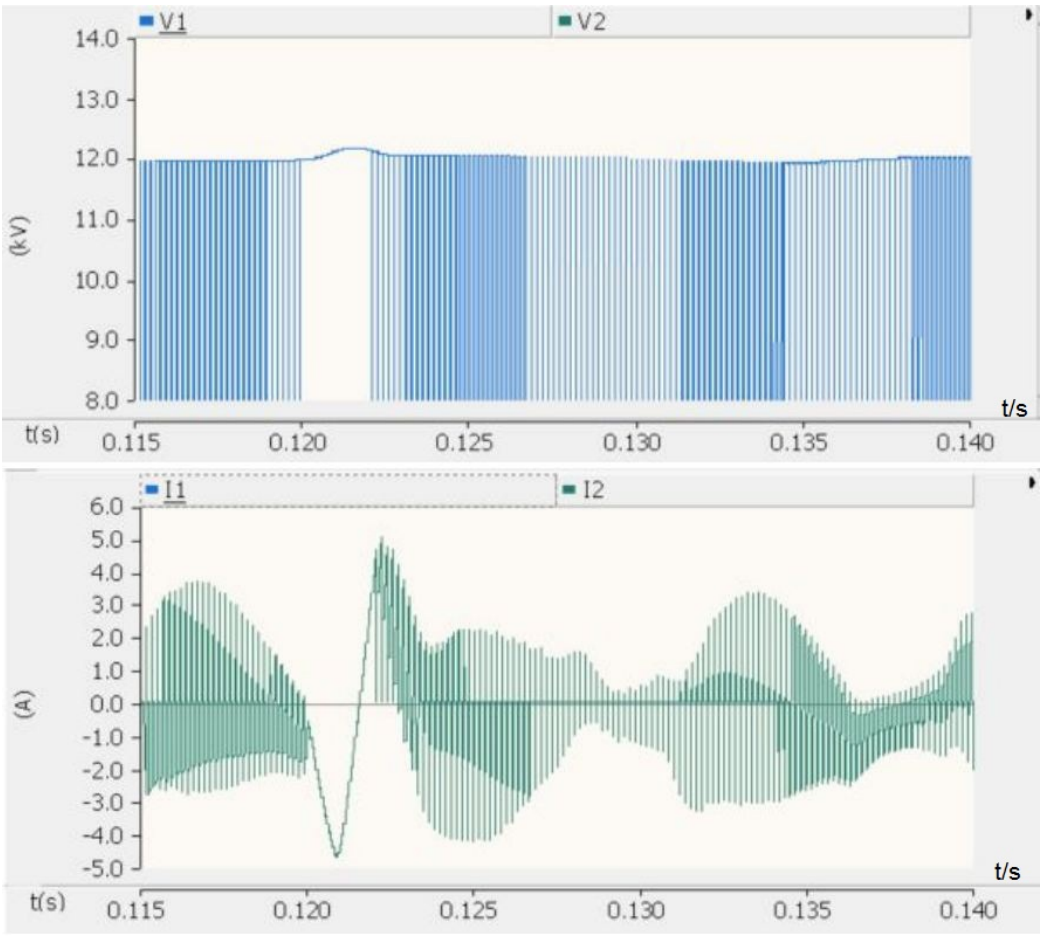

Figure 5.14: V_{r1} I_{r1} After the Filter Improvement

b. Upper Semiconductor

The voltage surge on the upper semiconductor is reduced from 12.72 kV to 12.43 kV, current surge drops from 28.34 A to 5.57 A, lower than rated 20 A.

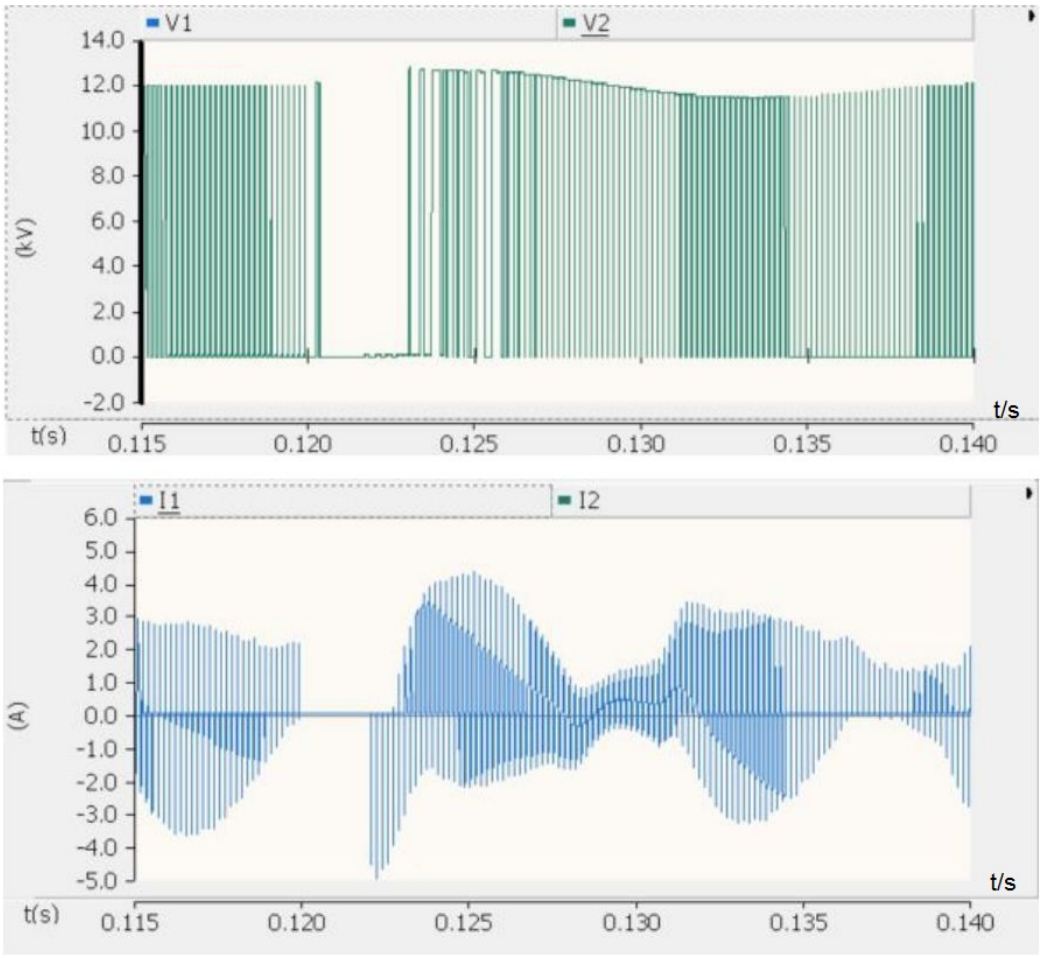

Figure 5.15: V_{r2} I_{r2} After the Filter Improvement

5.2.5 The Voltage and Current Across Capacitance C_h

The voltage surge on capacitance C_h is reduced from 12.72 kV to 12.43 kV, current surge drops from 28.26 A to 5.57 A. Thus the capacitance C_h is well protected, and voltage surge on high DC output caused by lightning strike is significantly reduced.

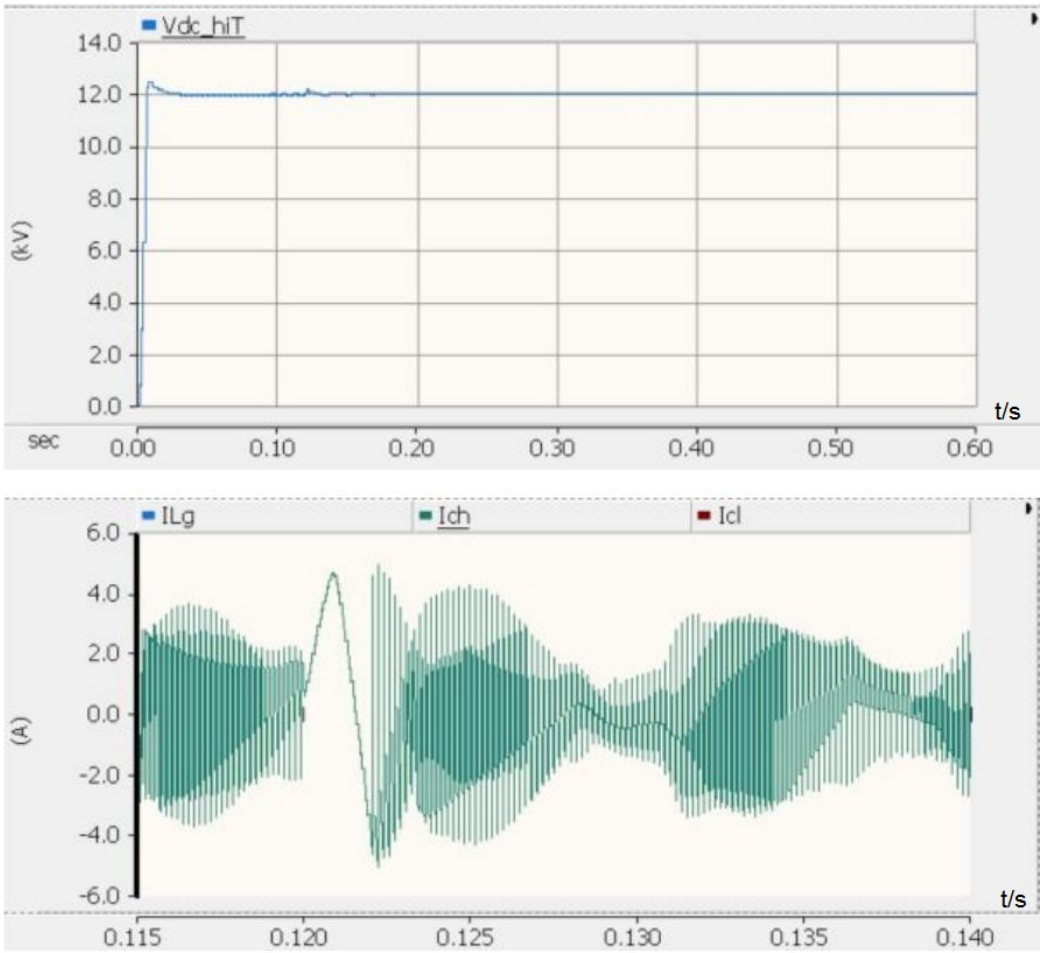

Figure 5.16: $V_{dc.hi}$ $I_{dc.hi}$ After the Filter Improvement

5.2.6 Conclusions

It can be seen in the table and figures that the surge arrester has effects on over-voltage and current protection if lightning happens, reducing amplitude of voltage and current surge on L_g, L_f and C_f by as much as 83%.

Chapter 6

CONCLUSIONS AND FUTURE WORK

6.1 Conclusions

Power electronic devices are widely used to interface DRERs and DESDs with the power grid. However, when connected directly to the power distribution system, the power electronic devices are under the risk of being exposed to the power transient caused by lightning strikes.

In this research, the FREEDM SST is taken as an example to simulate grid-tied power electronic devices in PSCAD software. The insulation coordination of the SST is analyzed under lightning strikes. The simulation is done when the devices are under non-operating condition and operating condition respectively. Similar analysis is also done to the VSC, another grid-tied power electronic device, to get more objective results. Operation conditions of other rid-tied converters, like STATCOM, are similar to that of the VSC.

The robustness of the devices is studied by applying a 60 kV 1.2/50 μs voltage impulse based on the IEC standards to represent a lightning strike. The over-voltage and over-current responses of the grid-tied power electronic devices are analyzed. Since the devices are connected to the power grid with an LCL front filter, the impulse can cause very high over-voltage on front filter components. Accordingly, the front filter inductances and capacitance need to be protected under lightning strikes.

The insulation coordination of the two types of devices is studied, and a methodology to implement MOSAs to reduce the voltage surge is proposed and explained in detail. The filter inductances are divided into three inductances in series to reduce

the voltage surge on each one. The MOSAs are selected and implemented based on ANSI standards. This methodology can reduce the over-voltage on the components inside the grid-connected power electronic devices by up to 90%.

The same simulation is performed on operating grid-tied VSCs under the same platform, the voltage surges on each element can also be reduced by up to 83% after protection.

6.2 Future Work

Both the analysis of the devices and the study of the protection methodology in this research are based on simulation. The protection method proposed in this research can be verified by physical experiments.

In this research, a 60 kV 1.2/50 μs voltage impulse is applied to the grid-tied devices to test the robustness and design the protection. In the high voltage lab in Arizona State University, a physical 60 kV impulse generator is going to be built for further insulation coordination tests.

REFERENCES

[1] X. Rong, D. Zhang, G. Karady, and G. Heydt, "Insulation coordination of freedm solid state transformer," in *2016 Grid of the Future Symposium, CIGRE US National Committee*, Oct 2016. (document), 2.4, 2.1.4, 2.1, 3.1, 3.2, 3.13, 4.2, 4.10, 5.2, 5.10

[2] G. T. Heydt, G. G. Karady, X. Rong, A. Q. Huang, and M. Steurer, "The direct connection of electronic components to power distribution primaries," in *North American Power Symposium, Morgantown, WV*, 2017. (document)

[3] R. Elmoudi, I. Grinberg, and M. Safiuddin, "Design and implementation of static var compensator for classroom and research applications in smart grid laboratory," in *2012 International Conference on Smart Grid (SGE)*, pp. 1–8, Aug 2012. (document), 2.1, 2.1.1

[4] L. Angquist and L. Lindberg, "Inner phase angle control of voltage source converter in high power applications," in *Power Electronics Specialists Conference, 1991. PESC '91 Record., 22nd Annual IEEE*, pp. 293–298, Jun 1991. (document), 2.2, 2.1.2

[5] Y. Ma, A. Huang, and X. Zhou, "A review of statcom on electric power system," in *2015 IEEE International Conference on Mechatronics and Automation (ICMA)*, pp. 162–167, Aug 2015. (document), 2.3, 2.1.3

[6] G. G. Karady, A. Q. Huang, and M. Baran, "FREEDM system: An electronic smart distribution grid for the future," in *PES T&D 2012*, pp. 1–6, May 2012. (document), 2.4.1, 2.10, 2.4.2

[7] A. Q. Huang, M. L. Crow, G. T. Heydt, J. P. Zheng, and S. J. Dale, "The future renewable electric energy delivery and management (freedm) system: The energy internet," *Proceedings of the IEEE*, vol. 99, pp. 133–148, Jan 2011. (document), 2.4.1, 2.11, 2.4.3

[8] Infineon, "Technical information for igbt fz250r65ke3," June 2014. 1.1, 4.1.4, 4.1.4

[9] IEC-61000, "Electromagnetic compatibility," 2014. 1.1, 1.2, 2.3.1

[10] IEC-60071, "Insulation coordination," 2006. 1.2, 3.1, 3.1

[11] M. Lindgren and J. Svensson, "Control of a voltage-source converter connected to the grid through an lcl filter – application to active filtering," in *Annual IEEE Power Electronics Specialists Conference*, vol. 1, pp. 229–235, May 1998. 2.1

[12] R. T. M. Rosyadi, S. Muyeen and J. Tamura, "Fuzzy logic controlled voltage source converter in grid connected application via lcl filter," in *International Conference on Electrical Machines and Systems (ICEMS)*, pp. 1–6, 2012. 2.1

[13] O. Clark and R. Gavender, "Lightning protection for microprocessor based electronic systems," *IEEE Transactions on Industry Applications*, vol. 26, pp. 947–953, Sep 1990. 2.1, 2.3.1, 2.3.1, 2.3.2

[14] Y. Ma, T. Zhao, and X. Zhou, "An overview on control methods used in static var compensator," in *2015 IEEE International Conference on Mechatronics and Automation (ICMA)*, pp. 92–97, Aug 2015. 2.1.1

[15] M. Mahdavian, G. Shahgholian, P. Shafaghi, M. Azadeh, S. Farazpey, and M. Janghorbani, "Power system oscillations improvement by using static var compensator," in *2016 13th International Conference on Electrical Engineering/Electronics, Computer, Telecommunications and Information Technology (ECTI-CON)*, pp. 1–5, June 2016. 2.1.1

[16] G. C. Sekhar, V. S. Kale, and G. V. Krishna, "Application of svc to improve voltage profile of indian railway traction system," in *2014 IEEE International Conference on Power Electronics, Drives and Energy Systems (PEDES)*, pp. 1–5, Dec 2014. 2.1.1

[17] M. Narimani and R. K. Varma, "Application of static var compensator (svc) with fuzzy controller for grid integration of wind farm," in *CCECE 2010*, pp. 1–6, May 2010. 2.1.1

[18] O. Benaissa, S. Hadjeri, and S. Zidi, "Impact of pss and svc on the power system transient stability," in *2016 8th International Conference on Modelling, Identification and Control (ICMIC)*, pp. 303–307, Nov 2016. 2.1.1

[19] B. S. Kumar, M. Suryakalavathi, and G. V. N. Kumar, "Optimal power flow with static var compensator based on flower pollination algorithm to minimize real power losses," in *Conference on Power, Control, Communication and Computational Technologies for Sustainable Growth (PCCCTSG)*, pp. 112–116, Dec 2015. 2.1.1

[20] A. Laka, J. A. Barrena, J. Chivite-Zabalza, M. . R. Vidal, and P. Izurza-Moreno, "New hexagonal three-phase voltage-source converter topology for high-power applications," *IEEE Transactions on Industrial Electronics*, vol. 62, pp. 30–39, Jan 2015. 2.1.2

[21] B. Huang, A. Shahin, J. P. Martin, S. Pierfederici, and B. Davat, "High voltage ratio non-isolated dc-dc converter for fuel cell power source applications," in *2008 IEEE Power Electronics Specialists Conference*, pp. 1277–1283, June 2008. 2.1.2

[22] M. E. Raoufat, A. Khayatian, and A. Mojallal, "Performance recovery of voltage source converters with application to grid-connected fuel cell dgs," *IEEE Transactions on Smart Grid*, vol. PP, no. 99, pp. 1–8, 2016. 2.1.2

[23] M. Farmad, S. Farhangi, S. Afsharnia, and G. B. Gharehpetian, "Application of voltage source converter in interphase power controller for power flow control and fault limitation," in *34th Annual Conference of IEEE Industrial Electronics*, pp. 2301–2306, Nov 2008. 2.1.2

[24] A. F. Abdou, A. Abu-Siada, and H. R. Pota, "Application of a statcom for damping subsynchronous oscillations and transient stability improvement," in *AUPEC 2011*, pp. 1–5, Sept 2011. 2.1.3

[25] P. M. Saradva, K. T. Kadivar, M. H. Pandya, and A. J. Rana, "Application of d-statcom to control power flow in distribution line," in *2016 International Conference on Energy Efficient Technologies for Sustainability (ICEETS)*, pp. 479–484, April 2016. 2.1.3

[26] T. Paulraj, I. S. Sherin, and M. A. Prakash, "Mitigation of power loss in transmission and distribution line using statcom," in *2016 International Conference on Advanced Communication Control and Computing Technologies (ICACCCT)*, pp. 432–435, May 2016. 2.1.3

[27] M. C. Falvo, L. Martirano, and D. Sbordone, "D-statcom with energy storage system for application in smart micro-grids," in *2013 International Conference on Clean Electrical Power (ICCEP)*, pp. 571–576, June 2013. 2.1.3

[28] F. Bignucolo, M. Bertoluzzo, and C. Fontana, "Applications of the solid state transformer concept in the electrical power system," in *2015 AEIT International Annual Conference (AEIT)*, pp. 1–6, Oct 2015. 2.1.4, 2.1.4

[29] G. Zhabelova, A. Yavarian, V. Vyatkin, and A. Q. Huang, "Data center energy efficiency and power quality: an alternative approach with solid state transformer," in *IECON 2015 - 41st Annual Conference of the IEEE Industrial Electronics Society*, pp. 001294–001300, Nov 2015. 2.1.4, 2.1.4

[30] J. Z. R. Xu, L. Xia and J. Ding, "Design and research on the lcl filter in three-phase pv grid-connected inverters," in *International Journal of Computer and Electrical Engineering*, vol. 5, June 2013. 2.1.4

[31] M. Liserre, F. Blaabjerg, and S. Hansen, "Design and control of an lcl-filter-based three-phase active rectifier," *IEEE Transactions on Industry Applications*, vol. 41, pp. 1281–1291, Sept 2005. 2.1.4

[32] C. Hunziker and N. Schulz, "Solid-state transformer modeling for analyzing its application in distribution grids," in *PCIM Europe 2016; International Exhibition and Conference for Power Electronics, Intelligent Motion, Renewable Energy and Energy Management*, pp. 1–8, May 2016. 2.1.4

[33] T. Yang, R. Meere, C. O'Loughlin, and T. O'Donnell, "Performance of solid state transformers under imbalanced loads in distribution systems," in *2016 IEEE Applied Power Electronics Conference and Exposition (APEC)*, pp. 2629–2636, March 2016. 2.1.4

[34] H. Wen and R. Yang, "Power management of solid state transformer in microgrids," in *2016 IEEE PES Asia-Pacific Power and Energy Engineering Conference (APPEEC)*, pp. 1399–1404, Oct 2016. 2.1.4

[35] IEEE, "Ieee standard for insulation coordination- definitions, principles and rules," 1996. 2.2

[36] IEEE, "Eee standard for metal-oxide surge. arresters for ac power circuits," 2012. 2.2, 2.3.2

[37] J. P. Bickford and A. G. Heaton, "Transient overvoltages in power system," *IEE Proceedings C - Generation, Transmission and Distribution*, vol. 133, pp. 201–225, May 1986. 2.3.1

[38] G. Tapiawala and R. K. Mishra, "Comprehensive modeling of dry type foil winding transformer to analyse inter turn insulation under lightning impulse voltage," in *2016 National Power Systems Conference (NPSC)*, pp. 1–5, Dec 2016. 2.3.1

[39] F. D. Martzloff, "Surge protection techniques in low-voltage ac power systems," in *INTELEC - 1979 International Telecommunications Energy Conference*, pp. 86–93, Nov 1979. 2.3.1

[40] IEC-60076, "Insulation levels, dielectric tests and external clearances in air," 2013. 2.3.1

[41] P. de Bruyne and P. Wetzel, "Improved overvoltage protection in power electronics using active protection devices," *IEE Journal on Electric Power Applications,*, vol. 2, pp. 29–36, February 1979. 2.3.2

[42] F. Noack, J. Pospiech, R. Brocke, and J. Schonau, "Reliable overvoltage protection of electronic devices in low-voltage power systems," in *International Symposium on Electromagnetic Compatibility (IEEE Cat. No.99EX147)*, pp. 298–301, 1999. 2.3.2

[43] C. Gomes and V. Cooray, "Surge protection of low voltage systems and relevant standards," in *2010 30th International Conference on Lightning Protection (ICLP)*, pp. 1–8, Sept 2010. 2.3.2

[44] F. B. Golden, "A new component-the metal oxide varistor suppressor," in *IEEE Power Processing and Electronics Specialists Conference*, pp. 134–139, May 1972. 2.3.2

[45] D. W. Durbak, "Surge arrester modeling," in *IEEE Power Engineering Society Winter Meeting. Conference Proceedings (Cat. No.01CH37194)*, vol. 2, pp. 728–730 vol.2, 2001. 2.3.2

[46] P. F. Evangelides, C. A. Christodoulou, I. F. Gonos, and I. A. Stathopulos, "Parameters selection for metal oxide surge arresters models using genetic algorithm," in *30th International Conference on Lightning Protection (ICLP)*, pp. 1–5, Sept 2010. 2.3.2

[47] I. W. G. 3.4.11, "Modeling of metal oxide surge arresters," *IEEE Transactions on Power Delivery*, vol. 7, pp. 302–309, Jan 1992. 2.3.2

[48] L. F. Casey, L. E. Zubieta, J. T. Mossoba, B. S. Borowy, and B. Semenov, "Power devices for grid connections," in *24th International Symposium on Power Semiconductor Devices and ICs*, pp. 1–7, June 2012. 2.4.3

[49] Online, "$www.mcmaster.com/standard-electrical-wire/=181vb4l$." 3.1.1, 3.1.2, 3.2, 3.2.1, 3.2.2, 4.1.1, 4.1.2, 4.2.1, 4.2.2, 5.1.1, 5.1.2, 5.2.1, 5.2.2

[50] Online, "$www.engineeringtoolbox.com/wire-gauges-d_419.html$." 3.1.1, 3.1.2, 3.2, 3.2.1, 3.2.2, 4.1.1, 4.1.2, 4.2.1, 4.2.2, 5.1.1, 5.1.2, 5.2.1, 5.2.2

[51] Online, "$http://hvstuff.com/0-04uf-10kv-high-voltage-capacitor-hv-tesla-coil-ham$." 3.1.3, 3.2.3, 4.1.3, 4.2.3, 5.1.3, 5.2.3

[52] K. Vechalapu, S. Bhattacharya, E. V. Brunt, S. H. Ryu, D. Grider, and J. W. Palmour, "Comparative evaluation of 15-kv sic mosfet and 15-kv sic igbt for medium-voltage converter under the same dv/dt conditions," *IEEE Journal of Emerging and Selected Topics in Power Electronics*, vol. 5, pp. 469–489, March 2017. 5.1.4

APPENDIX A

MOSA SELECTION BASED ON ANSI STANDARD

Typical ANSI System Voltages			Suggested ANSI Arrester MCOV Rating			
Nom Line to Line Voltage	Max Line to Line Voltage	Max Line to Grnd Voltage	Solid Multi-grounded Systems (4 wire)	Uni-grounded Systems (3 wire)	Impedance grounded, Ungrounded and Delta Systems	Transmission Line Arresters for Lightning Protection Only
kV rms	kV rms	kV rms	MCOV	MCOV [*]	MCOV [*]	
2.40	2.52	1.46			2.55	
4.16	4.37	2.52	2.55	5.1	5.1	
4.80	5.04	2.91			5.1	
6.90	7.25	4.19			7.65	
8.32	8.74	5.05	5.1	7.65		
12.0	12.6	7.28	7.65	10.2		
12.5	13.1	7.57	7.65	12.7 [7.65]		
13.2	13.9	8.01	8.4	12.7 [8.4]		
13.8	14.5	8.38	8.4	12.7 [8.4]	15.3 [8.4]	15.3
20.8	21.8	12.6	12.7	15.3 [12.7]		21
22.9	24.0	13.9	15.3	19.5 [15.3]		22-24
23.0	24.2	14.0	15.3-17		24.4 [15.3]	22-24
24.9	26.2	15.1	15.3	22 [15.3]		24-29
27.6	29.0	16.8	17	24.4 [17]		24-29
34.5	36.2	20.9	22	29 [22]	36-39 [22]	29-36
46.0	48.3	27.9		29	39	29-39
69.0	72.5	41.9		42-48	53-67	48-67
115.0	121	69.8		70-76	84-98	76-98
138.0	145	83.8		84-98	106-115	98-115
161.0	169	98		98-115	115-131	115-131
230.0	242	140		140-152	182-190	152-190
345.0	362	209		209-245	230-289	245-289
500.0	525	303		318-452		>452
765.0	800	462		462-490		>490
[*] Cooper Power Systems Evolution Arrester Rating						

APPENDIX B

AWG GAUGES AND THEIR CURRENT RATINGS

AWG	Typical Max. Current Load Ratings - Copper *(amps)*[1)]					
	Single Core	Multicore				
		up to 3 cores	4 - 6 cores	7 - 24 cores	25 - 42 cores	43 and above
40						
39						
38						
37						
36						
35						
34						
33						
32						
30						
28						
27						
26						
25						
24	3.5	2	1.6	1.4	1.2	1
22	5	3	2.4	2.1	1.8	1.5
20	6	5	4	3.5	3	2.5
18	9.5	7	5.6	4.9	4.2	3.5
16	20	10	8	7	6	5
14	24	15	12	10	9	7.5
13						
12	34	20	16	14	12	10
10	52	30	24	21	18	15
8	75	40	32	28	24	20
6	95	55	44	38	33	27
4	120	70	56	49	42	35
3	154	80	64	56	48	40
2	170	95	76	66	57	57
1	180	110	88	77	66	55

APPENDIX C

MATLAB CODE FOR FREQUENCY ANALYSIS

```
% LCL Frequency Analysis
% Parameters
Lg=121.3e-3;
Lf=170e-3;
Cf=0.04e-6;
Rg=36.87;
Rf=11;
Cdc=84e-6;
fs=6000;
% Transfer Function for Voltage
Gcf=tf(1,[Cf,0]);
Gl1=tf([Lg,Rg],1);
Gl2=tf([Lf,Rf],1);
Gc=tf(1,[Cdc,0]);
T1=(Gc+Gl2)*Gcf/(Gc+Gl2+Gcf);
T2=T1/(T1+Gl1);
Gv=T2*Gc/(Gc+Gl2);
Gi=T2/(Gc+Gl2);
margin(Gv);
figure(2);
margin(Gi);
% Lightning
a1=-61.223e3;
a2=-a1;
b1=48.3472e5;
b2=0.1425e5;
Gt=tf(a1,[1,b1])+tf(a2,[1,b2]);
figure(3);
margin(Gt);
% voltage response
figure(4);
margin(Gv*Gt);
% current response
figure(5);
margin(Gi*Gt);
% margin(Gt*tf([Cdc,0],1));
% Tranferfucntion with MOVs
Gv1=Gc/(Gc+Gl2+Gl1);
figure(6);
margin(Gv1);
figure(7);
margin(tf(1,[1,0])*Gv1);
Gi2=1/(Gc+Gl2);
figure(8);
margin(Gi2);
figure(9);
margin(tf(1,[1,0])*Gv1);
```